Anomalous Modulation of Photoinduced Electron Transfer of Coumarin Acceptors in Solvent Mixtures: Effect of Excited-State Hydrogen Bonding

A dissertation

as partial fulfilment of requirement

for the degree of Doctor of Philosophy in Chemistry

by

Nabajeet Barman

11612246

Department of Chemistry

Indian Institute of Technology Guwahati

Guwahati-781039,

Assam, India

Declaration

I do hereby declare that the work contained in this thesis entitled **"Anomalous Modulation of Photoinduced Electron Transfer of Coumarin Acceptors in Solvent Mixtures: Effect of Excited-State Hydrogen Bonding"** is the outcome of the research work carried out by me under the supervision of Dr. Kalyanasis Sahu, Associate Professor, Department of Chemistry, Indian Institute of Technology Guwahati, India.

In keeping with the general practice of reporting scientific observations, due acknowledgements have been made whenever work described here has been based on the findings of other investigators. This work has not been submitted elsewhere for the award of any degree.

Dated:

Department of Chemistry

Indian Institute of Technology Guwhati, (Nabajeet Barman)

Guwahti-781039, India

Certificate

It is certified that the work included in this thesis entitled **"Anomalous Modulation of Photoinduced Electron Transfer of Coumarin Acceptors in Solvent Mixtures: Effect of Excited-State Hydrogen Bonding"** is the results obtained from the research work carried out by Nabajeet Barman under the supervision of me.

Dr. Kalyanasis Sahu

Department of Chemistry

Indian Institute of Technology Guwhati,

Guwahti-781039, India

Acknowledgement

At this stage of ending my PhD programme, I would like to appreciate the people around me all throughout my academic journey without whom this thesis would not have been a reality. First of all, I take this opportunity to convey my earnest gratitude and respect to my supervisor, Dr. Kalyanasis Sahu who has been an excellent supervisor and taught me how to carry out research supervision. With his enthusiasm, inspiration and efforts to explain things lucidly, he helped me in making this thesis a reality. His integral vision on research, meticulous eye for details and simple yet scientific approach towards any problem will always leave a deep impression in my mind. Besides this he has provided me scientific knowledge and experimental skills and also made me to understand a broader perspective of the life as well. I find myself privileged to have worked under his guidance.

I would like to acknowledge my doctoral committee members Dr. Aditya N. Panda (Chairman), Dr. Debpratim Das, and Dr. Sumana Dutta who have been constantly guiding me with their valuable suggestions, encouragements and constructive criticism which helped to improve my thesis. I take this opportunity to thank Prof. B. K. Patel (HOD) and Prof. A. Chattopadhyay (former HOD).

I really thank my labmates Debabrata Singha, Aparajita Phukon, and Dilip Kr. Sahu for creating a good environment in the lab. They are always there providing their help whenever I need.

At this stage I would like to thank Prof. Kankan Bhattachayya and his students-Rajdeep Chowdhury and Shyamtanu Chattoraj for generous help in the fluorescence upconversion measurement. I am thankful to Sougata Sahu for teaching me how to operate the TRPL instrument. I will remain thankful to Prof. G. Krishnamoorthy for allowing me to operate the TRPL instrument.

I take this opportunity to thank IIT Guwahati for providing me Fellowship for my PhD programme. I thank the Department of Chemistry for providing instrumental and computational facilities, and CIF for instrumental facilities. I am thankful to all the faculties and scientific staff of the department of chemistry.

I remain thankful to my friends namely Nayanjyoti Rajbangshi, Manash Deka, Prakash Hazam, Pankaj Hazarika, Durlov Saikia, Suraj Pathak, Jiban Saikia, Sukanya Baruah for their help and inspiration.

Finally I would like to thank my parents for their unreserved endurance, encouragement and support throughout my life.

Sincerely

Nabajeet Barman

Contents

Synopsis

Abstract

The thesis describes our results on anomalous fluorescence modulation to illustrate the much debated role of hydrogen bonding on photoinduced electron transfer (PET). The content of the thesis has been spread out into seven chapters. Chapter 1 briefly accounts recent experimental and theoretical developments in the field of excited-state H-bonding and H-bonded mediated PET, which motivate us to undertake the project. Chapter 2 summarises experimental and theoretical methods used in our studies. In chapter 3, we first experimentally confirmed the theoretical prediction that PET becomes facilitated through donor-acceptor H-bonding between coumarin 102 (C102, acceptor) and phenol (donor). In chapter 4, we showed that PET depends unusually on the mole fraction of H-bond donor (aniline) in a mixture where an additional inert component is present along with the donor. The results may be attributed to possible modulation of polarity or H-bonding environment around the acceptor in the mixture. In chapter 5, we demonstrated that the anomalous PET behaviour retains even in similar polarity mixture of aniline (AN) and *N,N*-dimethylaniline (DMA). Chapter 6 emphasizes that the competitive H-bonding concept can account for the anomalous behaviour of PET for a different H-bonding donor- phenol as well. We revisited the system studied in chapter 3 with much fuller mole fraction range of phenol. In Chapter 7, we have utilized fluorescence up-conversion measurements to detect much more ultrafast H-bond assisted PET of a better electron acceptor coumarin 153 (C153) in AN-cyclohexane mixture. In the end, a future outlook is provided.

Chapter 1: Introduction

Photoinduced electron transfer (PET) is an excited state process where an electronically excited molecule can take up (Reductive PET) or releases an electron (Oxidative PET) from/to another molecule (called donor or acceptor, respectively). The factors governing the PET such as free energy, substituent effect, isotope effect have been reviewed in this chapter.[1-6] A special focus has been attributed to the issue of the fate of H-bonding in the electronic excited state i.e. whether H-bond breaks or becomes stronger in the

excited state.[7-13] The studies related to the effect of H-bonding on PET have been reviewed.[14-20] The scope of the current project in the context of the existing literature has been discussed.

Chapter 2: Experimental and theoretical methods

Theoretical calculation methodology, mainly density functional theory (DFT) and time-dependent density functional theory (TD-DFT) on C102-phenol systems were presented. Specifications of all the instruments (e.g. UV-Visible spectrophotometer, steady state spectrofluorometer, time correlated single photon counting (TCSPC), femtosecond up-conversion, FT-IR spectrophotometer etc.) are provided. Chemicals used and sample preparation procedures have also been included.

Chapter 3: Hydrogen-Bond induced photoinduced electron transfer of coumarin 102-phenol complex[21]

To understand the H-bonding effect on fluorescence, we have chosen three phenol derivatives- phenol, *p*-Cl-phenol and anisole (Figure 3.1) of varying H-bonding strength. First, we have discussed the results of DFT and TD-DFT calculations of C102-phenol H-bonded complex. Using TD-DFT methods we have demonstrated that H-bond of C102-phenol (1:1 complex) is strengthened in the electronic excited-state which was in agreement with the results of Zhao and co-workers.[12-13] The strengthening of the H-bond in the electronic excited-state is quite evident from the potential energy curves constructed from TD-DFT calculation followed by fitting with Morse type equation.

This follows experimental results on fluorescence quenching of C102 in cyclohexane in the presence of phenol. Steady-state fluorescence measurement showed that fluorescence of C102 in cyclohexane drastically quenches in the presence of phenol. This was in agreement with the prediction of the theoretical study of Zhao and co-workers.[12-13] Fluorescence quenching was found to be even more pronounced in the presence of *p*-Cl-phenol which has stronger H-bonding ability. However, fluorescence quenching was absent for anisole, where H-bond formation is not possible. Fluorescence quenching of C102 in the presence of different H-bond donor was correlated well with the H-bonding strength using Stern-Volmer plot. Fluorescence quenching was explained on the basis of internal conversion

(IC) from a locally excited (LE) state to a charge transfer (CT) state within the H-bonded complex. This study shows that excited-state hydrogen bonding dynamics, which are typically proposed to occur on a ultrafast time scale, may alter the fluorescence characteristics of a H-bonded complex on much slower time scale as well. The work was limited to lower concentration of phenol to avoid contributions from the higher order C102-$(phenol)_{n\geq 2}$ complexes.

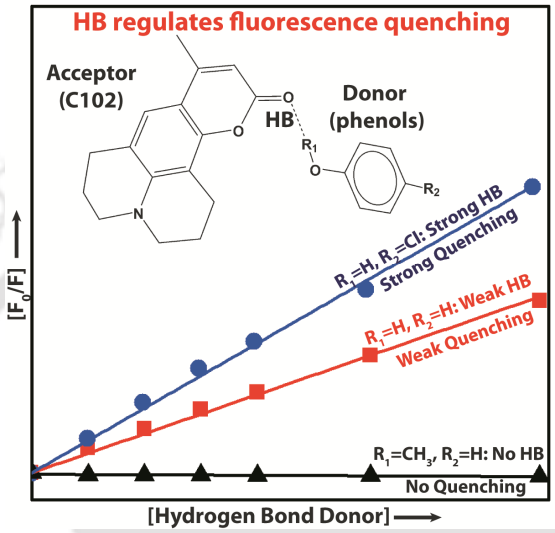

Figure 3.1: Schematic representation of H-bond controlled fluorescence quenching of C102-phenol complex for different H-bonding strength of the donor.

Chapter 4: Enhancement of H-bond mediated photoinduced electron transfer upon addition of inert solvent: Coumarin 102 in cyclohexane-aniline and toluene-aniline mixtures[22]

In the previous chapter, we demonstrated the important role of H-bonding in assisting PET within a H-bonded complex. In this chapter, we have shown that under appropriate condition, H-bonding can enhance PET rate to such an extent that the rate could eventually exceed the PET rate observed in neat electron-donating solvent. This apparently opposes the conventional idea that higher amount of donor should increase PET. Surprisingly, we observed dramatic acceleration of PET (6-10 fold enhancement compared to neat AN), for C102 dissolved in a binary mixture of AN and an inert solvent (cyclohexane or toluene). The PET induced fluorescence follows an anomalous trend against the mole fraction of AN (X_{AN}); first quenches up to certain X_{AN} (0.075 for cyclohexane; 0.13 for toluene), thereafter,

enhances with increase in X_{AN}. Although, the non-interacting component cannot directly participate in the PET process, it may modulate C102-AN H-bonding association by changing the polarity of the medium or by disruption the AN-AN H-bond so that the key donor-acceptor (C102-AN) H-bond become more effective for efficient PET (Figure 4.1). The study clearly illustrates the dominant role H-bonding in activating the electron transfer rate where standard thermodynamics predicts very weak donor-acceptor interaction.

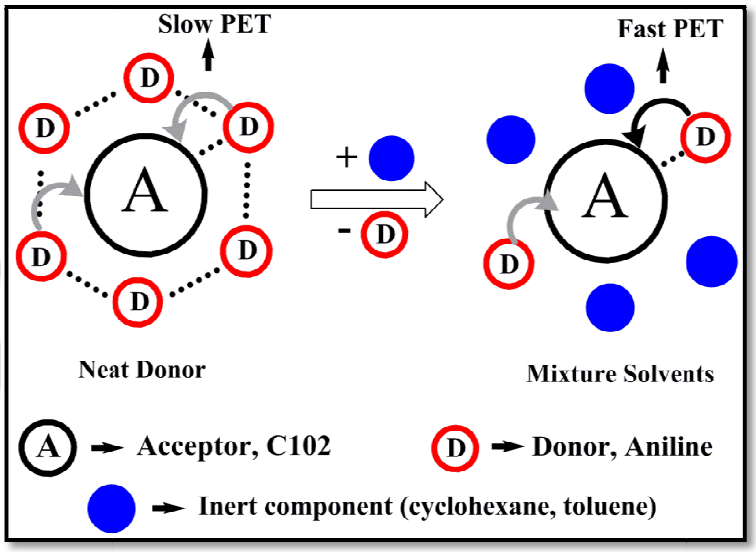

Scheme 4.1: A scheme summarising the concept of chapter 4. Hydrogen bonding activated photoinduced electron transfer is found to be more efficient in diluted donor than in neat aniline.

Chapter 5: Anomalous photoinduced electron transfer of coumarin 102 in aniline-*N*,*N*-dimethylaniline mixture[23]

In the previous chapter the unusual PET modulation of C102 with X_{AN} was attributed two possibilities: (1) the D-A (AN-C102) H-bonding itself may be modulated due to change in polarity of the medium as the donor and the inert solvent may have very different polarity or (2) the additional D-D (AN-AN) H-bonding may restrain the D-A H-bonding to adjust optimally for the PET. To decipher these two effects, in this chapter, we have investigated the PET of C102 in AN-DMA mixture. Both AN and DMA have similar polarity as evident from the Kamlet-Taft parameters of the two solvents (Table 5.1), hence, the effect of polarity change in the mixture may be eliminated. Interestingly, we still observed anomalous PET modulation for C102 in the mixture. The PET rate increases with increase in the X_{AN} upto a particular mole fraction, followed by a decrease of the rate with further increases in X_{AN}

(Figure 5.1). The observed anomalous PET modulation may be rationalized by considering efficient PET in the 1:1 H-bonded C102-AN complex (only D-A H-bond, non-competitive H-bonding) but less efficient in higher order C102-$(AN)_{n\geq 2}$ complexes (both D-A and D-D H-bonds, competitive H-bonding) where additional D-D (AN-AN) H-bonding may influence the key C102-AN H-bonding and thus retard the PET process.

Table 5.1: Kamlet-Taft parameters, π^* (polarity); α (hydrogen bond donor) and β (hydrogen bond acceptor) of aniline and DMA.

Solvent	π^*	α	β
Aniline	0.73	0.50	0.50
DMA	0.73	0.0	0.43

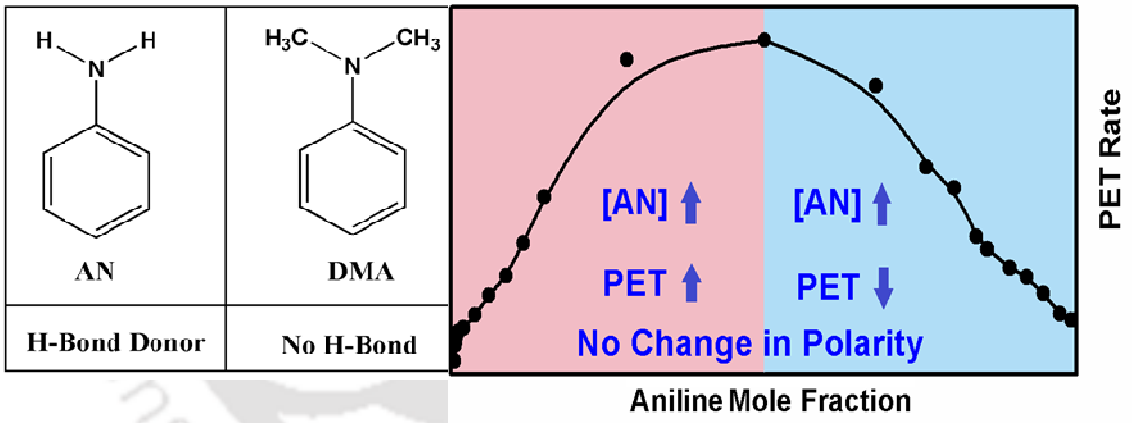

Figure 5.1: Schematic presentation of the main concept of the work done in the chapter 5. The PET of C102 in the uniform polarity AN-DMA mixture is found to be unusually modulated by the change in H-bonding conditions.

Chapter 6: Reduced fluorescence quenching of coumarin 102 at higher phenol mole fractions in cyclohexane–phenol and anisole–phenol solvent mixtures[24]

In chapter 3, we have already discussed that fluorescence of C102 drastically quenches upon H-bonding with phenol in a non-polar solvent cyclohexane due to H-bond induced PET. However, that work was limited upto low concentration of phenol where only

1:1 C102-phenol complex predominantly exists. In this chapter, we have revisited the same system upto much higher mole fractions of phenol. We found an unusual fluorescence modulation of C102 over mole fractions of the H-bond donor (phenol) in the cyclohexane-phenol mixture. We observed that both the quantum yield (φ_f) and fluorescence lifetime ($<\tau>$) decrease steadily with increase in the mole fraction of phenol upto a particular X_{PhOH},(= 0.013), but thereafter, both the quantities increase with further increase in X_{PhOH} (Figure 6.1). The results can be attributed to the competitive nature of the C102–phenol and the phenol–phenol H-bonding. Since the PET quenching operates through the H-bond between the C=O group of C102 and the HO– group of phenol, the H-bond may fail to attain an optimum geometry when the phenol is linked with other phenols via the H-bond. The variation of the C102–phenol H-bonding nature with the mole fraction of phenol was supplemented by FT-IR measurements. Similar unusual variation of the C102 fluorescence is observed in the phenol–anisole mixtures to a lesser extent, but is completely absent in the anisole–cyclohexane mixtures, where H-bonding is practically impossible (Figure 6.1).

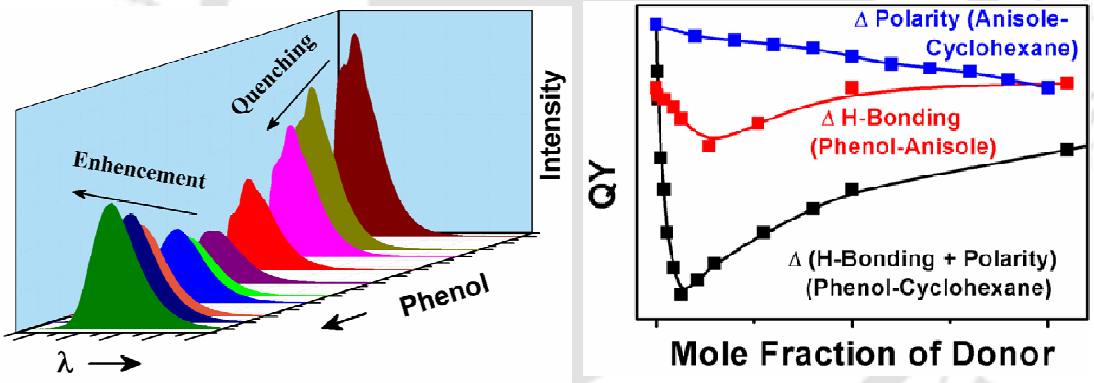

Figure 6.1: A comprehensive representation of chapter 6. The H-bond mediated fluorescence quenching of C102-phenol H-bonded complex is found to be unusually modulated by the variation of H-bonding conditions.

Chapter 7: An inert component mixed with donor solvent can make ultrafast H-bond assisted photoinduced electron transfer even faster[25]

The case of C102 discussed in the earlier chapters, cannot be a representative for ultrafast PET observed usually for other coumarins as C102 is reluctant to undergo PET in the absence of H-bonding. This implies that PET could occur favourably even in the absence of H-bonding. In this regard, we have chosen another acceptor coumarin 153 (C153) in

cyclohexane-AN and cyclohexane-DMA mixtures. C153 is known to undergo ultrafast PET in both neat AN and DMA.[2] Structurally, C153 has similar skeleton to C102; only the methyl group is substituted by trifluoromethyl group (Figure 3.1). The $-CF_3$ substitution has a profound effect on the reduction potential and hence, on the free energy of electron transfer becomes much more favorable. We observed that ultrafast PET from electron donating solvent (AN/DMA) to a dissolved acceptor (C153) shows very contrasting modulation when an inert component cyclohexane is added. In the case, where the donor solvent (AN) has the potential to form H-bond with the acceptor, the PET rates are found to accelerate by the presence of the inert component. On the other hand, for the donor solvent (DMA) incapable of forming H-bond with the acceptor, addition of cyclohexane retards the PET (Figure 7.1). This differential modulation of PET is justified by the possible rearrangement around the acceptor and the H-bonding situation in the mixture.

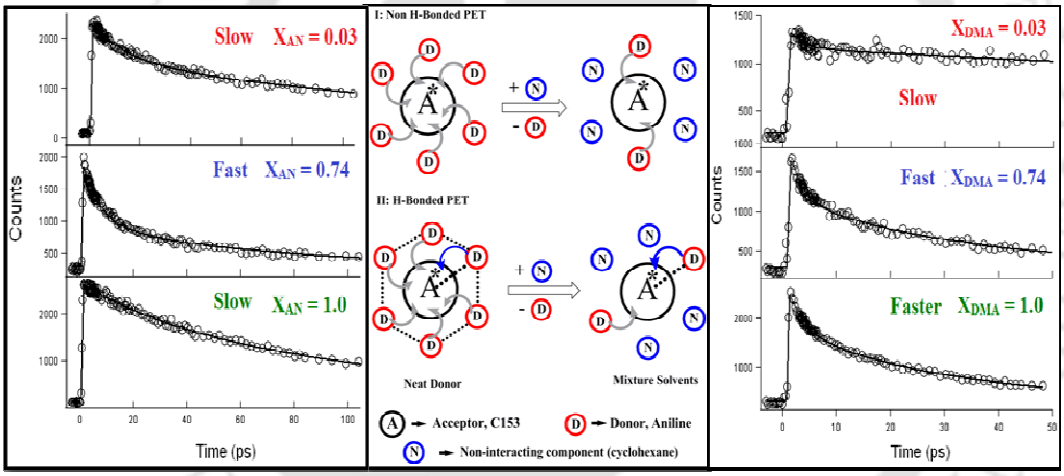

Figure 7.1: Schematic representation of chapter 7. The ultrafast PET of C153 is found to be unusually modulated in the presence diluted electron donor having H-bonding ability.

Future Outlook

This thesis investigates very important role of H-bonding on PET using coumarin acceptor and aniline and phenol donors. To obtain more insight into the mechanistic details of intermolecular PET process various effects such temperature, isotopic substitution, substituent effect should also be considered. Isotopic substitution is an important technique. It will give valuable information about the detail mechanism of PET in hydrogen-bonded complex. This work can be extended to study of the effect isotopic substitution on PET of coumarins as well as other system also. To validate the competitive PET in neat vs non-

competitive PET in mixture, MD simulation should be taken to look at the local structural arrangement of donor around the acceptor. So far we have considered only the fundamental aspects of H-bonded PET in mixture, it is interesting to see how this could affect photophysics under real competitive H-bonding condition. For example, in an enzyme pocket, a substrate forming a H-bond with a particular functional group at an active site, may also simultaneously make a H-bond with other amino acids.

References

1. P. F. Barbara, T. J. Meyer and M. A. Ratner, *J. Phys. Chem.*, 1996, **100**, 13148-13168.
2. Y. Nagasawa, A. P. Yartsev, K. Tominaga, P. B. Bisht, A. E. Johnson and K. Yoshihara, *J. Phys. Chem.*, 1995, **99**, 653-662.
3. H. Pal, Y. Nagasawa, K. Tominaga and K. Yoshihara, *J. Phys. Chem.*, 1996, **100**, 11964-11974.
4. H. Shirota, H. Pal, K. Tominaga and K. Yoshihara, *J. Phys. Chem. A*, 1998, **102**, 3089-3102.
5. E. W. Castner, D. Kennedy and R. J. Cave, *J. Phys. Chem. A*, 2000, **104**, 2869-2885.
6. Y. Nagasawa, A. P. Yartsev, K. Tominaga, A. E. Johnson and K. Yoshihara, *J. Chem. Phys.*, 1994, **101**, 5717-5726.
7. C. Chudoba, E. T. J. Nibbering and T. Elsaesser, *J. Phys. Chem. A*, 1999, **103**, 5625-5628.
8. C. Chudoba, E. T. J. Nibbering and T. Elsaesser, *Phys. Rev. Lett.*, 1998, **81**, 3010-3013.
9. E. T. J. Nibbering, C. Chudoba and T. Elsaesser, *Isr. J. Chem.*, 1999, **39**, 333-346.
10. E. T. J. Nibbering, F. Tschirschwitz, C. Chudoba and T. Elsaesser, *J. Phys. Chem. A*, 2000, **104**, 4236-4246.
11. E. T. J. Nibbering and T. Elsaesser, *Chem. Rev.*, 2004, **104**, 1887-1914.
12. G.-J. Zhao and K.-L. Han, *J. Phys. Chem. A*, 2007, **111**, 2469-2474.
13. G.-J. Zhao and K.-L. Han, *Acc. Chem. Res.*, 2011, **45**, 404-413.
14. G.-J. Zhao, J.-Y. Liu, L.-C. Zhou and K.-L. Han, *J. Phys. Chem. B*, 2007, **111**, 8940-8945.
15. G.-J. Zhao and K.-L. Han, *Biophys. J.*, 2008, **94**, 38-46.
16. G.-J. Zhao and K.-L. Han, *ChemPhysChem*, 2008, **9**, 1842-1846.
17. G.-J. Zhao, J.-Y. Liu, L.-C. Zhou and K.-L. Han, *J. Phys. Chem. B*, 2007, **111**, 8940-8945.
18. G.-J. Zhao and K.-L. Han, *J. Comput. Chem.*, 2008, **29**, 2010-2017.
19. Y. Liu, J. Ding, D. Shi and J. Sun, *J. Phys. Chem. A*, 2008, **112**, 6244-6248.
20. Y.-H. Liu and P. Li, *J. Lumin.*, 2011, **131**, 2116-2120.
21. N. Barman, D. Singha and K. Sahu, *J. Phys. Chem. A*, 2013, **117**, 3945-3953.
22. N. Barman, D. Singha and K. Sahu, *Phys. Chem. Chem. Phys.*, 2014, **16**, 6159-6166.
23. N. Barman and K. Sahu, *Phys. Chem. Chem. Phys.*, 2014, **16**, 27096-27103.

24. N. Barman and K. Sahu, *RSC Advances*, 2014, **4**, 58299-58306.

25. N. Barman and K. Sahu.(Under Preparation).

List of Publications

Paper included in this thesis:

1. **Nabajeet Barman**, Debabrata Singha, Kalyanasis Sahu, "Fluorescence Quenching of Hydrogen-Bonded Coumarin 102-phenol Complex: Effect of Excited-State Hydrogen Bonding Strength"†
   J. Phys. Chem. A **2013**, *117*, 3945-3953.

2. **Nabajeet Barman**, Debabrata Singha, Kalyanasis Sahu, "Faster Photoinduced Electron Transfer in a Diluted Mixture than in a Neat Donor Solvent: Effect of Excited-State H-Bonding"†
   Phys. Chem. Chem. Phys. **2014**, *16*, 6159-6166.

3. **Nabajeet Barman**, Kalyanasis Sahu, "Anomalous Modulation of Photoinduced Electron Transfer of Coumarin 102 in Aniline-Dimethylaniline Mixture: Dominant Role of Hydrogen Bonding"†
   Phys. Chem. Chem. Phys. **2014**, *16*, 27096-27103.

4. **Nabajeet Barman**, Kalyanasis Sahu, "Reduced Fluorescence Quenching of Coumarin 102 at Higher Phenol Mole Fractions in Cyclohexane-Phenol and Anisole-Phenol Solvent Mixtures: Role of Competitive Hydrogen Bonding"†
   RSC Adv. **2014**, *4*, 58299-58306.

5. **Nabajeet Barman**, Koushik Mondal, Kalyanasis Sahu, "Sharply Contrasting Influence of a non-interacting Co-solvent on Photoinduced Electron Transfer in Two Mixtures: New Evidence on H-Bonding on Ultrafast PET"†
   (*Communicated*).

Paper not included in this thesis:

6. Debabrata Singha, **Nabajeet Barman**, Kalyanasis Sahu, "A Facile Synthesis of High Optical Quality Silver Nanoparticles by Ascorbic Acid Reduction in Reverse Micelles at Room Temperature"†
   J. Colloid Interface Sci. **2014**, *413*, 37-42.

7. Debabrata Singha, **Nabajeet Barman**, Aparajita Phukon, Kalyanasis Sahu, "Selective Probing of Reverse Micelle Interfacial Layer Upon Silver Nanoparticle Formation Using Dynamic Stokes Shift Measurements"†
   J. Phys. Chem. C **2014**, *118*, 10366-10374.

Conference Proceedings:

1. **Nabajeet Barman**, Kalyanasis Sahu, "Excited-State Hydrogen Bond Strengthening of Coumarin102-phenol Hydrogen Bonded Complex: Facilitation of Fluorescence Quenching via Photoinduced Electron Transfer"†
   Advances in Spectroscopy and Ultrafast Dynamics (International Symposium),
   Kolkata, India, December **2014.**

2. **Nabajeet Barman**, Debabrata Singha, Kalyanasis Sahu, "Anomalous Modulation of Photoinduced Electron Transfer in Binary Mixture of Electron Donating Solvent: Effect of Hydrogen Bonding"†
   Frontiers in Chemical Sciences (National Conference)
   Guwahati, India, December **2014.**

List of Abbreviations

ADC	Analogue to digital converter
AN	Aniline
AN-*d*2	Amino Deuterated Aniline
AN-*d*7	per-Deuterated Aniline
$BP(OH)_2$	2,2-Bipyridine-3,3-diol
CT	Charge Transfer
C102	Coumarin 102
C153	Coumarin 153
C151	Coumarin 151
C337	Coumarin 337
C500	Coumarin 500
DFT	Density functional theory
DEA	Diethylamine
DMA	*N,N*-Dimethylaniline
DMA-*d*6	Deuterated *N,N*-Dimethylaniline
DMSO	Dimethylsulfoxide
DPA	*N,N*-Dipropylaniline
DAC	Donor-Acceptor Complex
DSS	Dynamic Stokes Shift
ET	Electron Transfer
ESPT	Excited State Proton Transfer
FN	Fluorenone
FTIR	Fourier Transform Infrared
HOMO	Highest Occupied Molecular Orbital
H-bonding	Hydrogen Bonding
IR	Infrared
IC	Internal Conversion
ISC	Inter System Conversion
ICT	Intramolecular Charge Transfer
LE	Locally Excited
LUMO	Lowest Unoccupied Molecular Orbital

MAN	*N*-Methylaniline
MCP	Micro-Channel Plate
MD	Molecular Dynamics
MO	Molecular Orbital
NR	Non-radiative
OX750	Oxazine 750
PET	Photoinduced Electron Transfer
PMT	Photomultiplier Tube
QY	Quantum Yield
R800	Rhodamine 800
TCE	Tetrachloroethylene
TC	Thiocoumarin
TCSPC	Time Correlated Single Photon Counting
TDDFT	Time-Dependent Density Functional Theory
TAC	Time to Amplitude Converter
TEA	Triethylamine
TICT	Twisted Intramolecular Charge Transfer

List of Tables

Table 7.2: Fluorescence decay components of coumarin 153 (C153) in the cyclohexane-AN mixture at different mole fractions of the AN, X_{AN}. Excitation wavelength was at 405 nm and decays were measured at corresponding emission maxima.

List of Schemes

Chapter 1

may suppress the effect of H-bonding of PET (gray arrow). In a liquid mixture, the non-interacting component may disrupt the donor–donor H-bond, and hence, strengthens/orients donor–acceptor H-bond for a faster PET process (black arrow).

Scheme 1.14: Anomalous variation of PET in a mixture of electron donating (also H-bond donating) and non-interacting solvents. PET rate increases with increase in the mole fraction of the donor upto a particular mole fraction and thereafter decreases with further enrichment of the donor.

Chapter 3

Scheme 3.1: Structures of C102 and different phenol derivatives of varying H-bond strength.

Chapter 4

Scheme 4.1: Photoinduced electron transfer (PET) for an excited acceptor (e.g. coumarin 102) in two different situations: in a neat solvent having simultaneous electron donating and H-bonding abilty (e.g aniline) and in a liquid mixture of the solvent containing another non-interacting component. In a neat solvent, competitive H-bonding between acceptor-donor and donor-donor H-bonds suppress the effect of H-bonding of PET (gray arrow). In a liquid mixture, the non-interacting component intervenes the donor-donor H-bond, and hence, strengthens/orients donor-acceptor H-bond for a faster PET process (black arrow).

Scheme 4.2: Relaxation scheme of the H-bonded complex – absorption and emission are indicated by upward and downward solid arrows respectively; electron transfer (ET) from the S_2 (LE) state to the S_1 (CT) state is shown by a blue curved arrow; and non-radiative (NR) transition is represented as wavy arrow.

Scheme 5.1 The different states of the acceptor C102 and their assigned PET rates.

Chapter 7

Scheme 7.1: Addition of inert co-solvent leads to different modulation of PET depending on the H-bonding ability of the donor. Gray and blue arrows indicate non-H-bonded and H-bonded PET, respectively. In the mixture, H-bonded PET dominates while non-H-bonded PET diminishes.

List of Figures

Chapter 3

Figure 7.3: The FTIR spectra of 20 mM coumarin 153 in the carbonyl stretching region in the cyclohexane-AN mixtures at different mole fractions of the electron donor (AN). Gradual disappearance of the free C=O stretching frequency (at 1748 cm^{-1}) and appearance of a new peak at 1736 may be due to H-bonding.

Chapter 1

Introduction

1.1. Photoinduced electron transfer

Photoinduced electron transfer (PET) is a process, where an electronically excited molecule (upon absorption of light), can either take up an electron from another molecule (Reductive PET) or release an electron to another molecule (Oxidative PET).[1] The notation donor and acceptor usually imply to the species which gives up or receives an electron, respectively, irrespective of its electronic state. Generally, electron accepting or donating tendency of a molecule is enhanced upon excitation to higher electronic states. Thus, electronic excitation may trigger a redox process (oxidation or reduction) between a pair of molecules which may not undergo electron transfer in the ground state.[1] Oxidative and reductive electron transfer processes between two neutral species can be expressed, respectively, in the following equations -

$$D^* + A \rightarrow D^{\cdot+} + A^{\cdot-} \qquad (1.1)$$

$$D + A^* \rightarrow D^{\cdot+} + A^{\cdot-} \qquad (1.2)$$

where, D and A represent donor and acceptor molecules, respectively, in the ground state while asterisk denotes their electronically excited states.[1] $A^{\cdot-}$ and $D^{\cdot+}$ represent radical anion and radical cation respectively, formed after the electron transfer reaction.

Note, PET reactions can also be further classified based on the interaction of the D-A pair. If the D and A molecules are covalently linked or D and A sites belong to same

molecule, PET is often referred as intramolecular (unimolecular). On the other hand, if D and A are separate molecules, PET is called intermolecular (bimolecular).[2-3] However, an intermediate situation can also arise, where D and A involve in some non-covalent interactions (e.g. Hydrogen-bonding, π-stacking) interaction. In such cases, a D-A complex may pre-exist in the ground state and is commonly referred to as a charge transfer complex (CT complex) or donor-acceptor complex (DAC).[2-3] On the other hand, if the D-A interaction is favoured in the excited state, such complex is termed as exciplex.[1-3] In general, PET requires close proximity of D and A, so that there is an overlap between their molecular orbitals. Thus any pre-existing interaction between D-A acceptor may be expected to assist PET. Through-space ET usually occurs by electron tunnelling, which decreases exponentially with distance.[2-3]

Electron transfer (ET) is undoubtedly one of the most important ubiquitous elementary processes in Chemistry and Biology.[4-7] Understanding the mechanism and control parameters of electron transfer reaction comprises one of the broadest and most ever-green research areas in Physical Chemistry.[6-21] In nature, PET plays a key role in photosynthesis and allows conversion of solar light into chemical energy. In the photosynthetic reaction centre, PET reaction creates charge imbalance across a membrane, which drives a proton pumping mechanism to produce ATP.[2-3] Many artificial photosynthesis systems have been developed which can mimic the light harvesting mechanism of green plants for utilizing solar energy. Since PET is fundamental to these systems, much effort has been made to understand the underlying principles of PET. The ultimate goal is to achieve the best possible efficiency and economy of the natural light-harvesting systems. In addition, PET is important in the design of a variety of optoelectronic devices, in photo-polymerization and in photography.[22] Organic Chemists have also paid great interest in PET as it involves in facile photochemical synthesis of many organic compounds that are often difficult to synthesize otherwise. After

being oxidized or reduced by a photosensitizer, an organic substrate can be easily transformed into a reactive intermediate allowing the progress of the reaction.[23-25] Due to its extensive importance, PET has been subject to numerous theoretical and experimental studies.[6-7, 9, 15-18, 21, 26-27]

1.2. Factors affecting photoinduced electron transfer

Several factors influence the rate of ET (or PET). These include the free energy difference between reactant and product, solvent relaxation, intra-molecular vibrations, and electronic coupling between donor and acceptor. Any factor that changes the relative energy of the reactant or product, solvation dynamics or the electronic coupling should influence the rate or efficiency of PET. The D-A distance and their relative orientation play an important role in determining the electronic coupling, which is controlled by the overlap of the electronic orbitals of D and A.[7, 28-29]

1.2.1. Free energy of photoinduced electron transfer

The thermodynamic efficiency or feasibility of photoinduced electron transfer (PET) can be determined by the free energy of reaction ΔG^0_{ET}, according to the Rehm-Weller equation-[10, 19, 30]

$$\Delta G^0_{\mathrm{ET}} = E(D/D^+) - E(A/A^-) - E_{00} - E_{\mathrm{IPS}} + \Delta E_{\mathrm{sol}} \qquad (1.3)$$

where, E_{00} represents the effective excitation energy i.e. the difference in energy between the lowest vibrational level of ground electronic state and the lowest vibrational level of first electronic excited state of the photoexcited species. $E(D/D^+)$ and $E(A/A^-)$, respectively, denote the oxidation and reduction potentials of the electron donor (D) and electron acceptor

(A) in the medium. E_{IPS} is the ion-pair stabilization energy in the medium and can be expressed by the following equation-

$$E_{IPS} = \frac{e^2}{\varepsilon_s r_0} \qquad (1.4)$$

where ε_s is the static dielectric constant for the solvent, e is the electronic charge and r_0 is the centre to centre distance between the D^+ and A^-. This accounts for the electrostatic interaction between the ions. It is important to note that the ions are formed at close distance (not at infinite seperation). This electrostatic interaction is generally weak in polar solvents but becomes significant in a non-polar medium. ΔE_{sol} is the correction term for the solvation energy of the D^+ and A^- ions in solvents of different dielectric constant ε_s. This term is useful when electrochemical measurements and PET measurements are carried out in two different media. ΔE_{sol} is usually calculated by using the empirical solvent parameters E_T (30) and donor number (D_N) of the solvents with the help of following equations[19]-

$$\Delta E_{sol} = \Delta G_s^0(-) + \Delta G_s^0(+) \qquad (1.5)$$

where $\Delta G_s^0(\pm)$ represents difference of the solvation energy of the anion (or cation) between two media (e.g. in acetonitrile and aniline). Their values can be estimated from the following equations[19]-

$$G_s^0(-) = -\left(\frac{N_0 z_i^2 e^2}{8\pi\epsilon_0}\right)\left(1 - \frac{1}{\epsilon_s}\right)\left(\frac{1}{\frac{1}{Ap} + r_i}\right) \qquad (1.6)$$

$$G_s^0(+) = -\left(\frac{N_0 z_i^2 e^2}{8\pi\epsilon_0}\right)\left(1 - \frac{1}{\epsilon_s}\right)\left(\frac{1}{\frac{1}{Bp} + r_i}\right) \qquad (1.7)$$

The value of Ap and Bp can be calculated by using the following two equations-

$$Ap = 1.29E_T(30) - 33.3 \qquad (1.8)$$

$$Bp = 10.14 + 0.108D_N \qquad (1.9)$$

where $E_T(30)$ is the polarity scale which is defined by Dimroth et al.[31] and donor number (D_N) is defined by Gutman.[32]

1.2.2. Substituent effect on photoinduced electron transfer

Chemical substitution of either donor or acceptor often leads to a strong impact on the rate of PET.[16, 18-20] Mainly, substitution has a profound effect on the reduction potential (or oxidation potential) of the acceptor (or the donor) and hence, on the overall free energy of PET.[16, 18-19] Yoshihara and co-workers have studied PET dynamics of a series of 7-amino coumarin dyes as photoexcited acceptor (**Scheme 1.1**) in neat aromatic amines (**Scheme 1.2**) as electron donor solvents using femtosecond up-conversion technique.[16, 18-21] A large variation of PET rate occurs ranging from a few nanoseconds to a couple of hundred femtoseconds depending on the structure of the acceptors as well as donors. As the length of the alkyl chain on the 7-NH_2 group becomes longer, PET becomes slower and becomes slowest when the amino group was fixed by a double-hexagonal ring.[16, 18-19] It was evident from the fluorescence lifetimes of the coumarins. For coumarin 151 (C151), the average fluorescence lifetime in *N,N*-dimethylaniline (DMA) was reported to be 210 fs whereas for coumarin 153 (C153) it was 8.5 ps. Likewise, the substituent in the 4-position also modifies the electron-accepting ability of the coumarins. In comparison to C153 which shows ultrafast PET, coumarin 102 (C102) does not show any PET in neat DMA.[18]

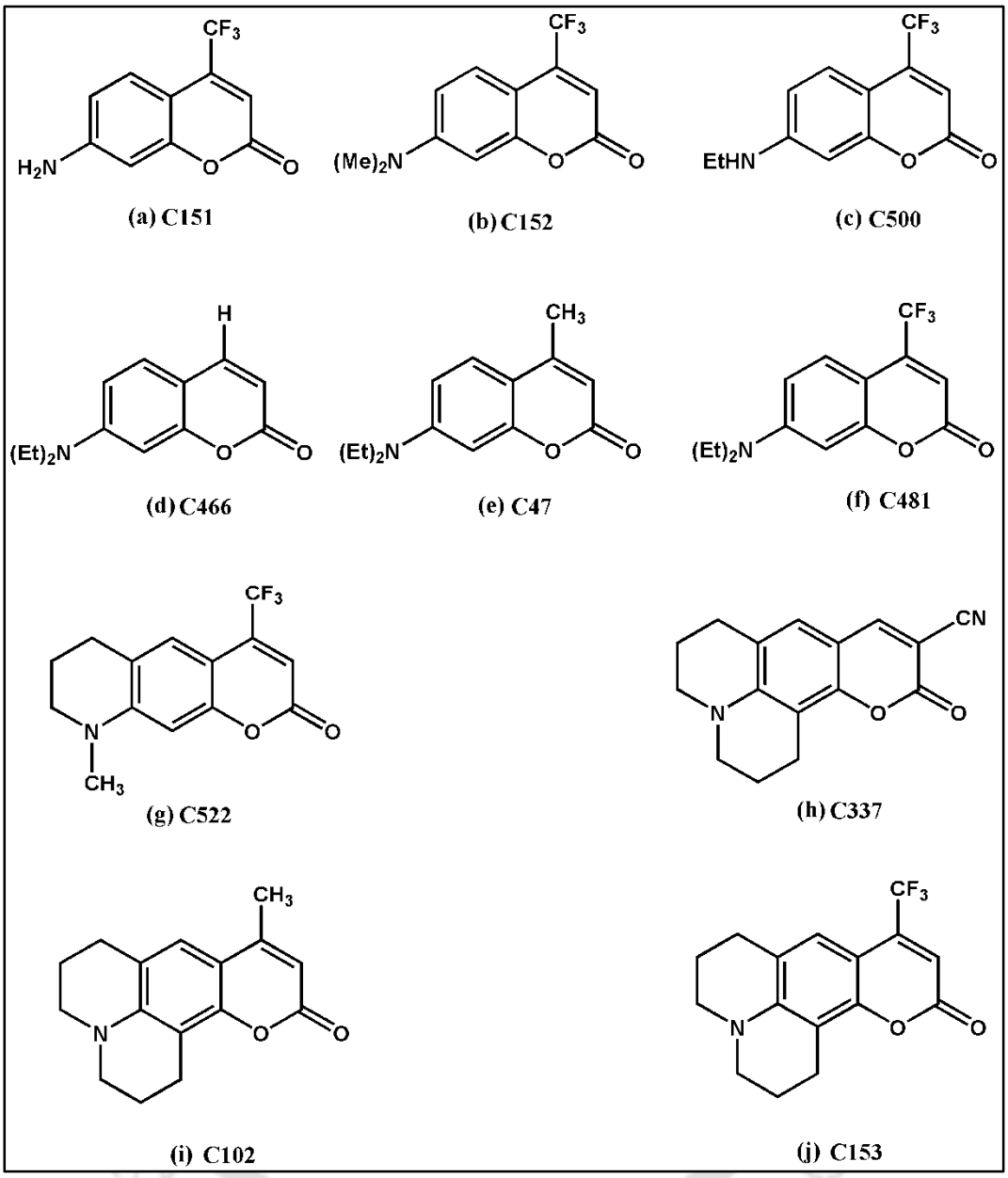

Scheme 1.1: Structures of some coumarin fluorophores that often used as electron acceptors.

Substituent effects on the PET dynamics were discussed from a number of considerations, such as free energy change (ΔG^0), frequencies of the vibrational modes involved in the ET process, flexibility of functional groups of the donor and the acceptor, and so on. The absorption and emission peak positions (and hence E_{00}) and the reduction potentials of the differently substituted acceptors (coumarin dyes) are substantially different.

For example, C151 has a NH_2 group at 7-position and its reduction potential is -0.21 V (in DMA).[18] However, For C153 where the 7-amino group is fixed with a double hexagonal alkyl ring, the reduction potential changes to -0.24 V.[18] Since alkyl group is an electron donating substituent, extending the alkyl chain on the amine group decreases electron-accepting ability in the excited state. For example, the standard free energy of PET from DMA to C151 is -0.67 eV, whereas, the free energy for C153 is only 0.0 eV.[18]

Similarly, substituent on donor also has a large effect. PET from aniline donors having alkyl substitution on either the $–NH_2$ group or in the aromatic ring (**Scheme 1.2**) to a series of coumarins was studied.[19] The free energy of PET (ΔG^0) for all the acceptors was significantly different in aniline (AN), *N*-methylaniline (MAN) and DMA.

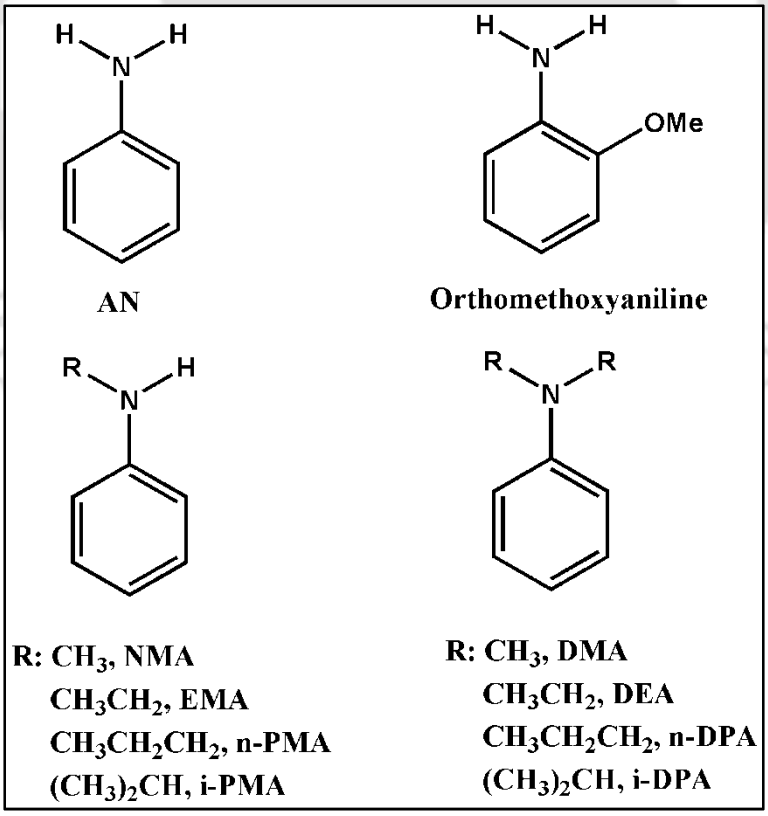

Scheme 1.2: Structures of aromatic amines (electron donors).

A variation in PET rate with the alkyl chain length was observed for *N,N*-dialkylanilines. In *N,N*-dialkylanilines, the PET rate becomes markedly slower with increase in the size of the alkyl substituent. For example, the average fluorescence lifetime of C151 increases from 220 fs in DMA to 610 fs in *N,N*-dipropylaniline (DPA).[19] This less efficient PET mainly arises from the increased distance of the donor-acceptor separation due to the bulkier alkyl groups. Interestingly, the ET dynamics for *N*-monoalkylanilines was quite insensitive on the alkyl group variation. Probably, the un-substituted N-H hydrogen of the amino group keeps enough space on the amino nitrogen for favourable approach of an acceptor. Alternatively, it may be possible that the N-H may involve in H-bond formation with the C=O group of the coumarins. We will discuss later that H-bonding have a crucial effect in inducing PET. Alkyl substitution in the aromatic ring also has a profound effect on PET. PET rate for coumarins were found faster in orthomethoxyaniline (also called orthoanisidine) compared to the rate in AN.[20]

1.2.3. Solvation dynamics

Solvation dynamics process is defined as the relaxation of solvent dipoles about a instantaneously created solute dipole. To study salvation dynamics time-resolved fluorescence spectroscopy is a useful technique. The fluorescence probe (solvation probe) used in the study of solvation dynamics usually has small dipole moment in the ground state but very large dipole moment in the excited state. As a result of the electronic excitation by an ultra short pulse creates an instantaneous large dipole change in the fluorophore.[33-41] Hence, there is an abrupt change in interaction of the excited probe with the neighbouring solvent molecules. Subsequently, to establish a new equilibrium, the solvent molecules around the probe rearrange themselves i.e. the excited solute dipole gets stabilized with time

due to salvation. Thus, emission maximum of the solute exhibits a gradual red shift with increase in time which is known as dynamic Stokes shift (DSS). The direct consequence of this is a marked wavelength dependence of the fluorescence decays (decay at the blue end and rise at the red end). Solvation dynamics is monitored by the decay of the solvent response function, C(t) which is defined as[42-47]-

$$C(t) = \frac{\nu(t) - \nu(\alpha)}{\nu(0) - \nu(\alpha)} \qquad (1.10)$$

where, ν(0), ν(t) and ν(α) denote the emission maxima (in cm^{-1}) of the fluorophore at time zero, t and infinity, respectively.

Solvation dynamics is very important for detailed understanding of the ET dynamics. In the theory of electron transfer, it is often considered that solvent polarization has a dominant role on ET.[48-53] The energy of relaxation due to solvent orientational polarization is considered as the driving force for ET reaction. A solvent coordinate describing the solvent polarization, expresses the free energy surface for ET. To minimize the free energy of the system polar solvent molecules rearrange them around the solute molecule. Therefore, ET is considered as a process for the reactant to cross the transition state to the product by fluctuation of surrounding solvent molecules.[54-56]

1.3. Hydrogen bonding: Ground state vs excited state

Hydrogen bonding (H-bonding) is a well-known attractive interaction of the type –X-H···Y-, where X and Y (usually N, O and F) are more electronegative than H. The X-H and Y are respectively, called H-bonding donating and accepting sites. The two sites may belong to same molecule (intramolecular H-bonding) or different molecules (intermolecular H-bonding). H-bonding has dominant consequence in controlling physical states (solid, liquid,

gas) of substances, self assembly, 3D structures of biological macromolecules (protein secondary and tertiary structures, H-bonding within DNA and RNA bases etc), enzyme-substrate binding etc.[28, 57-64]

The intermolecular hydrogen bond (H-bond) of a photo-excited complex may have a key role in tuning the photochemistry and dynamics.[65-68] The statics and dynamics of H-bonding have been extensively studied both experimentally and theoretically in the ground state.[69-74] However, H-bonding in the higher electronic excited states is relatively less explored. Photo-excitation of a H-bonded complex leads to charge redistribution, consequently, the H-bonding parameters such as distance, energy, relative orientation of the complex also changes. The dynamics of this reorganization of H-bonding after instantaneous excitation is known as hydrogen bonding dynamics (or excited-state hydrogen bonding dynamics).[68, 75-79]

Recent advancement in ultrafast laser spectroscopy and calculation methods revealed many new information about the excited-state H-bonding. The excited-state H-bonding dynamics usually occurs on hundreds of femtoseconds.[75, 80-82] To monitor the ultrafast dynamical behaviour of H-bonding in the excited states, various ultrafast spectroscopic techniques such as femtosecond vibrational spectroscopy, femtosecond absorption and fluorescence spectroscopy have been applied. High level quantum computations have also been performed to elucidate the nature of H-bonding in the electronic excited-states.[75, 83]

Using ultrafast IR spectroscopy, Nibbering and co-workers studied H-bonding dynamics on a model acceptor molecule coumarin 102 (C102) in the presence of several H-bond donating molecules such as phenol, methanol, chloroform etc. (**Scheme 1.3a-c**).[65, 77] The choice of C102 as a probe for H-bonding dynamics lies to the following facts. In C102, C=O is the only H-bond accepting site which can form H-bond with potential H-bond donors like phenol, methanol, chloroform etc.[79, 84] The C=O group, due to its polarized nature, shows

a strong stretching band in Fourier transform infrared (FTIR) spectra and its position is very sensitive towards H-bonding environment. Thus, H-bonding dynamics can be studied very effectively by probing the C=O stretching vibration of C102. Furthermore, it has very high molar extinction coefficient and can also be excited by the visible laser pulse (400 nm).

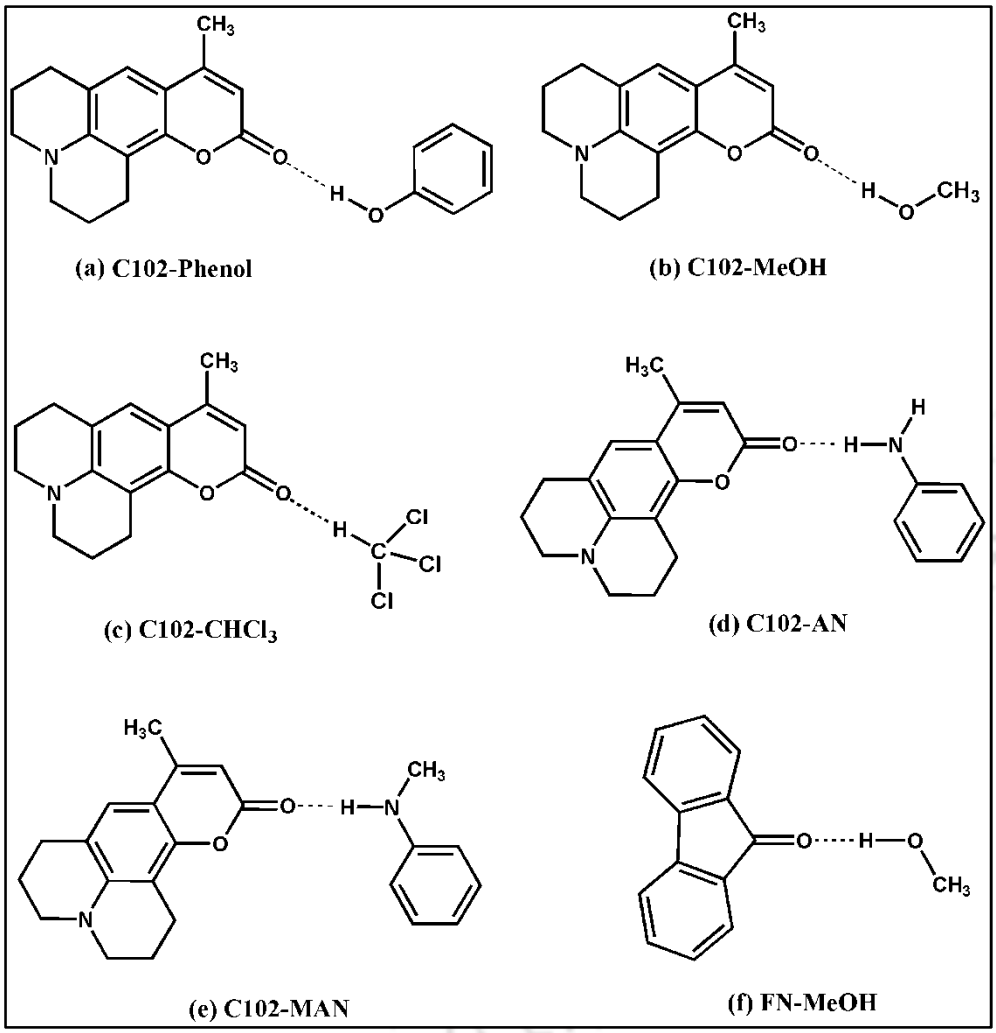

Scheme 1.3: Hydrogen bonded complex of some donor-acceptor pairs. Donors and acceptors are held by a single hydrogen bond.

Hence, in the ground state, the site-specific H-bonding of C102 with the H-bond donating group of the donors (e.g., –OH groups of phenol, methanol and –CH group of

$CHCl_3$) can be effectively probed by FTIR spectroscopy. Formation of the C=O···H-O H-bond significantly lowers (downshift) the C=O stretching vibrational frequency in the H-bonded complex compared to the C=O stretching frequency of free C102. In a non-interacting (i.e. non-H-bonding) solvent tetrachloroethylene (TCE) the C=O stretching band was observed at 1735 cm^{-1} (**Figure 1.1**). The C=O stretching band of C102 exhibited significant downshift to 1695 cm^{-1} in the presence of phenol. This marked red-shift by ~40 cm^{-1} indicates the formation of strong H-bond between the C=O group of C102 and –O-H group of phenol in TCE. However, upon photoexcitation, the C=O stretching frequency of H-bonded complex shifted back to 1740 cm^{-1} in the excited state within ~200 fs. The C=O stretching frequency of the H-bonded complex in the excited state (1740 cm^{-1}) resembles to the C=O stretching frequency of un-complexed C102. Thus, they concluded that the H-bond between C102 and phenol cleaved in the excited state just after excitation.[65] The fate of the C=O···H-O H-bond was also simultaneously probed by the O-H stretching vibrational frequency. C102-phenol H-bond strongly affects the O-H stretching vibrational frequency of phenol. In neat TCE, phenol shows a stretching band at 3610 cm^{-1} due to free –O-H group and a broader band between 3450 cm^{-1} and 3550 cm^{-1} which may be due to 1:1 phenol-phenol complex formation. The O-H stretching frequency of phenol is strongly red-shifted to 3380 cm^{-1} indicating the formation of C102-phenol H-bond. Upon photoexcitation, the excited complex exhibited a stretching band of free phenol O-H groups at 3610 cm^{-1} indicating the cleavage of C=O···H-O H-bond for both C102-phenol and C102-$(phenol)_2$ complexes.[65]

On the contrary, time-dependent density functional theory (TDDFT) calculations of Zhao and Han showed for the first time that the intermolecular H-bond between C102 and phenol becomes remarkably stronger and shorter in the electronic excited state of the H-bonded C102-phenol complex rather than being cleaved (**Figure 1.2**).[75]

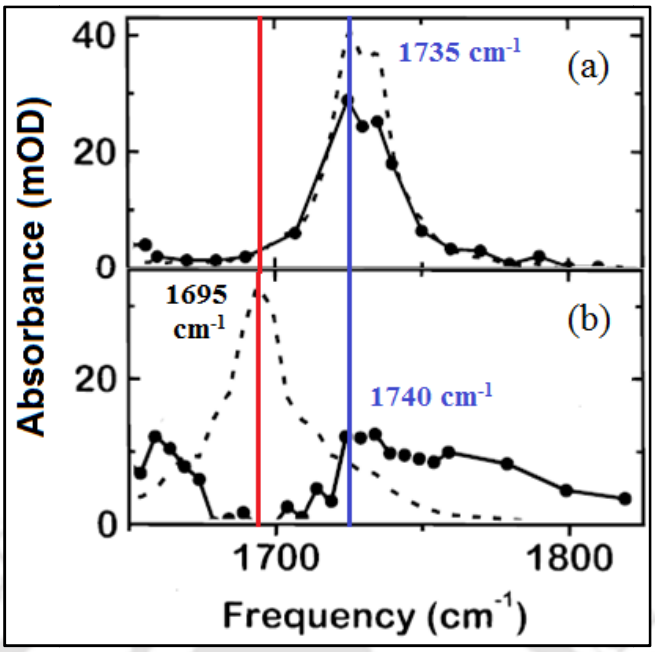

Figure 1.1: Ground state (dashed lines) and excited state (dotted lines) C=O stretching bands of (a) C102 and (b) C102-phenol complex in TCE. Reprinted with permission from ref 77. Copyright © 2000, American Chemical Society.

Isolated C102 as well as H-bonded 1:1 C102-phenol complex were optimized using both (B-P86 functional and TZVP basis set) calculations. They computed the potential energy curves along the H-bonding coordinate in the different electronic states. The minimum of the potential energy curve in the excited state was found at 1.691 Å which is considerably shorter than the minimum (at 1.785 Å) in the ground state (**Figure 1.3**). Thus, they concluded that the H-bond in the excited state becomes shorter rather than being cleaved.

Strengthening of the H-bond in the excited state was evident from the calculated H-bond energy of C102-phenol H-bonded complex. The H-bond energy increases from 36.8 kJ mol^{-1} in the ground state (S_0) to 51.5 kJ mol^{-1} in the excited state (S_2). H-bond energy in the ground state was computed by subtracting the individual energies of C102 and phenol in the ground state from the energy of C102-phenol complex in the ground state. For the excited state H-bonding energy the S_2 excited state was considered due to its locally excited (LE)

nature. The H-bonding energy was estimated by subtracting the energy of C102 in the S_1 state and the energy of phenol in the ground state from this energy. Strengthening of H-bond in the excited state has been further demonstrated by computing the infrared (IR) spectra of H-bonded and isolated C102. In the ground state isolated C102 shows a C=O stretching frequency 1741 cm^{-1}. However, in the excited state C=O stretching frequency exhibited blue shift to 1761 cm^{-1}. In the ground state, C=O stretching frequency exhibited a strong red-shift by 55 cm^{-1} from 1741 cm^{-1} (isolated C102) to 1686 cm^{-1} (C102-phenol) due to the formation of H-bond in accordance with the experimental result.[65, 77] However, the C=O stretching frequency of H-bonded C102-phenol complex in the excited state rather downshifted in comparison to the stretching frequency of isolated C102. The C=O stretching frequencies of isolated C102 and C102-phenol complex in the excited state were reported to be 1761 cm^{-1} and 1686 cm^{-1}, respectively. The larger red-shift of the C=O stretching frequency in the excited state (75 cm^{-1}) compared to the ground state (55 cm^{-1}) suggested that H-bond between C102 and phenol strengthened in the excited state.[75]

The TDDFT method has been proved to be successful tool to probe H-bonding dynamics[75] as well as to calculate the infrared spectra in the electronic excited state to many other H-bonded complexes.[63, 85-89] In addition to the strengthening of the H-bond in the excited state, significant weakening of the H-bond also observed.[66] Using TDDFT calculation Han and co-workers demonstrated that C=S···H-O H-bond between thiocoumarin (TC) and methanol significantly weakened in the excited state.[66]

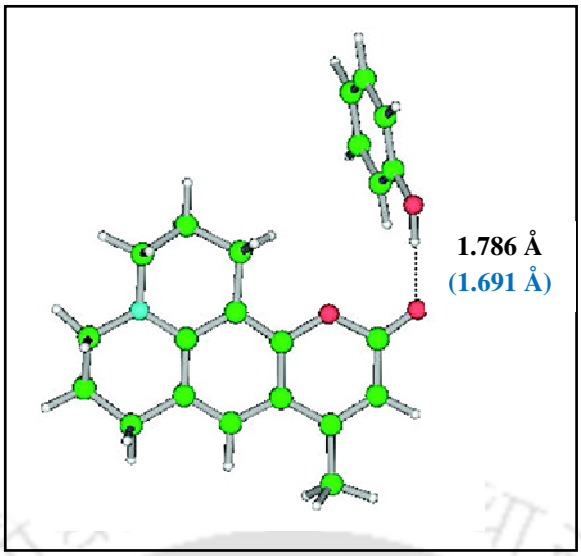

Figure 1.2: Optimized structure of 1:1 hydrogen bonded complex of C102 and phenol in the ground state. The calculated H-bond lengths are displayed and the excited state H-bond length is given in the bracket. Reprinted with permission from ref 75. Copyright © 2007, American Chemical Society.

It is very important to understand how the ultrafast H-bonding dynamics could influence the photophysics or electronic relaxation of a H-bonded complex. Han and co-workers have demonstrated that excited-state H-bond strengthening have a stronger influence on controlling the emission characteristics of the H-bonded complex and subsequently applied the excited-state H-bond strengthening and weakening concept on many ultrafast nonadiabatic dynamic processes, such as internal conversion (IC),[80, 90] intersystem crossing (ISC),[90] photoinduced electron transfer (PET),[82, 91-92] intramolecular charge transfer (ICT), and site-specific solvation,[93] excited-state proton transfer (ESPT),[94-96] twisted intramolecular charge transfer (TICT)[96] and metal-ligand charge transfer.[97-98]

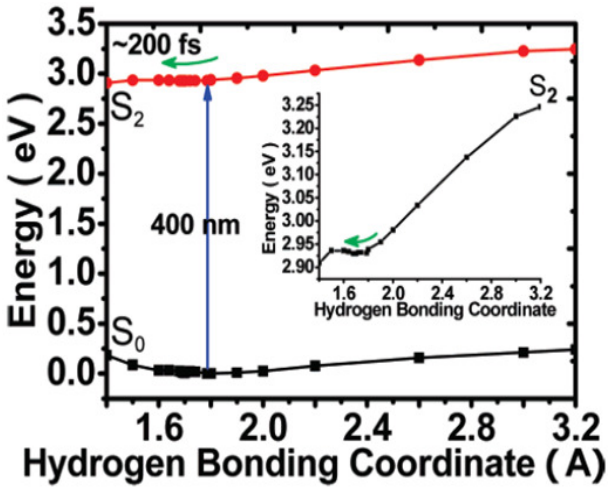

Figure 1.3: Potential energy curves along H-bond co-ordinates for ground state (S_0) and the excited state (S_2, inset) of the H-bonded C102-phenol complex. The minimum of the curve in S_2 state shifted towards shorter distance compared to S_0 state indicating strengthening of the H-bond in the excited state. Reprinted with permission from ref 75. Copyright © 2007, American Chemical Society.

Fluorenone (FN) is another interesting model fluorophore which have a single C=O site for H-bond acceptance. It has been anticipated that intermolecular H-bonding has a dominant role in the fluorescence quenching of fluorenone in protic solvents. Zhao and co-workers studied the H-bonding dynamics of FN in methanol (**Scheme 1.3f**).[99] TDDFT calculations showed that the ground state H-bonding between FN and methanol further strengthened in the electronic excited state. The H-bond distance of FN-MeOH complex in the ground state (S_0) and in the excited state (S_1) was calculated to be 1.906 Å and 1.802 Å respectively, while the corresponding H-bond energies were 27.85 $kJmol^{-1}$ and 42.62 $kJmol^{-1}$, respectively. They also checked the influence of electronic excitation and H-bonding on the IR spectra. The C=O stretching frequency of isolated FN was at 1780 cm^{-1} and 1592 cm^{-1}, respectively in the ground and in the excited state. For the FN-MeOH complex, the C=O stretching frequencies were at 1756 cm^{-1} and 1595 cm^{-1} in the ground and in the excited state, respectively.

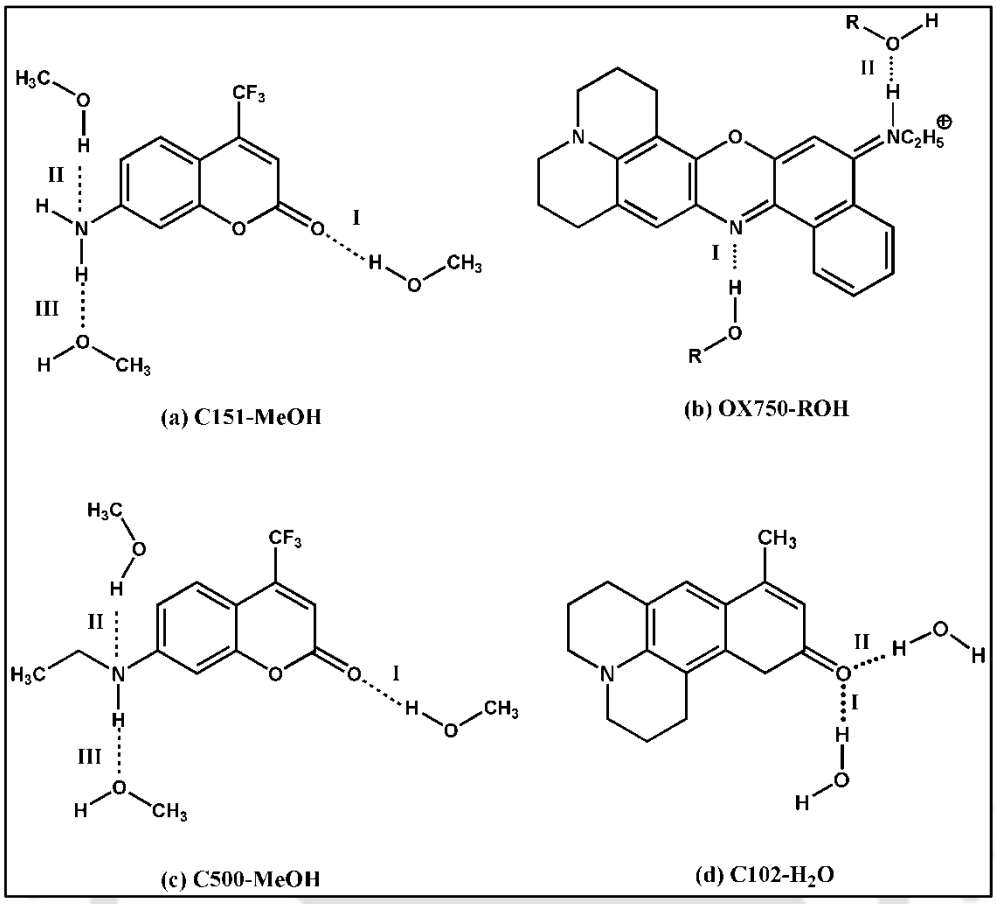

Scheme 1.4: Hydrogen bonded complexes of some fluorphores with solvents where there is possibility of multiple hydrogen bond formation.

Interestingly, a dramatic red shift of 188 cm^{-1} was noted just for electronic excitation of the free FN while a very small shift of 24 cm^{-1} was due to H-bonding in the ground state. Hence they concluded that the C=O frequency may not be a good indicator of H-bond dynamics in FN. However, they found that –OH frequency of methanol served a much better indicator of the H-bonding. They found an addition red shift of 159 cm^{-1} due to H-bond strengthening in the excited state. The strengthening of the H-bond in the excited state, shifts the equilibrium towards the H-bonded complex where radiationless deactivation through internal conversion (IC) leads to quenching of fluorescence of FN in polar protic solvent.[80]

Another chromophore oxazine750 (OX750) shows quite different fluorescence behaviour in protic and aprotic solvents.[29] The fluorophore shows intense emission in acetone (aprotic solvent) but very weak emission in protic alcoholic solvent. Han and co-workers systematically investigated the relaxation time scale and pathways of the chromophore in alcohols using combination of TDDFT and femtosecond time-resolved stimulated emission pumping fluorescence depletion spectroscopy.[29] They detected a very fast PET of ~200 fs from the alcoholic solvent to the excited chromophore. OX750 has two H-bonding sites - one H-bond accepting (aromatic N) and other one is H-bond donating (–NH) and hence, forms two intermolecular H-bonds (O-H···N(I) and N-H···O (II)) in alcohol (**Scheme 1.4b**). TDDFT calculations showed that H-bond I (O-H···N) becomes significantly strengthened while the H-bond II (N-H···O) remains nearly unchanged in the electronically excited state.[29] The strengthening of the H-bond in the excited state enhances the electronic coupling between the solute and solvent and hence, strongly facilitates PET through this site but not through the other site. Hence, the PET showed an explicitly site selectivity for the intermolecular hydrogen bond.[29]

The excited-state H-bonding dynamics have also been investigated by many other groups, and intermediate situations rather than these two extremes (H-bond breaking or strengthening) were also prescribed. Using sub-picosecond time-resolved infrared absorption spectroscopy, Palit et al. studied H-bonding dynamics of C102-AN complex in non-interacting solvent TCE. Their absorption transient monitored at 1736 cm^{-1} (characteristic stretching frequency of free carbonyl) for C102-AN complex dissolved in TCE arises immediately (<250 fs) following the electronic excitation suggesting release of free or unbound C102. However, the transient signal decays within a few tens of picosecond.

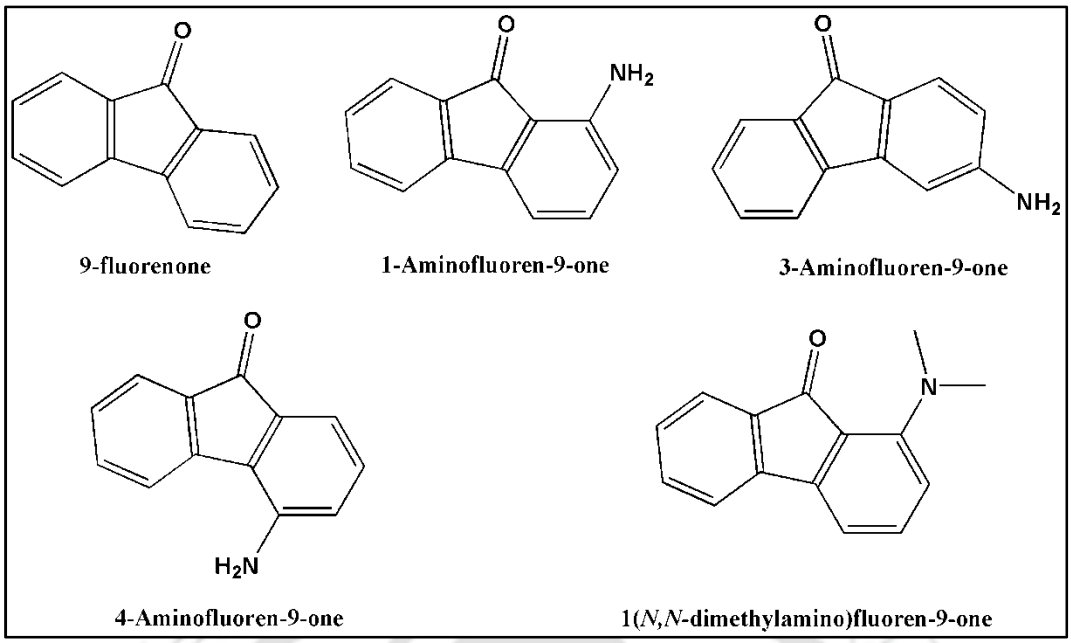

Scheme 1.5: Structures of some fluorenone derivatives.

As the lifetime of C102 in aniline is quite long (1.4 ns), the decay was attributed to the reformation of hydrogen-bond. Thus, they concluded that the H-bond in the excited state, the H-bond between C102 and AN first breaks within ~250 fs of photoexcitation, then, part of the free C102 reforms H-bond with aniline within ~30 ps.[84] Palit and co-workers also reported similar dynamic equilibrium between H-bond breaking and reformation in the excited state of fluorenone and amino-fluorenone in H-bond donating solvents (**Scheme 1.5**).[100-102] Blank and co-workers studied the H-bond dynamics of C102 in acetonitrile-water binary mixtures by using femtosecond time resolution with a technique that employs resonant optical excitation of chromophore followed by probing a non-resonant third-order Raman signal of the solvent (**Scheme1.4d**).[103-105] To visualize the local composition around C102, Monte Carlo simulations were also performed. Simulation studies revealed that the C=O group of C102 forms a bifurcated H-bond with two water molecules in the ground state, out of which one H-bond weakens while the other one strengthens upon electronic excitation.[106]

Recently, Ding and co-workers studied the hydrogen bonding dynamics of coumarin 500 (C500) (**Scheme 1.1c**) in 1,4-dioxane and methanol solvents using both femtosecond transient absorption measurements and TDDFT calculations.[107] They observed very fast intramolecular charge transfer (ICT) component of 500 fs in methanol which was absent in aprotic solvent 1,4-dioxane. TDDFT calculations revealed simultaneous strengthening of C=O···H-O (I) and N-H···O-H (III) hydrogen bonds as well as weakening of N···H-O H–bond (II) in the electronic excited state of the C500-$(MeOH)_3$ H-bonded complex (**Scheme 1.4c**). They concluded that this simultaneous strengthening and weakening of the H-bond in the excited state facilitated the ICT from the 7-NHEt group to the CF_3 group and also induced the formation of TICT state in the H-bonding with MeOH.

1.4. Effect of H-bonding on photoinduced electron transfer in neat electron donating solvent

Photoinduced electron transfer (PET) reactions in H-bonded D-A complexes, in which the donor and acceptor are linked to each other by a hydrogen bond, represents a new and unique area of research.[108] Electron transfer (ET) within a H-bonded complex is of fundamental importance as the H-bond linking the electron donating and accepting sites is ubiquitous in biological systems (e.g. proteins and DNA).[4, 108-113] H-bonding may tune ET by controlling the donor-acceptor distance and relative orientations.[28-29] Electronic coupling is thus strongly affected by the H-bonding networks making up the three-dimensional structure of those biological systems.[114-115] Moreover, several studies have demonstrated that H-bond can mediate electron transfer efficiently.[108, 113, 116] As the timescale and efficiency of ET depends on the electronic coupling between a donor and acceptor,[6-7, 117] Several studies have

attempted to interpret the role of H-bonding on photoinduced electron transfer (PET) process.[19, 118-119]

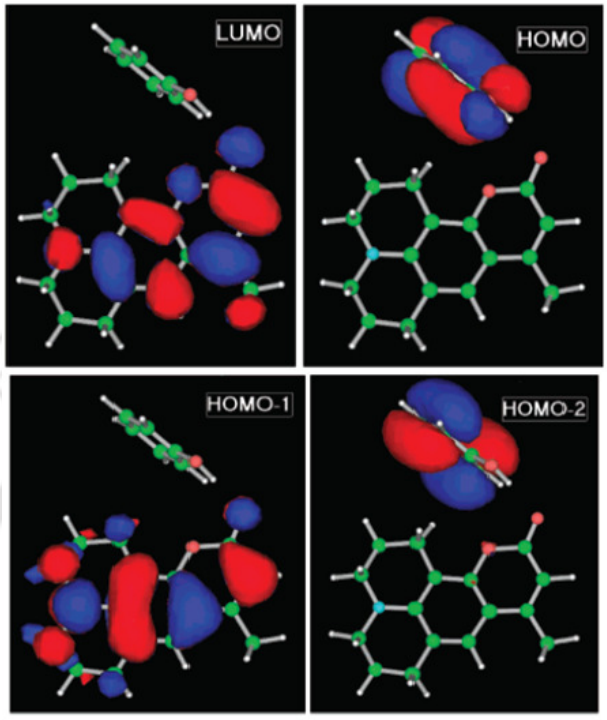

Figure 1.4: Frontier molecular orbitals (MOs) of hydrogen bonded C102-phenol complex. Reprinted with permission from ref 75. Copyright © 2007, American Chemical Society.

Recent TDDFT calculations revealed a new mechanism of PET within H-bonded complex. For the C102-phenol complex (**Figure 1.2**), Zhao and Han proposed that the H-bonding in the excited-state may facilitate PET within the H-bonded complex.[74] The facilitation can be well understood from the nature of electronic distribution in the electronic states. In the absence of H-bonding, the S_1 state of isolated C102 is locally excited (LE) in character. However, H-bonding lowers the energy of the LE state of the H-bonded complex and also create a new charge transfer (CT) state which was absent in isolated C102. Molecular orbital (MO) analysis provides insight into the nature of the excited states (**Figure 1.4**).[120] The electron density of lowest unoccupied molecular orbital (LUMO) and HOMO-1 orbital are entirely localized over the C102 fragment of the H-bonded complex. In contrast,

electron densities of highest occupied molecular orbital (HOMO) and HOMO-2 orbital are completely localized in phenol moiety. TDDFT calculation revealed that S_2 state of the H-bonded complex have the largest oscillator strength and generated from the orbital transition HOMO-1 → LUMO. Thus, the S_2 state of the C102-phenol complex is LE in nature.[120] However, the S_1 state of the C102-phenol complex is a CT state which corresponds to the orbital transition HOMO → LUMO. Hence, charge transfer between C102 and phenol may take place in this state.

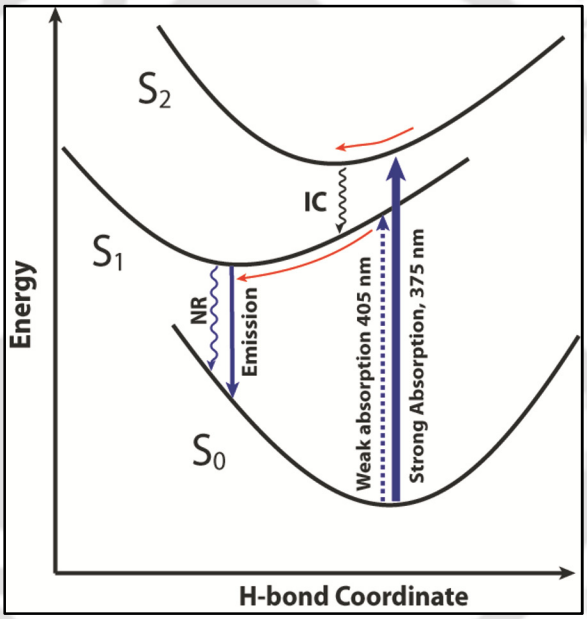

Scheme 1.6: Relaxation of the H-bonded complex. Absorption and emission are indicated by upward and downward arrows, respectively; whereas internal conversion (IC) and nonradiative transitions are represented as wavy arrows; red curved arrows show the excited-state hydrogen-bonding dynamics.

Hence, the PET event that take place in the C102-phenol H-bonded complex may be represented in the following way (**Scheme 1.6**). Photoexcitation initially prepares the complex in the S_2 (LE) state. The excited H-bonded complex may relax through radiative

pathway to the ground state (S_0) or undergo internal conversion (IC) to the low lying CT state depending upon the energy gap between the S_1 (CT) and S_2 (LE) states. If energy gap between the two states is very low, internal conversion (IC) from LE to CT is favoured. H-bond strengthening in the excited decreases this energy gap and hence, facilitates the IC (or PET) from a LE state to a CT state within the H-bonded complex.

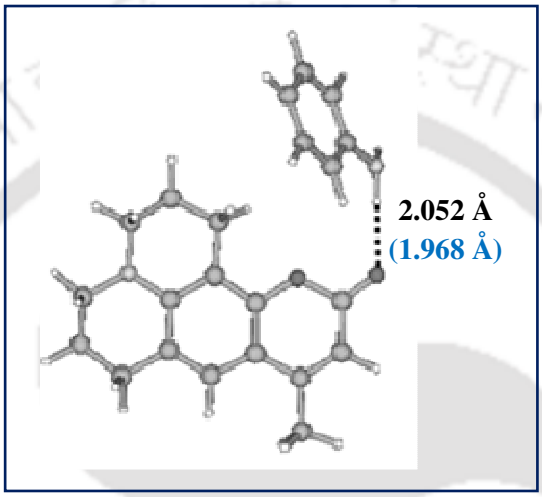

Figure 1.5: Optimized structure of 1:1 complex of C102 and aniline in the ground state showing the hydrogen bond distance in angstrom. Hydrogen bond distance in the excited state (in the bracket) becomes shorter. Reprinted with permission from ref 83. Copyright © 2008, American Chemical Society.

Similar mechanism of PET within H-bonded system was also proposed by Lui et al. for C102 and aniline.[82] Using TDDFT calculation for the 1:1 complex of C102 and aniline (**Figure 1.5**), they predicted that C=O···H-N H-bond of C102-AN complex become strengthened in the electronically excited state.[82] They demonstrated that the strengthening of the H-bond in the excited state (LE) enhances the electronic coupling between the C102 and AN and hence, electron transfer from the LE to CT state is facilitated by this strengthening.[82] Yang et al. also observed similar strengthening of H-bonding between coumarin 337 (C337)

and AN (or MAN) in the excited state (**Figure 1.6**). It was proposed that the strengthening of the H-bonding in the electronic excited state should significantly assist PET within the H-bonded complex.[118]

In summary, a series of theoretical studies emphasized that H-bond strengthening should assist PET within the H-bond complex.[75, 83, 118] However, experimental observations hardly support this proposal. Photoinduced electron transfer (PET), where either of the donor or the acceptor is fluorescence active, a convenient way to monitor the dynamics of electron transfer process is just to probe the fluorescence lifetime.

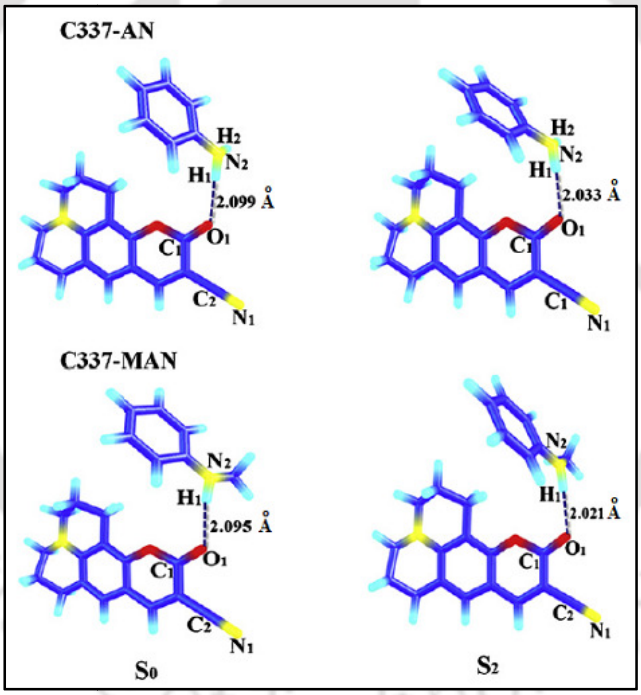

Figure 1.6: Optimized structures of 1:1 complex of C337-AN (top) and C337-MAN (bottom) in the ground (S_0) and excited state (S_2). The dashed lines represent the intermolecular hydrogen bonds between C337 and AN (or MAN). Corresponding H-bond distances in angstrom are also shown. Reprinted with permission from ref 119. Copyright © 2012 Elsevier B.V. All rights reserved.

Using fluorescence up-conversion measurements, Yoshihara and co-workers have extensively investigated PET for many fluorophores (Coumarins, Oxazines, Nile Blue etc.) in neat electron donating solvents such as DMA and AN.[16, 18-19, 21] The excited fluorophore serves as an acceptor and can receive a electron from the donor solvent. When the solvent acts as electron donor, naturally every acceptor is surrounded by many donors and hence, donor-acceptor interaction is not limited by diffusion.[121] Many coumarins show energetically favourable PET in their excited state with the AN/DMA donor and undergo PET even at a faster timescale than salvation dynamics.[19, 21] Thus in neat electron donating solvent, PET is usually very fast and fluorescence becomes severely quenched.[16, 18-19, 21] It was evident from the average fluorescence lifetime of the acceptors in different electron donating solvent. For example, C151 shows very fast PET in electron donating solvent such as AN or DMA. The average fluorescence lifetime of C151 in AN is 1.58 ps.[18-19] An important question is that is there any change in the PET rate, when the electron donating solvent also simultaneously can form a H-bond with the acceptor?

Since H-bond dynamics occurs in sub-picosecond time scales,[65, 68, 77, 79, 84, 122-124] its effect would likely to be dominant in ultrafast electron transfer. Several studies have attempted to understand the role of H-bonding in the PET process using series of coumarins as acceptor and aromatic as well as aliphatic amine as donor solvent.[19, 84, 118] A coumarin is an ideal system to study the effect of H-bonding on PET since the photoexcited coumarin serves simultaneously as an electron acceptor and also a H-bond donor through its C=O site. For example, C102 forms H-bond with electron donating solvent such as AN which can also acts as H-bond donor through its NH_2 group. H-bonding between C102 and AN in the ground state has been confirmed by the red-shift of the C=O stretching frequency of C102 in neat AN compared to the stretching frequency in a non-interacting solvent TCE.[84] C=O stretching

frequency of C102 in TCE appears at 1730 cm^{-1}, whereas in neat AN it is red shifted to 1703 cm^{-1}.[84]

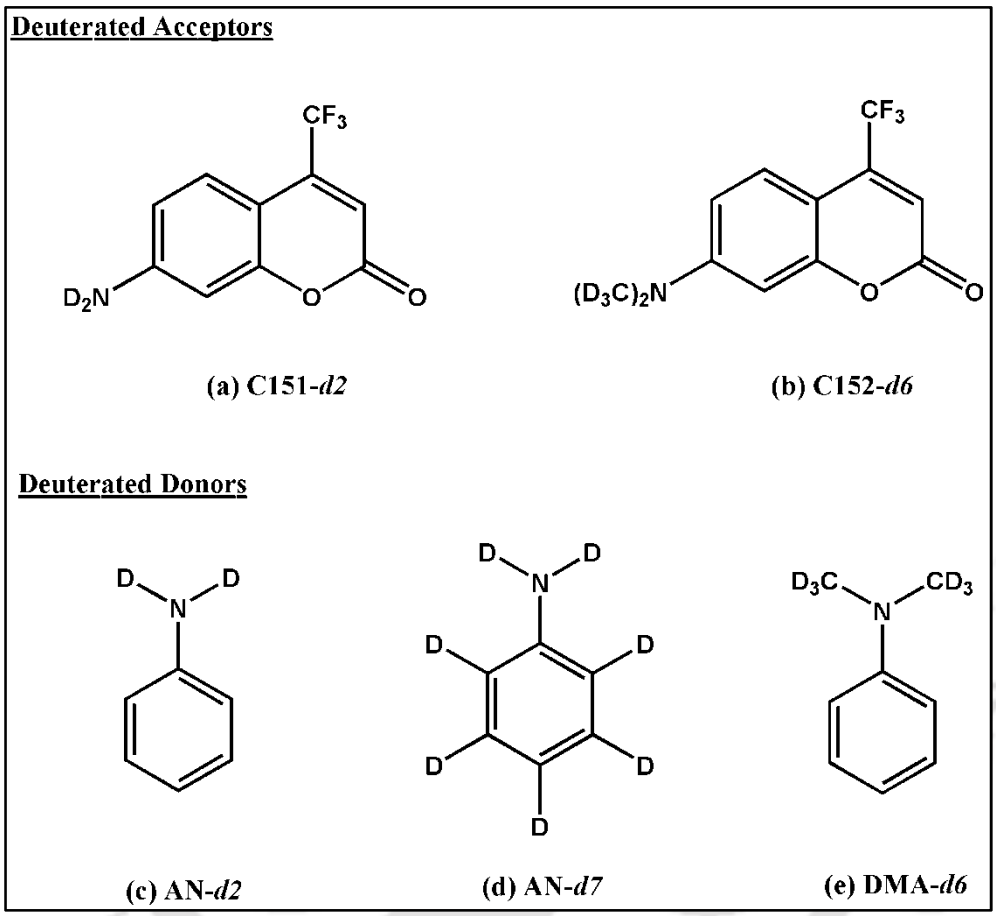

Scheme 1.7: Deuterated coumarin dyes (acceptor, a-b) and aromatic amines (donor, c-e).

To investigate the role of H-bonding, several groups studied deuterium isotopic substitution effect on PET.[19, 21] Isotopic substitution is a useful technique which can be used to elucidate the mechanistic pathways of intermolecular PET process in detail. Effect of isotopic substitution on the PET are usually discussed in the light of the changes in the electron transfer parameters such as the solvation time, vibrational frequencies, free energy change and so on.[19-21, 125-129] The isotope effect on the free energy of PET process can arise from two possible sources- one is zero-point energy effect and the other one is solvent

structural effect.[19, 21] As a result of isotopic substitution there is a reduction in the frequencies of some of the vibrational modes. This reduction in the vibrational frequency leads to decrease in the zero-point energy of the deutareted solute and hence, the ΔG^0 changes**.**

Yoshihara and co-workers investigated the effect of deuterium isotopic substitution of both the donor solvents and the acceptor dyes on PET in the coumarin-aniline system (**Scheme 1.7**).[19, 21] Significant deuterium isotope effects on the PET dynamics has been observed in the cases of per-deuterated aniline (AN-*d*7) and amino deuterated aniline (AN-*d*2) as the electron donors, but were not observed with deuterated DMA (DMA-*d*6) and deuterated coumarins as the electron donor and acceptors, respectively. The extent of the isotope effect on the PET is almost the same for both AN-*d*2 and AN-*d*7, which indicates that isotope effect is only linked with the NH_2 group of AN. For example, C153 shows faster PET in normal AN compared to the deuterated one. Effect of isotopic substitution on the PET rate is quite obvious from the average fluorescence lifetimes of the coumarins in normal and deuterated aniline. The average fluorescence lifetime of C153 in AN is 79 ps whereas, in deuterated AN-*d*7 the lifetime is 94 ps indicating slower PET in deuterated AN. However, in the case of DMA, they have not observed any isotope effect upon substituting all of the *N*-methyl group hydrogen by deuterium (DMA-*d*6). On the other hand, using deuterated coumarins, where the 7-amino group hydrogen atoms are substituted by deuterium, they have not observed any change in the ET dynamics.[19, 21] It was concluded that the isotope effect on the ET dynamics of coumarin-AN system arises due to the differences in the ΔG^0 values with normal and deuterated solvents. The change in the intermolecular hydrogen bonding with the solvent molecules due to deuteration was mainly responsible for the differences in ΔG^0 with normal and deuterated solvents. Similar isoptope effect on PET was also observed for coumarin in deuterated orthomethoxyaniline.[20] However, deuterium isotope effect on PET becomes insignificant for faster PET.[19]

In contrast, Ghosh et al. did not find any evidence for the role of H-bonding on PET of C337 in AN (or MAN).[118] Using ultrafast IR spectroscopy, they studied PET of C337 in aromatic amine-AN, MAN and DMA. Formation of H-bond between C337 and AN (or MAN) was confirmed by probing the C=O and C≡N stretching modes of C337. C337 shows C=O and C≡N stretching frequencies at 1722 and 2223 cm^{-1}, respectively and are red shifted upon H-bond formation with AN (or MAN). C337 shows fast PET of ~ 500 fs in all three solvents. Thus PET kinetics was same in AN, MAN and DMA, even though AN and MAN are involved in H-bond formation with C337. The results indicated that H-bonding does not play any significant role on PET of C337. Moreover, they have not observed any H/D isotope effect.

Nibbering and co-workers studied the PET dynamics between FN and amine solvents such as diethylamine (DEA) and triethylamine (TEA).[130] DEA can form H-bond with the C=O group of FN whereas no H-bond formation occurs with TEA and can be manifested from the C=O stretching frequency of FN in DEA and TEA. Fluorescence intensity of FN shows a drastic reduction in the emission intensity when TEA or DEA is used as the solvent. This indicates a substantial shortening of the S_1-state lifetime, probably caused by the ET reaction with the amine solvents. Ultrafast transient absorption showed that upon photo-excitation of FN to the S_1 state in addition to a bleach signal at 1621 cm^{-1}, a prominent transient absorption band at 1548 cm^{-1} appeared within a timescale of several tens of picoseconds in TEA and DEA. Fluorescence up-conversion measurements showed that the S_1 state of FN decays on picosecond timescales in TEA and DEA. It was proposed that ultrafast fluorescence quenching was caused by forward PET from the amine solvent to the optically excited FN. Comparing the experimental rate constants with the driving force (i.e free energy change) dependencies for forward and backward ET in amine solvents with and without H-

bonding capabilities has provided key insights into the important role of H-bonding in assisting ET processes.

1.5. Photoinduced electron transfer in solvent mixture: Regular and anomalous fluorescence modulation

Although, PET in neat electron donating solvent has been studied extensively, PET in binary solvent mixture is much less addressed till date. Castner and co-workers first addressed the issue that what happens to the PET rate if a non-interacting solvent is mixed with an electron donating solvent. To this end, they used two different coumarin acceptors (C151 and C152; **Scheme 1.1a-b**) in a mixture of DMA and a non-interacting solvent toluene using femtosecond up-conversion measurements and simulation.[121] They found that the PET rate gradually decreases on the addition of the non-interacting component. For instance, the rate of the electron transfer of C151 in neat DMA was 3.30 ps^{-1}, whereas at an intermediate mole fraction of X_{DMA} (= 0.638) the ET rate decreases to 0.415 ps^{-1}. Note that toluene and DMA have different sizes, dielectric constants and dipole moments, making the interpretation complex. To minimize these effects, they used chlorobenzene as a better co-solvent. They found similar trend of PET reduction on chlorobenzene addition also. The retardation of PET was explained as the exchange of the inert solvent molecules with some of the DMA molecules from the first solvation layer of the acceptor (C151 or C152) (**Scheme 1.8**). As a result of this replacement, there is significant reduction in the electronic coupling between the acceptor (coumarin) and the donor (DMA). As this trend seems obvious from the microscopic view of the solvent arrangement about the acceptor, we may term this trend as "regular PET" (**Scheme 1.9**).

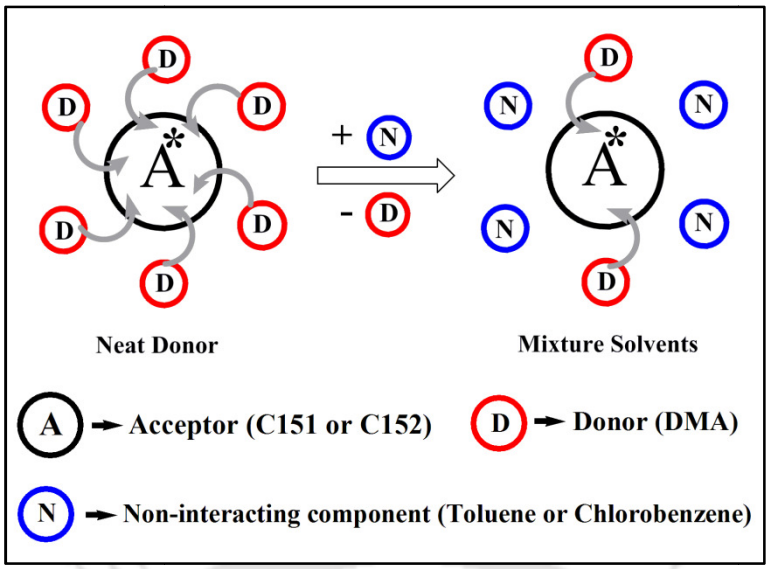

Scheme 1.8: Introduction of non-interacting solvent reduces the electronic coupling between the donor and acceptor.

On the contrary, Pshenichnikov and co-workers observed an unusual acceleration of electron transfer for rhodamine 800 (R800) (**Scheme 1.10**) upon addition of polar solvent acetonitrile to DMA.[131] Using frequency-resolved pump-probe transient spectroscopy they measured the backward ET rate for R800 at different mole fractions of acetonitrile. With increase in the content of acetonitrile the backward ET rate constant gradually decreased. At 0.25 mole fraction of acetonitrile the backward ET time constant decreased to ~2.5 ps from ~4.5 ps in neat DMA. Thus, the forward PET rate of the mixture was significantly higher than in neat DMA. Apparently, it appears that reduction of number of donors result in more facile PET. They interpreted this enhancement of PET to the change in dynamical properties of the medium.[131]

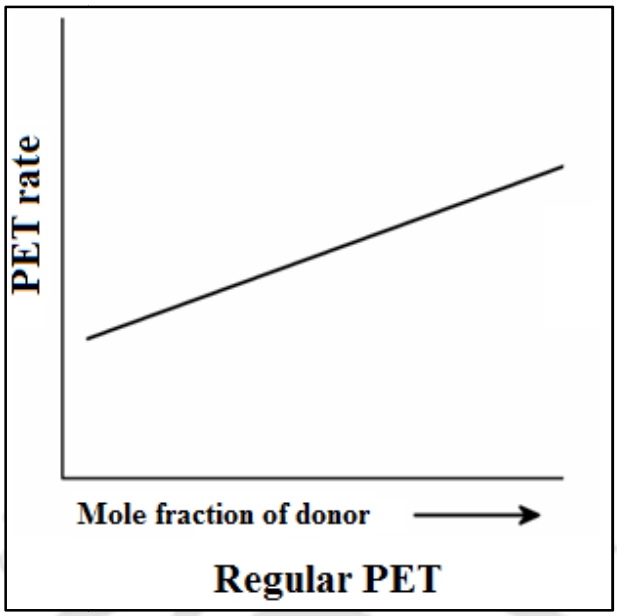

Scheme 1.9: Regular variation of PET in a mixture of electron donating and non-interacting solvents. PET rate increases with increase in the mole fraction of the donor.

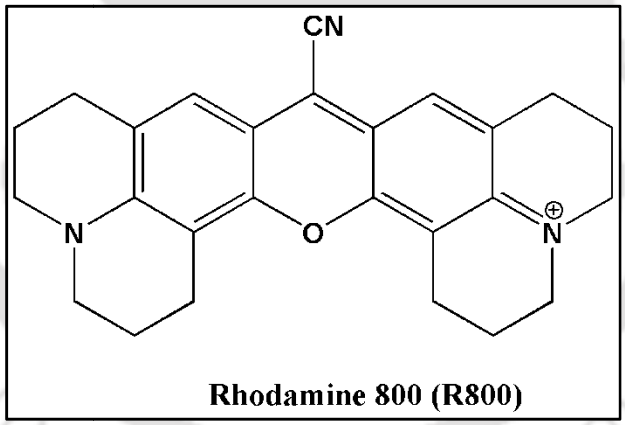

Scheme 1.10: Chemical structure of rhodamine 800 (R800).

Continuous variation of the H-bonding environment in a solvent mixture may shed new light on understanding the effect of H-bonding on photophysical processes which is competitive in nature. Competitive H-bonding may be considered as an important factor for governing chemical, photophysical and photochemical response in complex H-bonding environments. However, this aspect remains relatively unexplored in literature.

Recently, Saini et al. reported an anomalous fluorescence modulation of curcumin (**Scheme 1.11**) in toluene-methanol mixture. The emission intensity and lifetime first gradually increased with increase in methanol mole fraction, X_{MeOH} then reached to a maximum at X_{MeOH} = 0.14 and thereafter decreased with further increase in the methanol content.[132-133] The excited-state intermolecular H-bonding between the pigment and the H-bond donor solvent was proposed to reduce the non-radiative decay by the cleavage of the intramolecular H-bonding between the keto and the enolic –OH group curcumin. Interestingly, the intermolecular H-bonding interaction was found most effective at some intermediate mole fraction rather than in neat methanol. Similar anomalous modulation of fluorescence was also observed for a doubly H-bonded proton transfer probe 2,2-bipyridine-3,3-diol ($BP(OH)_2$) (**Scheme 1.12**), in a binary mixture of dimethylsulfoxide (DMSO) and water.[134] Using steady-state and time-resolved fluorescence measurements, Mandal et al. observed that the quantum yield of $BP(OH)_2$ varies anomalously with the mole fraction (X_{DMSO}) of DMSO, in a water-DMSO mixture displaying a maximum at X_{DMSO} = 0.12. After that, quantum yield of $BP(OH)_2$ decreased with further enrichment of DMSO in the mixture. They attributed this anomalously high fluorescence at this intermediate mole fraction of DMSO is due the enhanced pair hydrophobicity of the medium.[134]

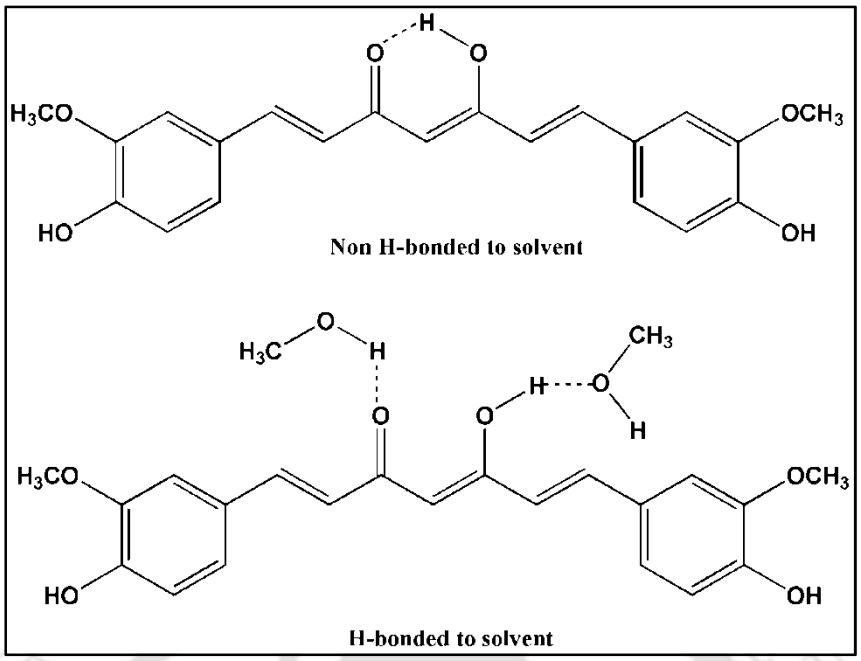

Scheme 1.11: Structure of curcumin in non-hydrogen-bonding (top) and hydrogen-bonding (bottom) solvents showing the intramolecular and intermolecular H-bonds. Reprinted with permission from ref 132. Copyright © 2012, American Chemical Society.

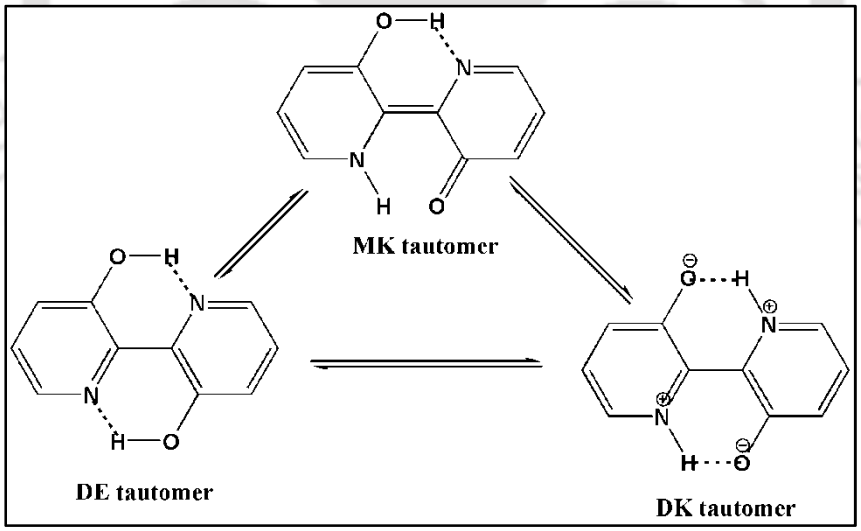

Scheme 1.12: Phototautomers of 2,2-bipyridine-3,3-diol in DMSO-water solvent mixture. Reprinted with permission from ref 134. Copyright © 2013, American Chemical Society.

1.6. Aim and scope of the present work

The primary aim of the present work is to understand the nature of D-A H-bonding in the electronic excited state of coumarin acceptors complexed with phenol, aniline donors and to correlate its effect on photoinduced electron transfer. For the C102-phenol complex, experimental results earlier showed that H-bond breaks quickly in the excited state upon excitation (**see section 1.3**). However, theoretical studies predicted that H-bond strengthened in the excited state rather than being cleaved and proposed that the strengthening of the H-bond in the excited state should facilitated PET. In our work, we confirmed the H-bond assisted PET of C102 in the presence of the H-bond donor observing fluorescence quenching. We think such evidence may be important towards the understanding of the effect of excited-state H-bond in other photophysical processes also.

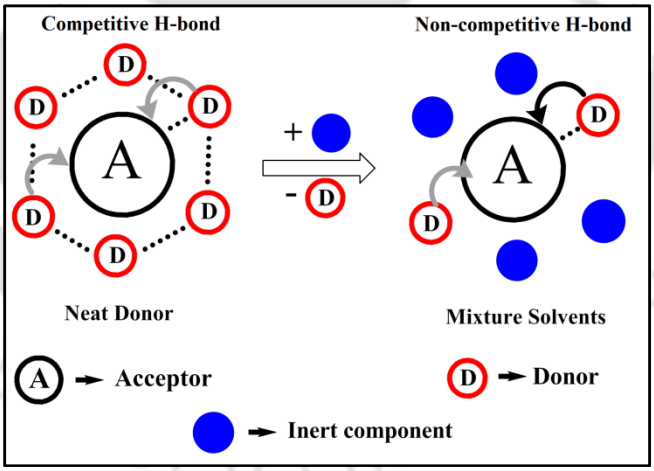

Scheme 1.13: Schematic representation of competitive and non-competitive hydrogen bonds. In a neat solvent, competitive H-bonding between acceptor–donor and donor–donor H-bonds may suppress the effect of H-bonding of PET (gray arrow). In a liquid mixture, the non-interacting component may disrupt the donor–donor H-bond, and hence, strengthens/orients donor–acceptor H-bond for a faster PET process (black arrow).

Another important discrepancy between theory and experiment existed while considering the effect of H-bonding on the PET of between C102 and aniline. Theory predicts facile PET within the H-bonded C102-aniline complex but actually no PET has been observed for C102 dissolved in neat aniline in the experimental studies. To resolve this, we conjectured that the effect of H-bonding required to activate PET may be suppressed in neat AN because of competitive nature of the donor-acceptor (D-A) and donor-donor (D-D) H-bonding (**Scheme 1.13**). The solvent aniline having H-bond donating and accepting ability together may form a hydrogen bond with itself, and may exist as H-bonded clusters. Hence, in pure aniline, the key H-bonding between the donor and the acceptor may not be fully effective in guiding electron transfer. Moreover, there are several donor molecules at close contact without forming H-bond with the acceptor; their contributions to overall PET may be overwhelmingly large. Hence, the effect of H-bonding on PET may be suppressed in neat aniline solvent. The situation may drastically change when an inert non-polar component is simply mixed with aniline. Although the inert component cannot participate in either H-bonding or electron transfer, it may replace some donors from the first salvation shell of the acceptor and disrupt the donor-donor H-bonding. The situation may shift from a competitive H-bonding (both C102-aniline and aniline-aniline H-bond co-exists) in neat aniline to non-competitive H-bonding (only C102-aniline H-bonding present) in the solvent mixture. As a proof of the concept, we have studied the PET of C102 in solvent mixture of aniline (donor) and inert solvent (cyclohexane or toluene). We observed faster PET for C102 at intermediate mole fraction of the donor compared to neat aniline. Thus, it can be inferred that under proper condition the H-bond assisted PET can be enhanced to that extent which exceeds the PET rate in neat electron donor which we may term as anomalous PET (**Scheme 1.14**).

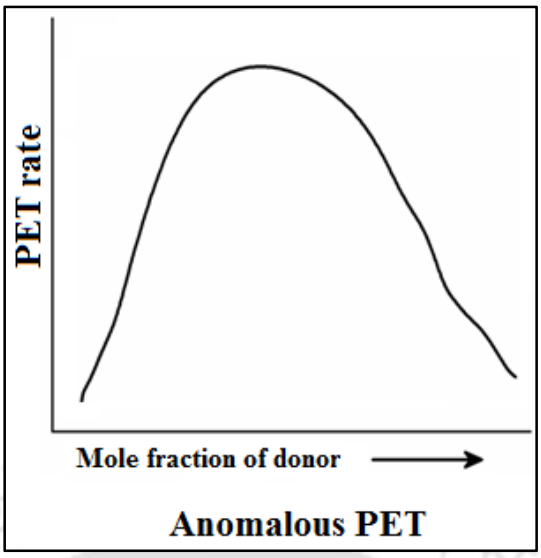

Scheme 1.14: Anomalous variation of PET in a mixture of electron donating (also H-bond donating) and non-interacting solvents. PET rate increases with increase in the mole fraction of the donor upto a particular mole fraction and thereafter decreases with further enrichment of the donor.

However, this anomalous trend of PET may possibly be attributed to either modulation of polarity or H-bonding environment around the acceptor (C102) in the mixture. To eliminate the role of polarity change we further studied PET of C102 in similar polarity AN-DMA mixture. The anomalous trend of PET remains preserved in the AN-DMA mixture. This supports the our postulate that competitive H-bonding may be responsible for less active H-bonding influence in neat donor solvent and is the main cause of the anomalous trend in H-bonding modulation not a polarity variation. Anomalous modulation of PET of C102 is also observed in cyclohexane-phenol and anisole-phenol mixtures indicating that it is a common feature of H-bonded system. However, we have not observed any PET modulation of C102 in cyclohexane-anisole mixture where only polarity change occurs. However, since C102 is reluctant to undergo PET in absence of H-bonding it cannot be considered as a representative for ultrafast PET. Unlike C102, C153 undergoes ultrafast PET with aromatic amine donors. We reproduced similar anomalous modulation for the ultrafast PET of C153 in cyclohexane-

aniline mixture. However, in cyclohexane-DMA mixture where no H-bond is formed ultrafast PET shows regular behaviour. To validate the competitive PET in neat vs non-competitive PET in mixture, MD simulation has been considered in our group to know about the local structural arrangement of donor around the acceptor.

Thus, this thesis investigates very important role of H-bonding on PET using coumarin acceptor and aniline and phenol donors. To obtain more insight into the mechanistic details of intermolecular PET process various effects such as temperature, isotopic substitution, and substituent effect should also be considered. Isotopic substitution is an important technique. This work can be extended to study of the effect isotopic substitution on PET of coumarins as well as other system also. So far we have considered only the fundamental aspects of H-bonded PET in mixture; it is interesting to see how this could affect photophysics under real competitive H-bonding condition. For example, in an enzyme pocket, a substrate forming a H-bond with a particular functional group at an active site, may also simultaneously make a H-bond with other amino acids.

Chapter 2

Experimental and theoretical methods

In this chapter, we have discussed theoretical methodologies especially density functional theory (DFT) and time-dependent density functional theory (TDDFT) that have been used in our studies. Specifications of all the instruments used (e.g. UV-Visible spectrophotometer, steady-state spectrofluorometer, time correlated single photon counting (TCSPC), femtosecond up-conversion, FTIR spectrophotometer etc.) are also provided. Chemicals used and details of sample preparation have been included along with the data analysis.

2.1. Theoretical methods

2.1.1. Density functional theory (DFT)

Density functional theory (DFT) is presently the most useful approach to compute the electronic structure of molecule and has been used for solving molecular parameters in the electronic ground state.[135-136] Due to its reasonable accuracy and less computational cost, considerable interest in modern computational chemistry has been gained in recent years. It is primarily based on the probability density function of electron. Using DFT calculations we can study various molecular properties such as molecular structures, vibrational frequencies, electronic properties etc.

In the last few years, there has been significant development of time-dependent density functional theory (TDDFT) methods for the calculation of the structure and electronic

properties of molecules in the excited state.[137-139] Recently, TDDFT has been applied to the H-bonding complexes to probe the H-bond dynamics in the excited state.[75, 81, 83, 137-141]

To understand the nature of the excited states as well as to estimate the H-bond strength, we have performed DFT and TDDFT calculations for isolated C102 and 1:1 complex of C102 and phenol derivatives. The results will be presented in the chapter 3. For this purpose, we have first optimized the individual structures of C102, phenol and *p*-Cl-phenol separately with DFT method using B3LYP functional and 6-31G** basis set. Using these optimized structures, 1:1 complexes- C102-phenol and C102-*p*-Cl-phenol are optimized at the same level of computation. To construct the potential energy surface of the hydrogen bonded complex, we performed single point energy calculation on each configuration by varying the H-bond distance by a step of 0.05 Å using DFT and TDDFT methods at the same level of computation. All of the calculations were performed with the Gaussian 03 package in the gas phase.[142]

2.2. Steady-state measurements

Absorption spectroscopy is the most useful spectroscopic tool which provides important information about the wavelength of a transition and the corresponding molar extinction coefficient (ε) of a chromophore under investigation. Throughout the studies, we have recorded the UV-Vis spectra of all the samples in Perkin-Elmer Lamda-35 and Perkin-Elmer Lamda-750 spectrophotometers. Lamda-750 spectrophotometer consists of deuterium, tungsten and halogen light source, double holographic grating monochromator, high sensitivity R928 PMT.

Steady-state fluorescence spectra of all the samples were recorded on Jobin Yvon Fluoromax4 spectrofluorometer. For all the steady-state measurements, we have used a

quartz cuvette of path length 1 cm. The most commonly used light source for spectrofluorometer is a high-pressure 150 W xenon (ozone free) arc lamp. Fluorescence is collected at right angles with respect to the incident beam while the emitted light is detected through a monochromator by a R928P photomultiplier tube (PMT).

2.3. Time-resolved fluorescence measurements

The details of any excited state process can be best probed by measuring the fluorescence intensity decay over time i.e. time-resolved fluorescence measurement. Often the decay of the excited population occurs on a wide range of timescales. Hence, usually different techniques or a combination of techniques are required for different studies. Here we have used two main techniques- time correlated single photon counting (TCSPC) and fluorescence up-conversion.

2.3.1. Time correlated single photon counting (TCSPC)

TCSPC is a very standard method to measure fluorescence lifetime from few tens of picosenconds to millisecond/microsecond time scale. The actual time resolution and time window depends on the nature of the light source and electronic components of the spectrometer. In the entire work, TCSPC measurements were performed on LifeSpec II from Edinburgh Instruments, UK. In this technique, the sample to be analyzed is excited with a short light pulse from a light source with sufficient delay between pulses. In our case, light sources were picosecond laser diodes (EPL-375 nm from Edinburgh and LDH-P-C-405 from PicoQuant) and maximum repetition rate was 10 MHz. In TCSPC method, the light source beam is split into start and stop signal pulses. The start signal pulse travels to a micro-channel

plate (MCP) photomultiplier which activates the time to amplitude converter (TAC). The stop signal pulse travels through the sample. The growth of ramp signal in TAC is stopped by this pulse. The TAC output can be amplified by an amplifier, and this analogue pulse of height corresponding to a measured time of the signal goes through further processing to convert to digital pulse through the analogue to digital converter (ADC).

Since the fluorophores emit photons at different times following their excitation by radiation, the decay time molecules must have a certain rate rather than occurring at a specific time with excitation. The principle of TCSPC is the detection of single photons and the measurement of their arrival times in respect to a reference signal from the light source. The TCSPC method needs a high repetitive light source to accumulate a sufficient number of photons since this is a statistical method and requires many numbers of statistical data precision. The time measurement of the start and stop sequence is represented by an increase of a memory value in a histogram. Thus, this experiment must be repeated many times to gather sufficient photons in the full range of delays between excitation and emission. The resulting histogram counts versus the time channels on the X-axis represents the curve of fluorescence decay profiles.

In most cases, the TCSPC technique has limits for the temporal and lifetime range measurable for the fluorescence lifetimes. Therefore, for the curve fittings the method involving linearization of the fitting function and least-squares fitting is the most widely used deconvolution technique. Time-resolved data were analyzed with reconvolution method based on discrete components analysis model using the FAST software provided by the Edinburgh Instruments Ltd.

2.3.2. Femtosecond up-conversion measurements

Fluorescence up-conversion is a nonlinear optical detection technique to achieve femtosecond time resolution. In this technique, fluorescence of the sample is not detected directly, but instead sent to an appropriate nonlinear optical crystal. The fluorescence signal (ν_F) is mixed with a time delayed gate pulse (ν_G) in this crystal and generates a signal at the sum frequency, $\nu_F + \nu_G$. The intensity of the light at the sum frequency is determined using a photon counting electronics. The fluorescence up-conversion was measured in FOG 100, (CDP) at the laboratory of Prof. Kankan Bhattacharya at Indian Association for the Cultivation of Science, Kolkata, India and the details of the up-conversion principle are given elsewhere.[143-144] The IRF (for SH excitation) displays a full width at half maximum (FWHM) of 350 fs.

2.4. Analysis of the picosecond (TCSPC) and femtosecond (up-conversion) decays

An observed decay, N(t) is a convolution of the actual intensity decay, I(t) with the lamp function, L(t). In order to extract the fluorescence lifetime it is essential to de-convolute the data and the convolution integral may be expressed as-

$$N(t) = \int_0^{t'} L(t)I(t' - t)dt \qquad (2.1)$$

The deconvolution is based on an iterative least square method. An excitation pulse profile is first recorded and then the deconvolution starts with the mixing of the excitation pulse and a projected decay to form a new reconvoluted set. This data is compared with the experimentally obtained data and the difference is summed, generating the χ^2 function for the fit. The deconvolution proceeds through a series of such iterations until an insignificant

change in χ^2 occurs between two successive iterations. The quality of fit is normally assessed by inspection of the reducedχ^2, plot of the weighted residuals and the autocorrelaion function of the residuals. The picosecond decays are de-convoluted using FAST software.

The femtosecond fluorescence decays are fitted using a Gaussian shape for the exciting pulse using IGOR Pro-5 software.

2.5. Fourier transform infrared (FTIR) spectroscopy

Fourier transforms infrared (FTIR) spectra in the range 450-4000 cm^{-1} were recorded in a Perkin-Elmer Spectrum Two FTIR spectrophotometer. For this purpose, we have used demountable liquid cell kit purchased from Sigma-Aldrich (097-3710, 2112003-1KT). For each measurement we have used 2 mm slit width. Concentration of C102 was taken 2 mM at each sample, whereas for cyclohexane-aniline mixture concentration of C153 at different mole fraction was 20 mM.

2.6. Estimation of quantum yield of coumarins in solvent mixtures

The excited molecules after absorption of light dissipate their absorbed energy by decomposition, reaction, emission or nonradiative de-excitation. The efficiency with which these processes take place is called the quantum efficiency. The fluorescence quantum yield is the fraction of excited molecules that return to the ground state S_0 with emission of fluorescence photons. Quantum yield of fluorescence (φ) is generally defined as the ratio of the number of photons emitted to the number of photons absorbed as given by the following equation.

$$\varphi = \frac{\text{Number of photons emitted}}{\text{Number of photon absorbed}} \qquad (2.1)$$

Generally, the fluorescence quantum yield of a sample (φ) is determined with respect to that of a standard known fluorophore using the following equation-

$$\frac{\varphi_s}{\varphi_r} = \frac{I_s A_r n_s^2}{I_r A_s n_r^2} \qquad (2.2)$$

where, φ_s is the fluorescence quantum yield of the sample, I_s and I_r are the integrated fluorescence area, and A_s and A_r are the absorbance values for the sample and reference solutions, respectively.

In our case quantum yield of the fluorophore (C102) was measured in different solvent mixtures with respect to the reported values in different solvents by Jones II et al.[145] Quantum yield of C102 in cyclohexane is almost unity (~ 1.05).[145] So we have calculated the quantum yields at different mole fraction of donor with respect to this value. For this purpose we have divided the respective area under curve of the OD-normalized emission spectra by the area under curve of the emission spectra of C102 in cyclohexane.

2.7. Chemicals

2.7.1. Fluorescence probes (acceptors)

Throughout the works, we have used two fluorophores, coumarin 102 (C102) and coumarin 153 (C153). C102 and C153 were purchased from Sigma-Aldrich and used as received.

2.7.2. Donors

We have used a series of hydrogen bond and electron donors in our work. Several phenol derivatives are used as hydrogen bond donors. Phenol was supplied by Sigma-Aldrich whereas *p*-Cl-phenol was purchased from Hi-Media. Anisole was purchased from Merck Chemicals. The electron donors, Aniline and *N,N*-dimethylaniline were purchased from Sigma-Aldrich and used without further purification.

2.7.3. Solvents

Throughout this work we have used various solvents with best available grade. Cyclohexane used was supplied by either Merck Chemicals or Rankem (HPCL grade). Acetonitrile and methanol were supplied by Merck Chemicals. Toluene (HPLC grade) was purchased from Spectrochem. All the solvents were used as received without further purification.

2.8. Preparation of samples

2.8.1. Preparation of binary mixture solution

Binary mixtures of electron donating (also acts as H-bond donor) solvent i.e aniline and non-interacting solvent (cyclohexane, toluene and *N,N*-dimethylaniline) having different composition were prepared and mole fraction of the donor was calculated. Since cyclohexane and aniline are not miscible at room temperature we were unable to prepare complete range of mole fractions. For toluene-aniline mixture we have prepared the solvent mixtures at different mole fraction of aniline ranging from 0.0 to 1.0. Here, *N,N*-dimethylaniline cannot form H-bond and without H-bond formation it cannot acts as electron donor towards C102,

hence termed as non-interacting component. Similarly, we have also prepared binary mixtures of cyclohexane-phenol, anisole-phenol and cyclohexane-anisole. In cyclohexane-phenol and anisole-phenol mixtures mole fraction of phenol was considered up to its solubility range in both the solvents.

2.8.2. Preparation of fluorophore solution

For fluorescence measurement, solutions of C102 and C153 were prepared in all the solvents used in our study. The fluorophores are completely soluble in the solvents.

A stock solution of ~4 mM concentration was prepared by vortexing C102 in 500 µL cyclohexane. After that a solution of C102 of ~12 µM concentration was prepared by adding 10 µL of the stock solution to 3 mL of cyclohexane and was used throughout all absorption, steady-state and time-resolved fluorescence measurements. For titration experiment, we have gradually added required amount of phenol (or *p*-Cl-phenol or anisole) to this solution. Similarly, we have also prepared the solution of C102 in other solvents-acetonitrile and methanol and performed all absorption and fluorescence measurements at different concentrations of phenol.

For cyclohexane-aniline and toluene-aniline mixtures, we have prepared two stock solutions of C102 having concentration of 1 mM in cyclohexane and toluene, respectively. After that we have added 10 µL of the stock solution to 2 mL of each solvent mixture having different mole fraction of aniline and concentration of C102 in the samples was maintained 5 µM.

For aniline-DMA mixture, we have prepared a stock solution of C102 in methanol having concentration of 4 mM. 10 µL of this stock solution is added to each samples of volume 3 mL of aniline-DMA mixture at different mole fraction of aniline. The concentration

of C102 in each sample was kept ~ 12 μM. Before adding to the solvent mixture methanol was evaporated.

For cyclohexane-phenol, anisole-phenol and cyclohexane-anisole, we have prepared two stock solutions of C102 in cyclohexane and anisole of concentration of ~ 2 mM. 10 μL of this stock solution was added to each samples of volume 2 mL of cyclohexane-phenol, anisole-phenol and cyclohexane-anisole at different mole fraction of phenol and anisole. The concentration of C102 in each sample was ~9 μM.

For, C153 we have prepared a stock solution of ~2 mM in cyclohexane. From this stock solution 10 μL was pipette out and added to each sample of cyclohexane-aniline mixture having different mole fraction of aniline. The final concentration of each sample was ~ 10 μM.

2.8.3. Preparation of FTIR samples

For FTIR measurement we have prepared samples at different mole fraction of aniline (or phenol). The concentration of C102 and C153 were respectively 5 mM and 20 mM throughout all the measurements.

Chapter 3

Hydrogen-Bond induced photoinduced electron transfer of coumarin 102-phenol complex*

3.1. Introduction

The nature of the H-bonding, whether it is strengthen or weaken in the excited state has been reviewed in the chapter 1 (**see section 1.3**). Using UV-visible pump and IR probe spectroscopy, Nibbering and co-workers suggested that H-bond between C102 and phenol formed in the ground state in a non-polar solvent TCE breaks in the electronic excited state just after excitation (`within ~200 fs of excitation).[65, 77, 122-123, 146] On the contrary, using TDDFT calculation, Zhao and Han demonstrated that C102-phenol H-bond strengthened in the excited state rather than being cleaved. They proposed that the strengthening of the C102-phenol H-bond in the electronically excited-state upon photoexcitation facilitates photoinduced electron transfer (PET) within the H-bonded complex. This H-bond strengthening assisted PET may lead to fluorescence quenching of C102.[75] From the literature it is clear that if H-bond breaks in the excited state then C102 and phenol will be apart and as a result there will be no fluorescence quenching. On the other hand, if H-bond strengthened in the excited state, C102 and phenol will come closer and PET will be facilitated. Thus, H-bond induced PET will lead to fluorescence quenching. Various groups have investigated the effect of excited state H-bonding on photophysics of many other complexes but C102-phenol remains ambiguous.[80, 119, 147]

In this chapter, we have revisited the C102-phenol system in a non-interacting solvent cyclohexane. To characterise the excited states of the H-bonded system, especially to observe the effect of the excited-state H-bond strengthening or weakening in the excited state

*This work has been published in *Journal of Physical Chemistry A* **2013,** *117*, 3945-3953.

relaxation, we have applied both steady-state and time-resolved fluorescence spectroscopy. Here, we have considered a series of phenol derivatives e.g. anisole and *p*-Cl-phenol having a variety of H-bonding strength (**Scheme 3.1**). Since –OH group is replaced by $-OCH_3$, anisole lacks H-bond formation ability. On the other hand, the presence of an electron withdrawing –Cl group at the *para* position makes *p*-Cl-phenol a better H-bond donor compared to phenol. The stronger H-bond formation ability of *p*-Cl-phenol compared to phenol with C102 is evident from the lower pK_a value of *p*-Cl-phenol (9.38) than phenol (9.98).[148] Since the oxidation potentials of the three phenol derivatives are similar,[149] interaction with C102 may be controlled by the effect of the excited-state H-bonding rather than by the free energy of electron transfer.[10] We observed that anisole has negligible or no effect on the emission spectra of C102, while the fluorescence of C102 quenches significantly in the presence of phenol. For *p*-Cl-phenol, fluorescence quenching of C102-quenching is even more prominent.

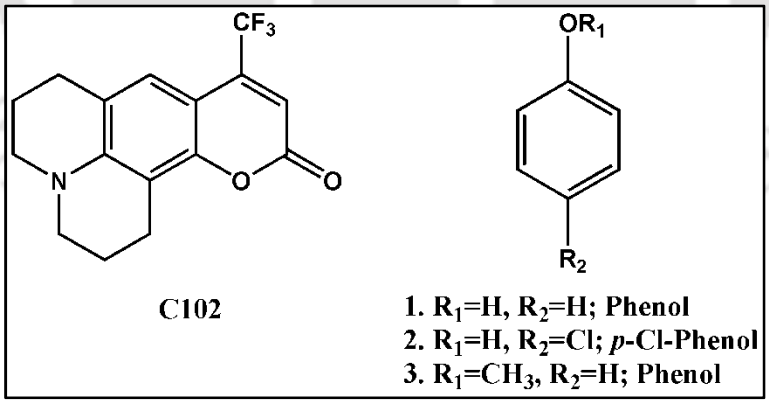

Scheme 3.1: Structures of C102 and different phenol derivatives of varying H-bond strength.

In order to understand the role of solvent in controlling the H-bond formation, we considered another two solvents- acetonitrile and methanol of different polarity. Both the

solvents have H-bond formation ability and can form H-bond with either C102 or phenol or both.

The results are discussed in the following order. First, we have discussed the theoretical results to characterize the spectroscopic states in the H-bonded complex, followed by results from the steady-state and time-resolved fluorescence measurements in the absence and in the presence of H-bond donor. Subsequently, we analyzed the results on the basis of excited state H-bonding effect on the electronic relaxation.

3.2. Results

3.2.1. Time-dependent density functional theory (TDDFT) calculations

Figure 3.1 represents the ground-state optimized geometry of the 1:1 H-bonded complexes of C102 and H-bonding donors- phenol and *p*-Cl-phenol. Here, we want to focus only on the 1:1 complex and hence, we covered only the low-concentration range of the donors (phenol and *p*-Cl-phenol). At these concentrations, formation of higher order complexes (C102-$(donor)_{n=2,3..}$) may be safely ignored. From the **figure 3.1**, C102 and phenol are held by the formation of H-bond between the C=O group of C102 and the HO− group of phenol and *p*-Cl-phenol. The H-bond distance, that is, the distance between the O atom of the C=O group and the H atom of the HO− group of phenol, was found to be 1.845 Å (**Table 3.1**). As a result of the H-bond formation between C102 and phenol, the H-bonding groups (C=O and −OH) of the donor and acceptor bonds are lengthened. The C=O bond (1.211 Å) of isolated C102 is elongated by 0.015 Å on the formation of 1:1 H-bonded complex with phenol (**Table 3.1**). The molecular planes of C102 and phenol were seen nearly orthogonal to each other in the 1:1 complex. The optimized geometry and the H-bond parameters of the C102-phenol complex showed good agreement with that reported by Zhao et al.[75] The

geometry of the C102-*p*-Cl-phenol complex was qualitatively similar to the C102-phenol complex (**Figure 3.1**). However, the H-bond length was shorter by 0.081 Å in the C102-*p*-Cl-phenol complex compared to the C102-phenol, indicating superior H-bonding ability of *p*-Cl-phenol.

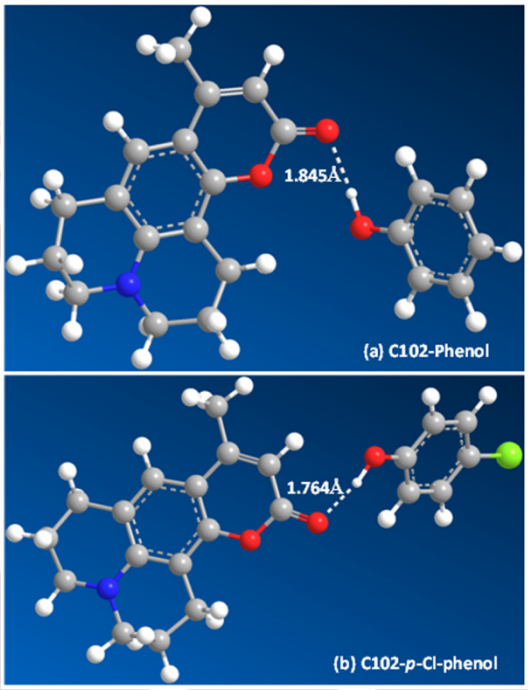

Figure 3.1: Optimized structures of 1:1 C102-phenol and C102-*p*-Cl-phenol hydrogen bonded complexes in the ground state (S_0). The shorter hydrogen bond length in the C102-*p*-Cl-phenol complex indicates stronger H-bond formation than in C102-phenol complex.

Figure 3.2 represents the potential energy curves of the first three electronic states (S_0, S_1, S_2) of the C102-phenol and C102-*p*-Cl-phenol H-bonded complexes, respectively. From the curves, it was evident that the minima of the S_1 and S_2 potential curves shift to a shorter distance than that of the ground state (S_0). Similar shifting of the potential minima towards shorter distance in the excited state was also reported earlier by Zhao et al. for C102-phenol using BP86 functional with TZVP basis set.[75] The potential energy curve, U(r) along

the hydrogen-bonding coordinate (r) was fitted with a Morse type equation for each of the electronic states-

$$U(r) = U(r_0) + D_e\,[1 - e^{-a(r-r_0)^2}] \qquad (3.1)$$

where, r_0, $U(r_0)$ and D_e represent the equilibrium H-bond distance, equilibrium potential energy and H-bond dissociation energy, respectively, and *a* is an adjustable Morse parameter. The fitted results for the three electronic states S_0, S_1, and S_2 for C102-phenol and C102-*p*-Cl-phenol are summarized in **Table 3.2**. The H-bond distance and energy for *p*-Cl-phenol were found to be shorter and greater, respectively than that of phenol. The fitted values for H-bond energy for C102-phenol complex in S_0 and S_2 states were 8.40 and 11.36 kcal M^{-1}, respectively, which were in excellent agreement with the calculated values (8.67 and 12.26 kcal M^{-1} respectively) of Zhao et al.[75] The excited-state H-bond strengthening was observed to be more drastic in the S_1 state for both of the complexes (**Table 3.2** and **Table 3.3**).

Table 3.1: H-Bond length ($L_{O..H}$) and the bond lengths of the H-bond accepting ($L_{C=O}$) and donating groups (L_{H-O}) in the ground state (S_0) before and after formation of the H-bonded complex.

	$L_{C=O}$ (Å)	L_{H-O} (Å)	$L_{H\cdots O}$ (Å)
Phenol	-	0.966	-
p-Cl-phenol	-	0.966	-
C102	1.211	-	-
C102-phenol	1.226	0.981	1.845
C102-*p*-Cl-phenol	1.228	0.985	1.764

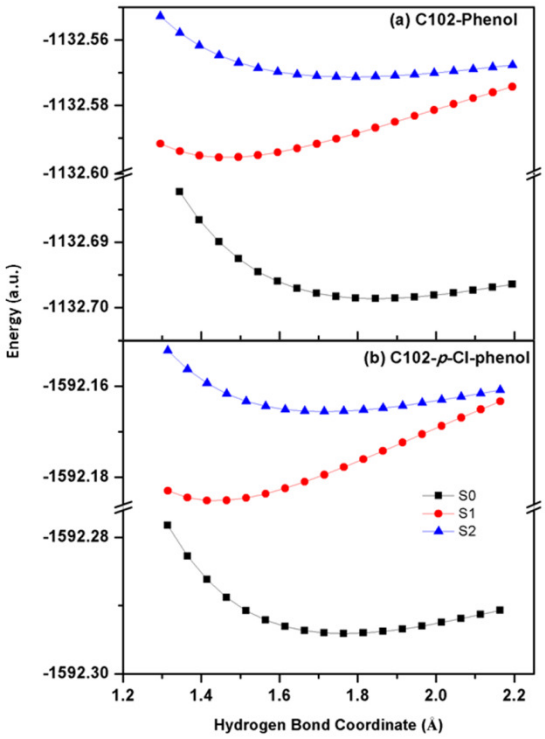

Figure 3.2: Potential energy variation along the H-bond coordinates (i.e., the distance C=O···H-O in angstroms) for the C102-phenol (a) and C102-*p*-Cl-phenol (b) complexes in the first three electronic states (S_0, S_1, S_2). The minima of the S_2 and S_1 potentials correspond to shorter H-bond than in the ground state. For *p*-Cl-phenol, H-bond is shorter than phenol in all electronic states. The H-bond shortening is more drastic in the S_1 state for both phenol and *p*-Cl-phenol.

Table 3.2: Fitting parameters according to the equation 3.1 to the calculated potential energy curve of the 1:1 C102-phenol complex in three electronic states.

Electronic States	r_0(Å)	$U(r_0)$ (a.u.)	D_e (kcalM^{-1})	a (Å^{-2})
S_0	1.845	-1132.6986	8.40	1.47
S_1	1.467	-1132.5958	31.21	1.47
S_2	1.777	-1132.5713	11.36	1.42

Table 3.3: Fitting parameters according to the equation 3.1 to the calculated potential energy curve of the 1:1 C102-*p*-Cl-phenol complex in three electronic states.

Electronic States	r_0(Å)	$U(r_0)$ (a.u.)	D_e (kcalM^{-1})	a (Å^{-2})
S_0	1.762	-1592.2941	10.26	1.52
S_1	1.439	-1592.1851	31.51	1.48
S_2	1.712	-1592.1656	12.41	1.50

Table 3.4: TD-DFT/B3LYP/6-31G** calculated electronic transition wavelengths (nm) of free C102, C102-phenol and C102-*p*-Cl-phenol complexes in gas phase. Corresponding oscillator strengths are given in the parentheses.

Transitions	C102	C102-phOH	C102-*p*-ClphOH
$S_0 \rightarrow S_1$	341 (0.3391)	407 (0.0011)	391 (0.0004)
$S_0 \rightarrow S_2$	298 (0.0045)	357 (0.3262)	354 (0.3938)

The energy, strength, and nature of the transitions in the H-bonded complex can be obtained from the TDDFT calculations. Two lowest energy transitions in isolated C102, C102-phenol and C102-*p*-Cl-phenol complexes are shown in **table 3.4**. C102 shows a strong $S_0 \rightarrow S_1$ transition band originating at 341 nm. Our theoretical calculation predicts a strong transition ($S_0 \rightarrow S_2$) at 357 nm for C102- phenol complex. In addition to this, a very weak low-energy transition ($S_0 \rightarrow S_1$) was predicted at 407 nm which may be ascribed as a dark state. In the C102-*p*-Cl-phenol complex, the transitions were similar to those of the C102-phenol complex. From the frontier molecular orbitals (**Figure 3.3**) of the H-bonded complex, it may be stated that the $S_0 \rightarrow S_1$ transition is of CT character, where electron density dominantly moves from the phenol moiety to C102. Because the excited-state hydrogen bond shortening is the most dramatic.

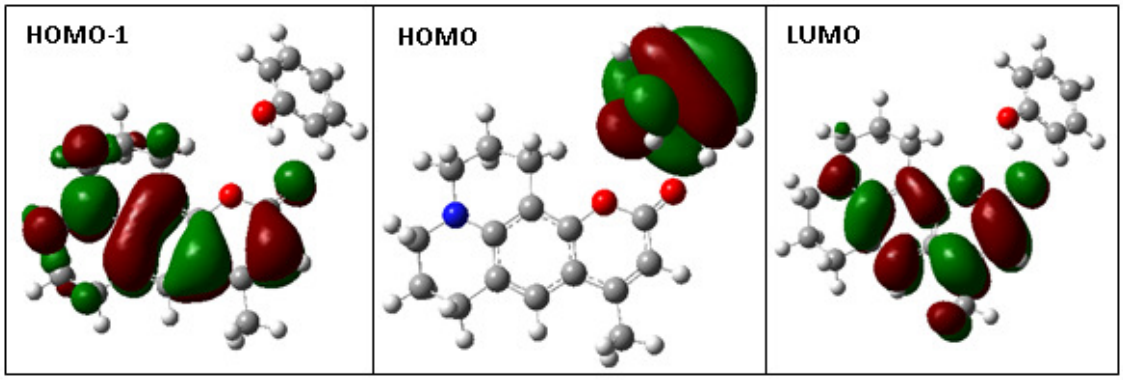

Figure 3.3: Frontier molecular orbitals (MOs) of C102-phenol hydrogen-bonded complex. For S_2 transition (HOMO-1 → LUMO) electron remains on coumarin moeity but for S_1 transition (HOMO → LUMO) electron moves from the phenol to the coumarin unit.

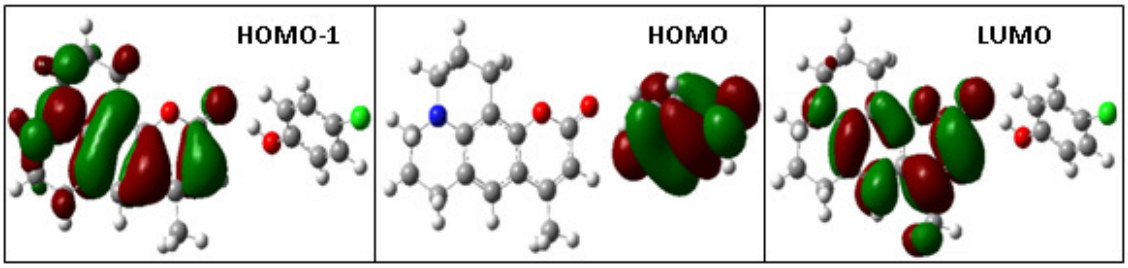

Figure 3.4: Frontier molecular orbitals (MOs) of C102-*p*-Cl-phenol hydrogen-bonded complex. For S_2 transition (HOMO-1 → LUMO) electron remains on coumarin moeity but for S_1 transition (HOMO → LUMO) electron moves from the *p*-Cl-phenol to the coumarin unit.

in the S_1 state of the complex, this CT may be aided by the excited-state hydrogen bonding. In the case of $S_0 \rightarrow S_2$ transition, electron density remains on C102 moiety of the C102-phenol complex before and after excitation, and hence it is locally excited (LE) in nature and possess a strong oscillator strength. This observation was also in accordance with that of Zhao et al.[75]

3.2.2. Steady-state absorption and emission measurements

Figure 3.5 represents absorption spectrum of ~12 μM C102 in cyclohexane in the presence of different concentrations of the H-bond donors (phenol or *p*-Cl-phenol). In the absence of any donor, the absorption spectrum of C102 exhibited vibrational structures (characteristics of absorption bands of most fluorophores in nonpolar solvents) with absorption maximum at 362 nm. Our calculation in the gas phase predicted the lowest energy $S_0 \rightarrow S_1$ transition at 341 nm (405 nm by Zhao et al.[75]). On addition of phenol the absorption band gradually shifted to longer wavelength along with the development of an additional shoulder at ~395 nm. Similar observation was reported for the C102-phenol in TCE.[77] From our theoretical calculation, it may be inferred that the absorption band originates from a superposition of both the absorption from the $S_0 \rightarrow S_2$ transition of the H-bonded complex and the $S_0 \rightarrow S_1$ transition of the free C102. The calculated absorption maximum of the $S_0 \rightarrow S_2$ transition of the complex was red-shifted by 16 nm from the $S_0 \rightarrow S_1$ absorption band of free C102. The relative contribution of the complex increases to that of the free C102 as the amount of phenol increases which accounts for the gradual red shifting of the absorption band at progressively higher concentration of phenol. Another noticeable feature was that at low phenol concentration (≤34 mM) a clear isosbestic point was observed at 368 nm indicating formation of the 1:1 C102-phenol complex between C102 and phenol. However, at the higher phenol concentration, the isosbestic region becomes defocused. This may be due to the formation of higher order C102-$(\text{phenol})_n$ complex (n = 2,3 etc). For *p*-Cl-phenol, the 395 nm band increases more effectively on increasing the *p*-Cl-phenol concentration, and the isosbestic point was found to be at 369 nm. The red-shifting of the absorption band was more prominent in *p*-Cl-phenol, indicating better H-bonding donating ability of *p*-Cl-phenol over phenol (**Figure 3.5**).

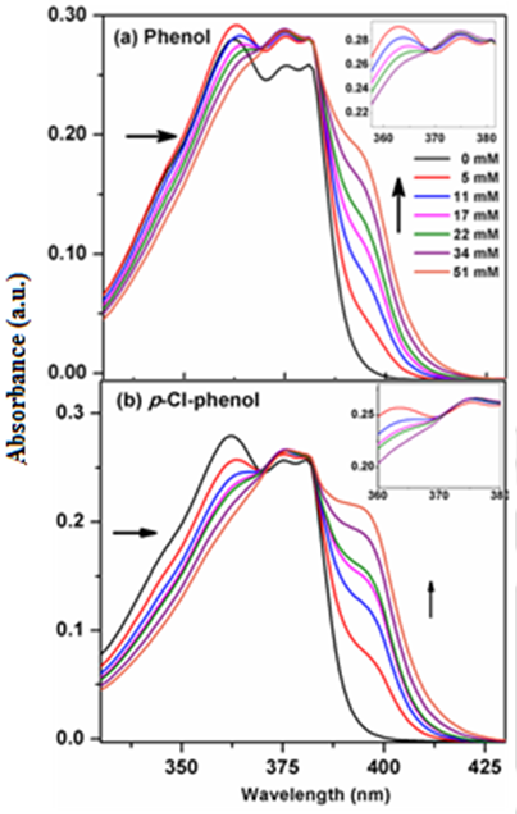

Figure 3.5: Absorption spectra of C102 in cyclohexane in the presence of different concentrations (0-51 mM) of phenol (a) and *p*-Cl-phenol (b). The inset shows the magnification of the isosbestic region in both cases.

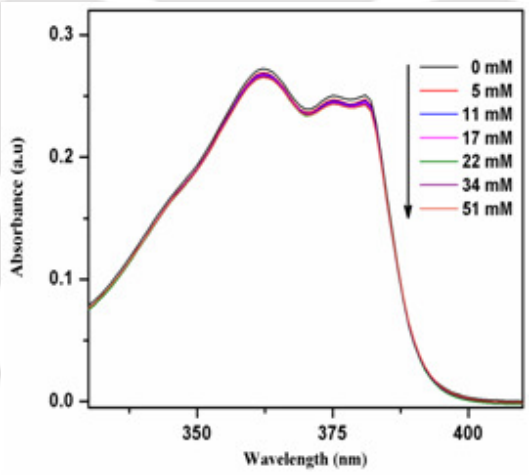

Figure 3.6: Absorption spectra of C102 in cyclohexane in the presence of different concentrations (0-51 mM) of anisole.

Interestingly, anisole did not show any effect on the absorption spectrum of C102 in the same concentration range (**Figure 3.6**). In polar solvents- acetonitrile or methanol, phenol

did not alter the absorption spectrum of C102 (**Figure 3.7**). This may be due to direct involvement of the solvent molecules in H-bond formation with either C102 or phenol or both, and hence, the intermolecular C102-phenol H-bonding may be masked.

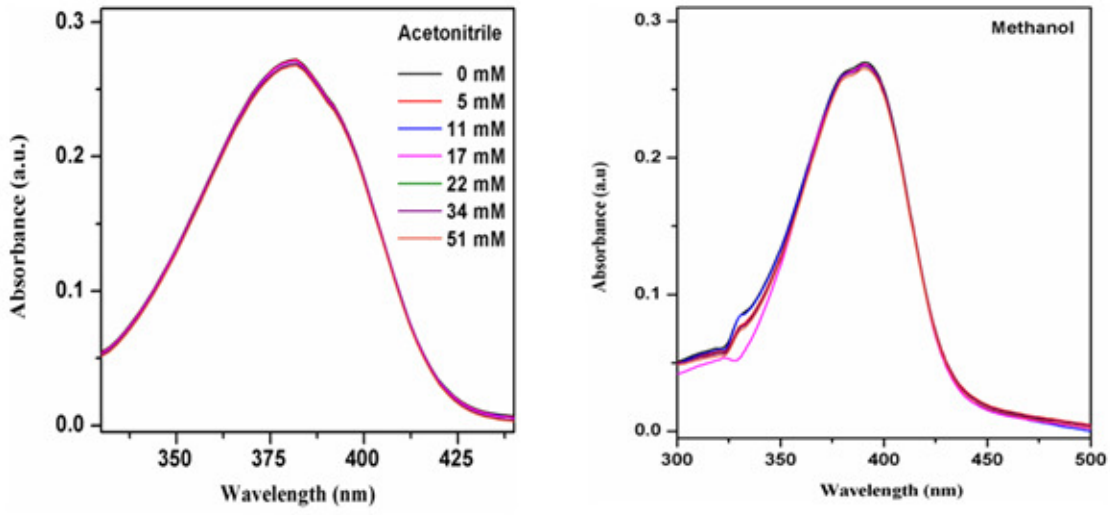

Figure 3.7: Absorption spectra of C102 in acetonitrile (left panel) and methanol (right panel) in the presence of different concentrations (0-51 mM) of phenol.

Emission spectra of C102 in the presence of different concentrations of phenol and *p*-Cl-phenol at an excitation wavelength of 370 nm are represented in **figure 3.8**. Since the excitation wavelength was close to the isosbestic point of the absorption spectra, the transition probability of the both species (free C102 and 1:1 C102-phenol) is the same. Hence, excited-state population will be proportional to the ground-state population of each species. We observed that on addition of phenol the emission intensity of C102 gradually diminishes (**figure 3.8a**).

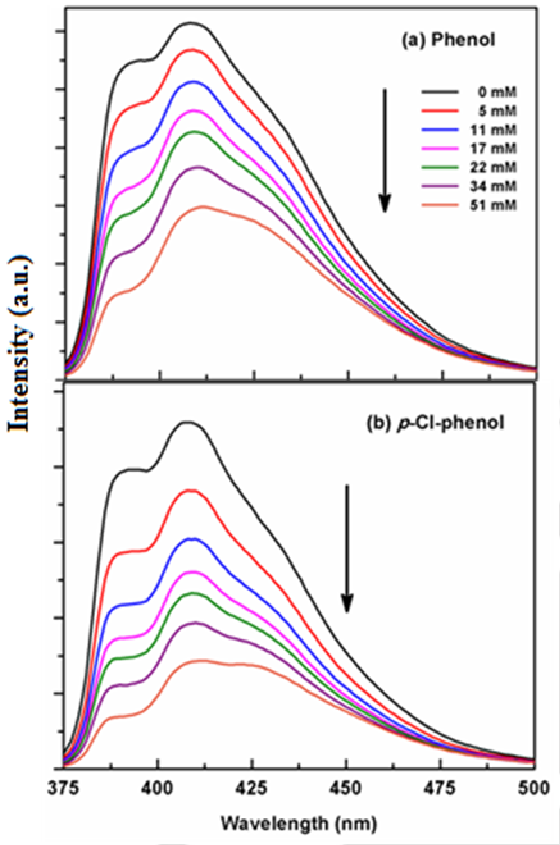

Figure 3.8: Emission spectra of C102 in cyclohexane in the presence of different concentrations (0-51 mM) of phenol (a) and *p*-Cl-phenol (b) at an excitation wavelength (λ_{ex}) of 370 nm.

For *p*-Cl-phenol, the quenching was even stronger (**figure 3.8b**). For example, at 34 mM *p*-Cl-phenol the emission intensity of C102 decreases by a factor of 2.4, while for same phenol concentration fluorescence intensity reduces by a factor of 1.7 from that in the absence of any donor. On the contrary, anisole does not have any effect on the emission spectrum of C102 (**Figure 3.9**). From theoretical calculation (**section 3.2.1**), it was found that *p*-Cl-phenol forms a stronger H-bond with C102 than phenol. Stronger fluorescence quenching by *p*-Cl-phenol and no quenching in anisole may indicate that the H-bonding-assisted mechanism was responsible for fluorescence quenching. Note that phenol did not alter the emission spectrum of C102 in polar solvents- acetonitrile or methanol (**Figure 3.10**).

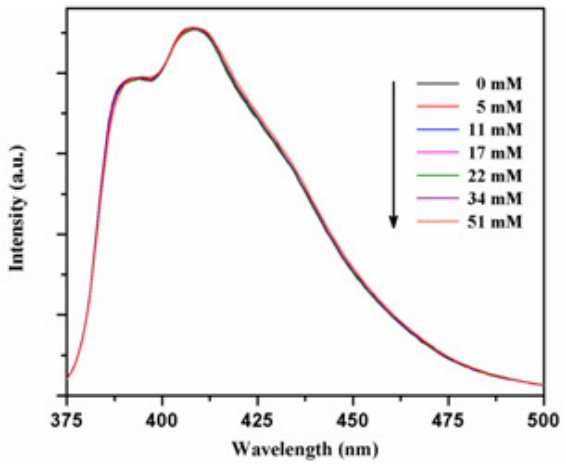

Figure 3.9: Emission spectra of C102 in cyclohexane in the presence of different concentrations (0-51 mM) of anisole at an excitation wavelength (λ_{ex}) of 370 nm.

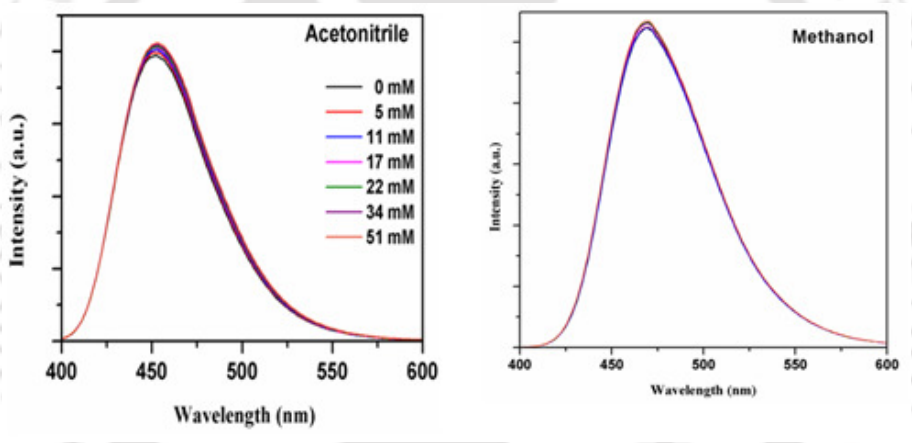

Figure 3.10: Emission spectra of C102 in the presence of different concentrations (0-51 mM) of phenol in acetonitrile and methanol at an excitation wavelength (λ_{ex}) of 370 nm**.**

The fluorescence quenching of C102 in the presence of phenol (or *p*-Cl-phenol) in cyclohexane can be quantified by the using the Stern–Volmer equation-

$$\frac{F_0}{F} = 1 + K_{SV}[Q] \qquad (3.2)$$

where F_0 and F are the fluorescence intensities of C102 in the absence and in the presence of quencher (phenol or *p*-Cl-phenol), respectively. Stern-Volmer plots for phenol and p-Cl-

phenol are presented in **figure 3.11**. The quenching constants (K_{SV}) for the phenol and *p*-Cl-phenol were found to be 25.8 M^{-1} and 42.7 M^{-1}, respectively. The higher quenching constant of *p*-Cl-phenol compared to phenol indicates that H-bonding should have a major role in fluorescence quenching.

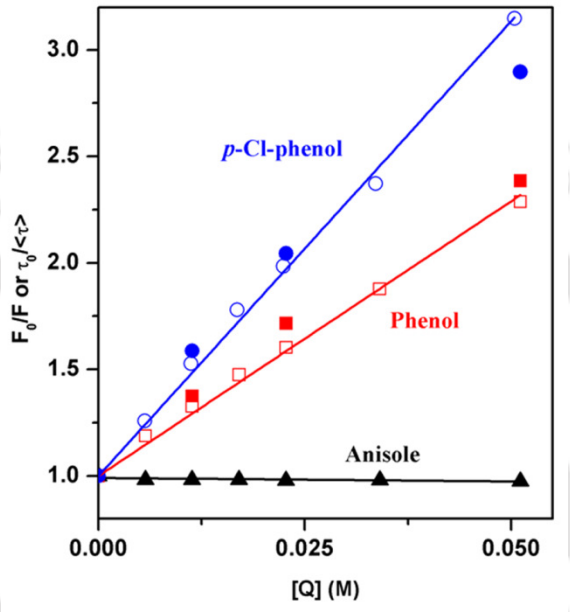

Figure 3.11: Stern-Volmer plot of the fluorescence quenching of C102 in cyclohexane in the presence of the quenchers- phenol (square), *p*-Cl-phenol (circle) and anisole (triangle). Fluorescence quenching is absent for anisole and the most drastic for *p*-Cl-phenol. Time resolved data ($\tau_0/\langle\tau\rangle$) for phenol and *p*-Cl-phenol are displayed as filled symbols.

From the absorption spectra of the C102-phenol systems (**figure 3.5**), it may be expected that excitation at 405 nm should have negligible contribution from the unbound C102 and thus, the emission spectrum will be representative of the H-bonded C102-phenol complex alone. It was confirmed that the emission of the H-bonded complex, when excited at this wavelength becomes almost independent of phenol concentration (**Figure 3.12**). Note that the emission of the complex was much weaker that free C102. For example, at 11 mM

phenol, the emission intensity of C102-phenol decreases dramatically by a factor of 16 compared to free C102.

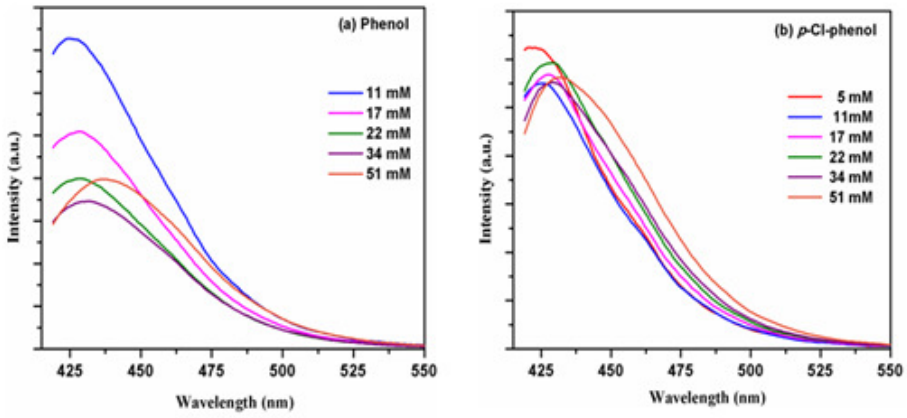

Figure 3.12: Emission spectra of C102 in cyclohexane in the presence of different concentrations (0-51 mM) of phenol (a) and *p*-Cl-phenol (b) at an excitation wavelength (λ_{ex}) of 405 nm.

3.2.3. Time-resolved fluorescence measurements

Time-resolved fluorescence measurements were performed by exciting the samples at two different wavelengths- 375 and 405 nm.

When excited at 375 nm, both the free and the H-bonded C102 may be excited. The relative contributions of the excited species should depend on their ground-state population (as the molar extinction coefficient at this wavelength is similar). In the absence of any donor (phenol or *p*-Cl-phenol), fluorescence decay of C102 was exponential with a decay time of 2.7 ns, which is in agreement with literature.[145]

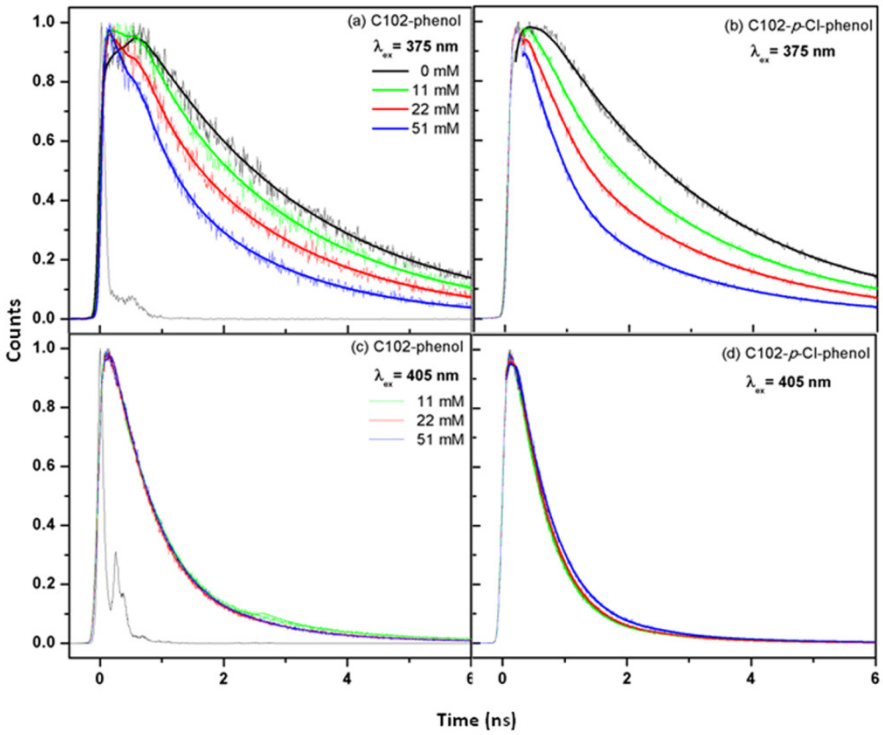

Figure 3.13: Fluorescence transients of C102 in cyclohexane in the presence of different concentrations (0-51 mM) of phenol or *p*-Cl-phenol excited at two different wavelengths- 375 nm and 405 nm. Fluorescence decays (at λ_{em} =405 nm) at 375 nm excitation gradually become faster on the addition phenol or *p*-Cl-phenol but at 405 nm excitation fluorescence decays (at λ_{em} =430 nm) remain almost invariant of phenol or *p*-Cl-phenol concentration.

Figure 3.13 displays the fluorescence decays of C102 in the presence of various concentrations of phenol and *p*-Cl-phenol at the excitation wavelengths of 375 nm and 405 nm, respectively. From the figure, it is clear that the fluorescence decays gradually become faster with increase in the concentration of the H-bond donor (phenol or *p*-Cl-phenol). The fluorescence transients at λ_{ex} = 375 nm could be fitted by a sum of two exponentials

$$F(t) = a_1 e^{-t/\tau_1} + a_2 e^{-t/\tau_2} \qquad (3.3)$$

In the presence of H-bond donor fluorescence decays of C102 were bi-exponential with two distinct time components. For example, the fluorescence transient of C102 in the presence of

11 mM phenol, showed a fast component of 400 ps and a slow component of 2500 ps. With increase in the concentration of phenol, the time constants did not change much but the relative contribution of the components increased. The contribution of the fast component increased from 25 to 54% with increase in the phenol concentration from 11 mM to 51 mM. The fast component was absent in free C102, hence, the decay time could be assigned to the H-bonded complex. Thus, the corresponding amplitude would represent their relative excited-state population. On addition of phenol, the slow component decreased slightly from the lifetime of free C102. Thus, this slower decay times may be attributed to the directly excited free C102 or a LE complex, where the H-bond has been ruptured. Hence, the slight decrease of decay time may be due to the preferential salvation of excited C102 by the polar phenol.

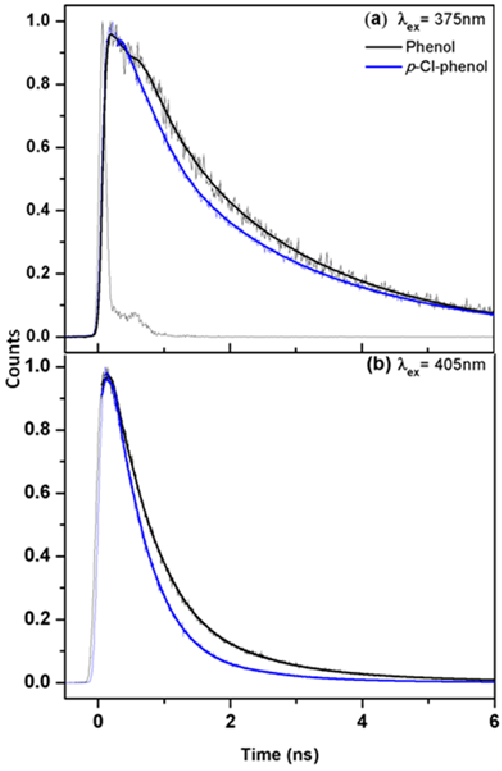

Figure 3.14: Comparison of the effect of phenol and. *p*-Cl-phenol on the fluorescence decay of C102 in cyclohexane at same concentration (22 mM) of phenol or *p*-Cl-phenol. Faster fluorescence decays are observed in the presence of *p*-Cl-phenol than in phenol at both the excitation wavelengths (375 nm and 405 nm).

The effect of excited-state H-bonding on the electronic relaxation can be manifested from the comparison of the fluorescence decays of C102 in the presence of phenol with that

of *p*-Cl-phenol at same concentration (**Figure 3.14**). At a particular concentration, the decay times for both phenol and *p*-Cl-phenol were similar, but the relative contributions of the fast and slow components were different. For example, at 22 mM phenol, the contribution of the fast (410 ps) component was 38%, while at same concentration of *p*-Cl-phenol, the fast component increased to 56%. This increase in the relative contribution of the fast component implied that the fluorescence decay is controlled by the H-bond-regulated mechanism.

The decrease in the relaxation time could be correlated to the Stern-Volmer quenching by-

$$\frac{\tau_0}{<\tau>} = 1 + K_{SV}[Q] \qquad (3.4)$$

where τ_0 is the decay time of C102 in the absence of any quencher (phenol or *p*-Cl-phenol) and $<\tau>$ is the average decay time in its presence. The average fluorescence decay time was calculated by the following equation-

$$<\tau> = a_1\tau_1 + a_2\tau_2 \qquad (3.5)$$

The time-resolved quenching data had a good agreement with the steady-state measurement (**Figure 3.11**).

It is to be noted that at 405 nm free C102 has negligible absorption (**figure 3.5**). Hence, at this excitation wavelength the H-bonded complex will be excited exclusively, thus, the fluorescence decay at 405 nm will be characteristics of relaxation of the hydrogen-bonded complex only. Interestingly, the fluorescence decay (at λ_{ex} = 405 nm) in the presence of 11 mM phenol (or *p*-Cl-phenol) is markedly different from the free C102. With further addition of phenol fluorescence decay remains almost unchanged. The fluorescence decay of the C102-phenol complex was bi-exponential with two distinct components of 610–630 ps and 2.7–1.8 ns. The contribution of the slow component was very small (10–16%) which may be due to directly excited free C102 or the C102-phenol complex with broken H-bond in the

excited state. In the presence of *p*-Cl-phenol, the fluorescence decay was slightly faster than phenol at the same concentration of the donors (**Table 3.5 and Table 3.6**).

Table 3.5: Fluorescence decay parameters of C102 in cyclohexane at various concentrations of phenol at two excitation wavelengths (λ_{ex}) -375 and 405 nm.

	λ_{ex} = 375 nm		λ_{ex} = 405 nm	
[Phenol] (mM)	τ_1/ps (a_1)	τ_2/ps (a_2)	τ_1/ps (a_1)	τ_2/ps (a_2)
0.0	-	2700 (1.00)	-	2700 (1.00)
11	400 (0.25)	2500 (0.75)	640 (0.90)	2500 (0.10)
22	410 (0.38)	2300 (0.62)	610 (0.86)	1800 (0.14)
51	420 (0.54)	2000 (0.46)	630 (0.84)	1700 (0.16)

Table 3.6: Fluorescence decay parameters of C102 in cyclohexane at various concentrations of *p*-Cl-phenol at two excitation wavelengths (λ_{ex}) -375 and 405 nm.

	λ_{ex} = 375 nm		λ_{ex} = 405 nm	
[*p*-Cl-Phenol] (mM)	τ_1/ps (a_1)	τ_2/ps (a_2)	τ_1/ps (a_1)	τ_2/ps (a_2)
0.0	-	2700 (1.00)	-	2700 (1.00)
11	350 (0.40)	2600 (0.60)	470 (0.94)	1700 (0.06)
22	400 (0.56)	2500 (0.44)	480 (0.92)	1400 (0.08)
51	390 (0.71)	2200 (0.29)	510 (0.91)	1500 (0.09)

3.3. Discussion

The most important observation of this work was strong fluorescence quenching of C102 in the presence of H-bond donors- phenol and *p*-Cl-phenol in cyclohexane. However, quenching was not observed in the case of anisole where no H-bond formation is possible. It was reported that absorption and emission spectra of C102 exhibited red-shift in the presence of phenol in another non-interacting solvent TCE[77] but fluorescence quenching was observed the first time using cyclohexane as a solvent. Although both TCE and cyclohexane are non-interacting solvents without any hydrogen bond accepting or donating ability strong fluorescence quenching of C102 observed in cyclohexane only. Fluorescence quenching was also absent in interacting solvents- acetonitrile and methanol and may be attribute to the masking of the intermolecular C102-phenol H-bond by the dominant H-bonding interaction of the solvent with either C102 or phenol. Although TCE cannot form hydrogen bond it may not be a totally non-interacting solvent. Yoshihara and co-workers observed a broad band in FTIR spectrum for the C=O group of C102 in TCE compared to that in DMA.[84] This may be due to the fact that the π electron of the unsaturated solvent or the chlorine atoms may weakly interact with C102 or phenol through halogen bonding [150-151] and as a result the fluorescence quenching may be obscured in TCE but not in cyclohexane.

The mechanism of fluorescence quenching may be clearly understood from the theoretically predicted potential energy states of the hydrogen-bonded complexes. In the absence of H-bonding, the S_1 states of the isolated C102 are LE in character and the S_0–S_1 energy gap is large. Hence, the excited-state relaxation exclusively follows the radiative pathway. This may be the reason for very high quantum yield of C102 in cyclohexane.[145] H-bond formation lowers the energy of the LE state of the complex. In addition to this H-boning creates a new CT state that was absent in the free coumarin. This CT state may be formed due to intermolecular interactions within the strongly H-bonded species in the excited state. On

the basis of the theoretical and experimental results, the excited-state relaxation of the H-bonded complex may be represented by the following relaxation scheme (**Scheme 1.6**). It is already mentioned that at λ_{ex} = 405 nm, only the hydrogen-bonded complex is selectively excited, whereas at λ_{ex} = 375 nm, both the free and the H-bonded complexes are excited. TDDFT calculations shows that oscillator strength of $S_0 \rightarrow S_1$ transition is very low hence, S_1 state is termed as dark state (non-fluorescent). Photoexcitation initially prepares the complex in the S_2 (LE) state. From this state the complex may relax radiatively to the ground state (S_0) or undergo internal conversion (IC) to the S_1 (CT) state. This nonradiative IC may be the main origin of fluorescence quenching, and the fast component (~600 ps) may be due to the dynamics of the process. Zhao et al.[75] first proposed that this local CT (or PET) within the H-bonded complex may lead to fluorescence quenching and is observed by us for the first time.[152] Fluorescence quenching due to PET in the absence of a H-bond has been extensively studied in coumarin–dimethylaniline (DMA) systems.[21, 153-154] However, the oxidation potential of the phenol derivatives is much less favorable for PET than DMA, and C102 is known to be less susceptible to PET among all other coumarins.[21, 153-154] Hence fluorescence quenching through PET without a H-bond could be neglected for the phenol derivatives. This may be the reason for lack of fluorescence quenching for anisole in cyclohexane and all the of phenol derivatives in acetonitrile and methanol. PET within the H-bonded system could be very facile due to the proximity of the donor–acceptor and proper orientation of the donor–acceptor compared with the non H-bonded system. Hence, fluorescence quenching is observed only in the H-bonded C102-phenol or C102-p-Clphenol pairs but not for anisole, although all have similar oxidation potential.

3.4. Conclusion

The theoretical assumption that excited-state H-bond strengthening or shortening may lead to the fluorescence quenching has been observed here for the first time for C102-phenol complex in cyclohexane. Fluorescence quenching was correlated well with the strength of H-bond. The quenching was completely absent for the C102-anisole system, where H-bonding is not possible, and was more prominent for the *p*-Cl-phenol, which forms stronger hydrogen bond with C102 than phenol. Time-resolved fluorescence measurement suggests that the observed quenching is mostly dynamics quenching and aided by excited-state H-bond strengthening. Theoretical calculations indicated that a dark CT state exists in the hydrogen-bonded complex and plays a major role in the fluorescence quenching mechanism. The observed fluorescence quenching of the selectively excited hydrogen bonded C102-phenol complex may be due to the internal conversion (or PET) from the S_2(LE) to S_1(CT) state, and the transfer occurs on a much faster time scale (~600 ps) than the electronic relaxation of the unbound C102. The H-bond may persist for most of the excited-state complex, and only a small fraction (10%) of the complex may dissociate in the excited state and display a slow relaxation similar to unbound C102. This study shows that excited-state hydrogen-bonding dynamics, which are typically proposed to occur on an ultrafast time scale, may alter the fluorescence characteristics of a H-bonded complex on much slower time scale as well.

Chapter 4

Enhancement of H-bond mediated photoinduced electron transfer upon addition of inert solvent: Coumarin 102 in cyclohexane-aniline and toluene-aniline mixtures*

4.1. Introduction

In the previous chapter (**chapter 3**), we have demonstrated the important role of H-bonding in assisting PET within a H-bonded C102-phenol complex.[152] In this chapter, we will represent result on the effect of H-bonding on the PET between C102-aniline complex.

A coumarin dissolved in neat aniline is an ideal model system to study the role of H-bonding in the photoinduced electron transfer (PET) process.[19, 118-119] The photoexcited coumarin may simultaneously serves as an electron acceptor and a H-bond acceptor through its C=O site, whereas, the solvent aniline may act as a donor for both electron and H-bonding through its $-NH_2$ group. For an acceptor dissolved in a neat electron donating solvent, many donors may surround the acceptor and hence, every acceptor molecule would be at contact distance with many donors. Hence, one may expect that effect of H-bonding on PET may be the most effective at this condition. Although theoretical study predicted that C102-AN H-bonding may facilitate PET, there is no experimental evidence of PET when C102 is dissolved in neat AN (**see section 1.4, chapter 1**).

The inefficient PET within C102-AN H-bonded complex may be explained as follows. Due to H-bond donating and accepting ability, aniline may form H-bond with itself and may exist as H-bonded cluster.[155-157]Thus in neat aniline, in addition to C102-AN H-bond AN-AN H-bond may exist and situation may be described as competitive H-Bonding (**scheme 4.1**).

*This work has been published in *Physical Chemistry Chemical Physics* **2014,** *16*, 6159-6166.

Hence, the key H-bonding between C102 and AN may not be efficient enough in guiding electron transfer. In addition to this, due to high polarity of aniline, the C102-AN H-bonding may be weak.[14] Several donor molecules may also present at close contact without forming a H-bond with the acceptor and their contributions to overall PET may be significant. Hence, the effect of H-bonding on PET may be decreased in a neat aniline solvent.

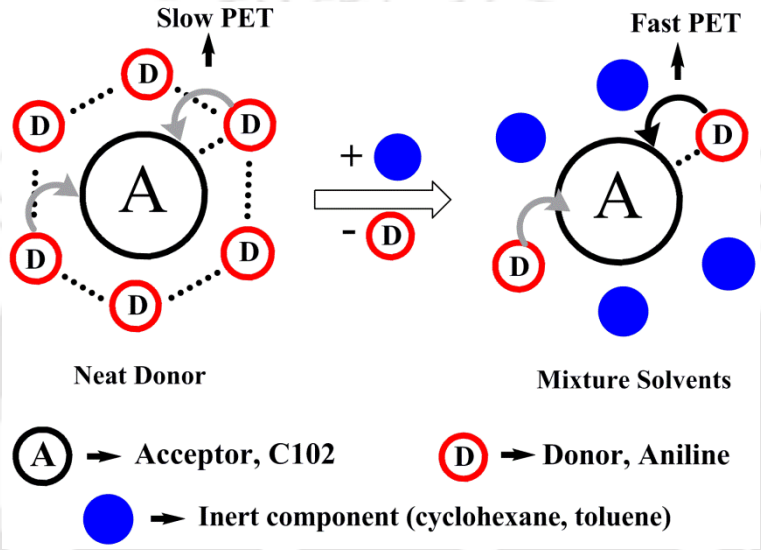

Scheme 4.1: Photoinduced electron transfer (PET) for an excited acceptor (e.g. coumarin 102) in two different situations: in a neat solvent having simultaneous electron donating and H-bonding abilty (e.g aniline) and in a liquid mixture of the solvent containing another non-interacting component. In a neat solvent, competitive H-bonding between acceptor-donor and donor-donor H-bonds suppress the effect of H-bonding of PET (gray arrow). In a liquid mixture, the non-interacting component intervenes the donor-donor H-bond, and hence, strengthens/orients donor-acceptor H-bond for a faster PET process (black arrow).

When an inert non-polar component is simply mixed with aniline the situation may change considerably. The main role of inert component is that it may replace some of the donors from the first solvation shell of the acceptor by disrupting D-D H-bond. Thus, in the solvent mixture, situation may be described as non-competitive H-bonding (**scheme 4.1**)

where only C102-AN H-bonding present. In the non-polar solvent H-bonded association may also be stronger than in the polar solvent.[14] These factors may help to accelerate the PET process.

To demonstrate this concept, we used a binary mixture of aniline and a non-interacting solvent, cyclohexane or toluene and studied PET from aniline to excited C102 by varying the mole fractions of aniline (X_{AN}).

Cyclohexane is a perfect choice for an inert solvent since the aliphatic solvent cannot participate in either electron transfer or H-bonding. This is evident from the Kamlet-Taft parameters of cyclohexane; H-bond donating (α), H-bond accepting (β) and polarity (π^*) parameters have zero contribution (**Table 4.1**).[158] However, cyclohexane and aniline are not miscible for certain compositions (from X_{AN} ~ 0.15 to ~ 0.70) at room temperature. To avoid this problem, we have selected another solvent toluene, which is completely miscible in all proportions with aniline. The quadrupolar solvent toluene is a much weaker electron or H-bond donor than aniline and hence, may practically serve the requirement of an inert solvent in this case.

Table 4.1: Kamlet-Taft parameters, α (hydrogen bond donor), β (hydrogen bond acceptor), and π^* (polarity); dielectric constant (ε_s), $E_T(30)$ and donor number (D_N) of the neat solvents.

Solvent	π^{*a}	α^a	β^a	$\varepsilon_s{}^b$	E_T (30)^b	$D_N{}^b$	λ_{em}^{max} (cal) (nm)	λ_{em}^{max} (exp) (nm)
Cyclohexane	0.0	0.0	0.0	1.9	30.9	0.0	409	408
Toluene	0.54	0.0	0.11	2.4	33.9	0.1	442	423
Aniline	0.73	0.26	0.50	6.7	44.3	35	461	463
DMA	0.73	0.0	0.43	4.4	36.5	27	448	436[c]

[a] From ref 159. [b] From ref 27. [c] From ref 18.

4.2. Results

4.2.1. Steady-state measurements

The absorption maxima (λ_{abs}^{max}) of C102 in the neat solvents –cyclohexane, toluene and aniline – were found to be at 362 nm, 372 nm and 398 nm, respectively. The absorption maximum of C102 showed slight red-shift in toluene compared to cyclohexane but was markedly red-shifted in aniline. This was consistent with the fact that the electronic transition energy of C102 depends highly on the polarity and H-bonding ability of solvents.[145, 147, 152] With increase in the AN content in the mixture, λ_{abs}^{max} shifted gradually towards higher wavelength. (**Figure 4.1**). This red-shift may be due to the formation of the H-bonded C102–AN complex and increase in the average polarity of the medium. Note that an increase in polarity may decrease the H-bonding between C102 and aniline. Hence, the relative contribution of the two effects may vary with mole fractions.

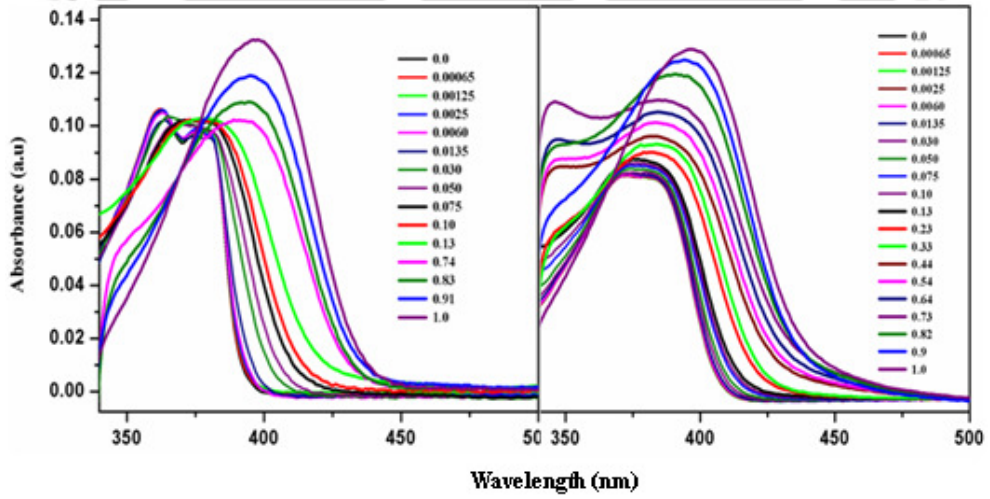

Figure 4.1: Absorption spectra of C102 in the cyclohexane-aniline (left panel) and toluene-aniline (right panel) mixtures at different mole fractions of aniline, X_{AN}.

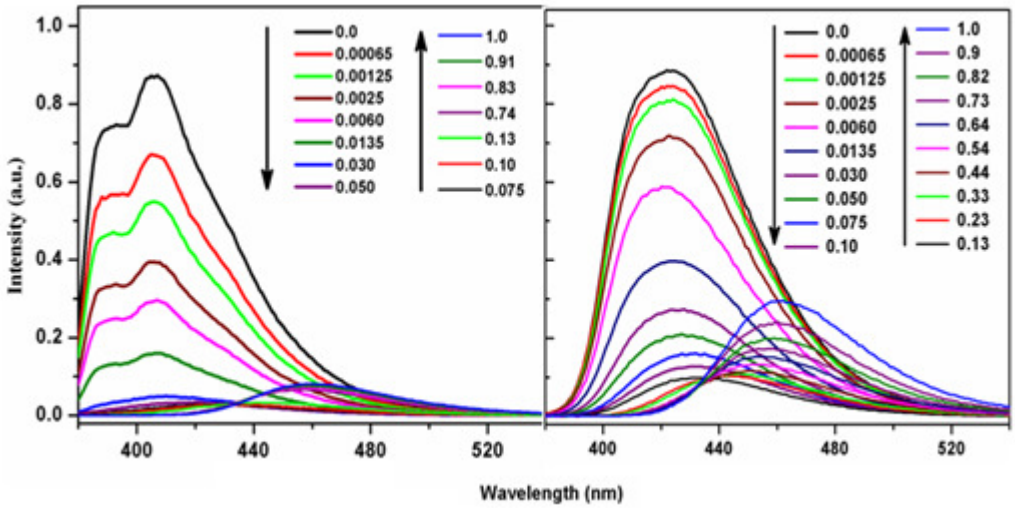

Figure 4.2: Steady-state emission spectra of C102 in the cyclohexane-aniline (left panel) and toluene-aniline (right panel) mixtures at different mole fractions of aniline, X_{AN}. The emission spectra were measured at an excitation wavelength λ_{ex} of 375 nm.

The emission maximum (λ_{em}^{max}) of C102 shows a strong dependence on the polarity and H-bond donating ability of the medium.[160] The emission maxima of C102 in neat cyclohexane, toluene and aniline were observed at 408 nm, 423 nm and 463 nm, respectively (**Figure 4.2**). Moog et al.[160] correlated the emission frequency (ν) of C102 with the Kamlet–Taft[158] polarity (π^*), H-bond donor (α) and H-bond acceptor (β) parameters of twenty different solvents as-

$$\nu = \nu_0 + a\alpha + s\pi^* \qquad (4.1)$$

where ν_0 denotes the emission frequency in the gas phase, a and s are the parameters representing the degree of emission shift due to H-bonding and polarity, respectively. Using reported correlation parameters ($\nu_0 = 24.4 \times 10^3$ cm^{-1}, $a = -2.3 \times 10^3$ cm^{-1} and $s = -2.9 \times 10^3$ cm^{-1} for C102 emission[160] and the Kamlet–Taft parameters of the solvents used in this study, we can calculate the emission maximum of C102 in those solvents (**Table 4.1**). Our observed emission maxima show good agreement with the calculated emission

maxima. Hence, it may be inferred that the red-shifted emission observed in aniline is mainly due to the polarity effect and H-bond donating ability of aniline, and other special solute–solvent interactions (e.g. π–π stacking) are of minor importance. Molecular dynamics (MD) simulation of Castner and co-workers demonstrated that the coupling between DMA and the C151 is very dynamic in nature.[121] No evidence of exciplex formation for C151 was found in the neat DMA or in the diluted mixture with a non-polar solvent. Using theoretical calculation Liu and co-workers demonstrated that the H-bonding strength increases in the excited state for the C102–AN system.[83] As the H-bonding is strengthened in the excited state, it may be attributed that the C102–AN complex as a H-bonded exciplex rather than π–π stacking exciplex.

Figure 4.2 displays the emission spectra of C102 in cyclohexane-aniline and toluene-aniline mixtures. The emission spectrum of C102 exhibited a gradual red-shift on the addition of aniline to the non-polar solvent (cyclohexane or toluene). However, the extent of the spectral shift was much higher at lower mole fractions compared to at higher mole fractions of aniline. This can be inferred by plotting the emission maxima of C102 at different mole fraction against the mole fraction of aniline (**Figure 4.3**).

$$\lambda_{\mathrm{em}}^{\max} = \lambda_{\mathrm{em}}^{\max}(0) + mX_{\mathrm{AN}} \qquad (4.2)$$

For the cyclohexane–aniline mixture, a linear fitting according to the equation 4.2 up to 0.1 mole fraction of aniline gave a slope of 190 ±25 nm per mole fraction but a much lower slope of 19 ±2 nm per mole fraction. Similarly, for the toluene–aniline mixture up to 0.3 mole fraction the slope is 77 ± 2 nm per mole fraction and 23 ± 2 nm per mole fraction at higher mole fraction. We may conclude that H-bonding association is stronger at low mole fractions of aniline than at higher mole fractions. This is consistent with the fact that H-

bonding is generally much stronger in a less polar medium than in a high polarity medium because of solvation.[14]

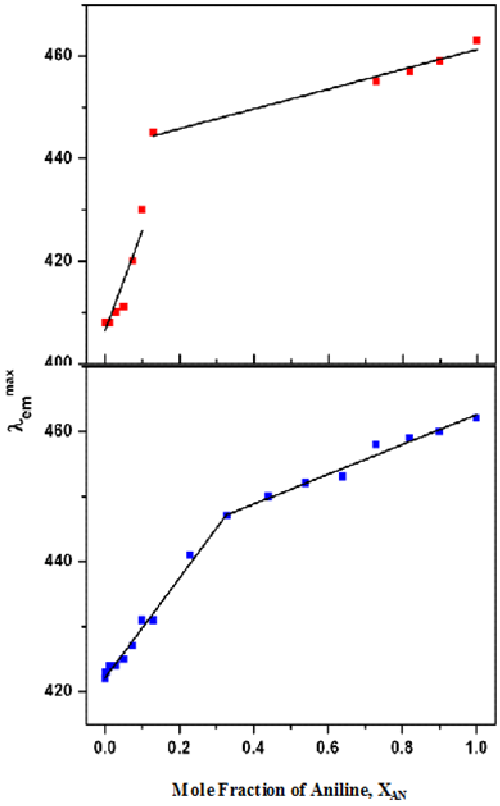

Figure 4.3: Variation of the emission maxima, λ_{em}^{max} (nm), of C102 in the cyclohexane-aniline (top panel) and toluene-aniline (bottom panel) mixtures against the mole fraction of aniline, $X_{AN.}$

The fluorescence quantum yield (QY) of C102 is very high in neat cyclohexane or toluene but moderately decreased in neat aniline (**Table 4.2 and Table 4.3**). However, the QY of C102 in neat aniline is much higher than most of the coumarin dyes indicating that PET from aniline to C102 is much slower compared to other coumarin dyes.[84] Upon the addition of aniline to a solution of C102 in cyclohexane, the emission intensity first decreased up to X_{AN} ~ 0.075, thereafter it increased with further increase in X_{AN} (**Figure 4.2**). The quantum yield at this composition was about 30 times lower than neat cyclohexane and ~15 times lower than neat aniline (**Table 4.2**). For toluene, we have observed similar trend but the extent of quenching was not as dramatic as in cyclohexane. In this case, the QY diminished from 1.0 to 0.14 as X_{AN} increased from 0.0 (neat toluene) to 0.13. At X_{AN} ~0.13 the QY was

~7 times lower than that of neat toluene and ~3.4 times lower than that of neat aniline (**Table 4.3**).

Table 4.2: Emission maxima (λ_{em}^{max}), quantum yield (φ), fluorescence lifetimes (τ) and PET rate constant (k_{ET}) of C102 in the cyclohexane-aniline mixture at different mole fractions of aniline. Excitation wavelength was at 375 nm. Fluorescence lifetimes were measured at corresponding emission maxima.

			Lifetimes (τ/ns)			
X_{AN}	λ_{em}^{max} (nm)	QY (φ)	$\tau_1(a_1)$	$\tau_2(a_2)$	<τ>	k_{ET} (ns^{-1})
0.0	408	1.0	-	2.720 (1.00)	2.720	0.00
0.00065	408	0.64	0.110 (0.24)	2.330 (0.76)	1.810	0.185
0.00125	408	0.56	0.120 (0.26)	2.000 (0.74)	1.500	0.295
0.00250	408	0.45	0.160 (0.27)	1.600 (0.73)	1.210	0.460
0.0060	408	0.27	0.130 (0.37)	1.080 (0.63)	0.760	1.00
0.0135	408	0.122	0.100 (0.55)	0.610 (0.45)	0.330	2.70
0.030	410	0.060	0.080 (0.70)	0.340 (0.30)	0.150	6.20
0.050	411	0.042	0.080 (0.81)	0.260 (0.19)	0.110	8.50
0.075	420	0.031	0.070 (0.92)	0.270 (0.08)	0.080	11.40
0.10	430	0.034	0.070 (0.90)	0.270 (0.10)	0.090	10.40
0.13	445	0.050	0.090 (0.84)	0.370 (0.16)	0.130	7.20
0.74	455	0.30	0.150 (0.29)	1.050 (0.71)	0.790	0.90
0.83	457	0.31	0.150 (0.26)	1.070 (0.74)	0.830	0.84
0.91	459	0.36	0.160 (0.21)	1.200 (0.79)	1.000	0.64
1.0	463	0.47	-	1.400 (1.00)	1.400	0.41

Table 4.3: Emission maxima (λ_{em}^{max}), quantum yield (φ), fluorescence lifetimes (τ) and PET rate constant (k_{ET}) of C102 in the toluene-aniline mixture at different mole fractions of aniline. Excitation wavelength was at 375 nm. Fluorescence lifetimes were measured at corresponding emission maxima.

			Lifetimes (τ/ns)			
X_{AN}	λ_{em}^{max} (nm)	QY (φ)	$\tau_1(a_1)$	$\tau_2(a_2)$	<τ>	k_{ET} (ns^{-1})
0.0	423	1.00	-	2.700 (1.00)	2.700	0.00
0.00125	423	0.75	-	2.430 (1.00)	2.430	0.043
0.0060	423	0.60	0.290 (0.14)	1.880 (0.86)	1.650	0.24
0.030	424	0.27	0.170 (0.23)	0.880 (0.77)	0.710	1.04
0.050	425	0.20	0.120 (0.28)	0.690 (0.72)	0.530	1.51
0.075	427	0.17	0.100 (0.29)	0.600 (0.71)	0.450	1.84
0.10	431	0.16	0.100 (0.34)	0.560 (0.66)	0.410	2.10
0.13	432	0.14	0.090 (0.39)	0.520 (0.61)	0.360	2.45
0.23	441	0.15	0.100 (0.38)	0.610 (0.62)	0.410	2.06
0.44	450	0.20	0.120 (0.35)	0.790 (0.65)	0.550	1.44
0.64	453	0.255	0.130 (0.32)	0.940 (0.68)	0.690	1.10
0.73	458	0.29	0.130 (0.30)	1.060 (0.70)	0.780	0.91
0.82	459	0.32	0.140 (0.26)	1.110 (0.74)	0.860	0.80
0.91	460	0.35	0.140 (0.22)	1.190 (0.78)	0.960	0.70
1.0	463	0.47	-	1.400 (1.00)	1.400	0.41

To ensure the effect of H-bonding on the observed fluorescence quenching of C102-AN, we have used DMA which has no H-bonding ability. **Figure 4.4** displays the absorption and emission spectra of C102 in cyclohexane-DMA mixture at various mole fractions of DMA. Upon addition of DMA to cyclohexane we have observed that both absorption and emission spectra of C102 remains unchanged. Yoshihara and co-workers has also observed no significant fluorescence quenching of C102 in neat DMA.[18] Hence, the observed fluorescence quenching in the case of the C102–aniline system in a nonpolar solvent may proceed via a H-bond assisted mechanism.

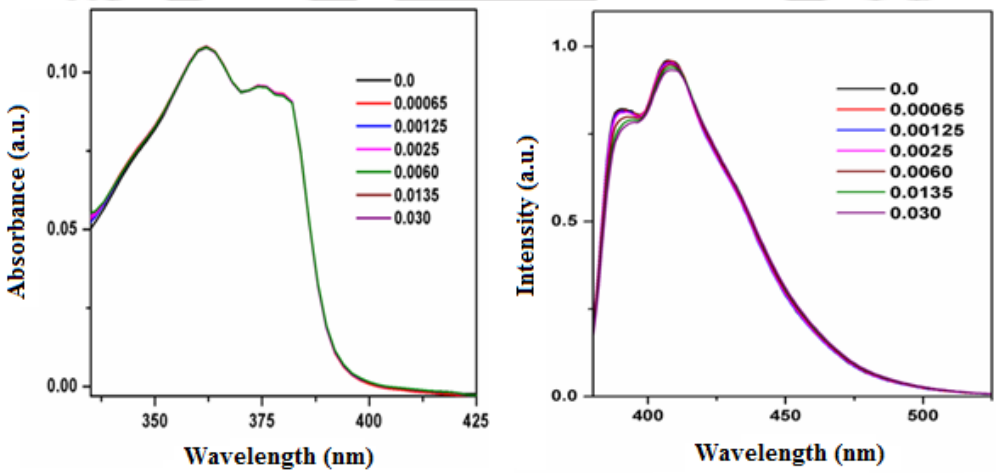

Figure 4.4: Absorption (left panel) and emission (right panel) spectra of C102 in cyclohexane-DMA mixture at different mole fractions of DMA, X_{DMA}.

4.2.2. Time-resolved measurements

The fluorescence decays of C102 were found to be single exponential in all the neat solvents – cyclohexane, toluene and aniline with lifetimes of 2.72 ns, 2.70 ns and 1.4 ns, respectively. Note that the lifetime of C102 is much higher than that of other coumarin dyes, which usually decays completely within few picoseconds.[84] The unusual modulation of

fluorescence observed in the steady-state measurement was also manifested in the lifetime measurements. The fluorescence decays of C102 measured at corresponding steady-state emission maxima at different mole fractions of aniline in cyclohexane-aniline and toluene-aniline mixtures are shown in **figure 4.5** and **figure 4.6**, respectively. The average fluorescence decay time of C102 decreased gradually up to the same critical mole fraction where the emission intensity was minimum. After that, the trend reversed and the average fluorescence lifetime increased with a further increase in X_{AN}. Fluorescence decays were found to be bi-exponential in the solvent mixtures with two distinct time components (**Table 4.2** and **Table 4.3**). The amplitude of the faster component (70–170 ps) increased gradually up to the critical mole fraction after that decreases with further increase in the mole fraction. The fast component may be due to the PET of the H-bonded complex. On the other hand the slower component may be due to either a non-H-bonded complex or an improperly oriented H-bonded complex.

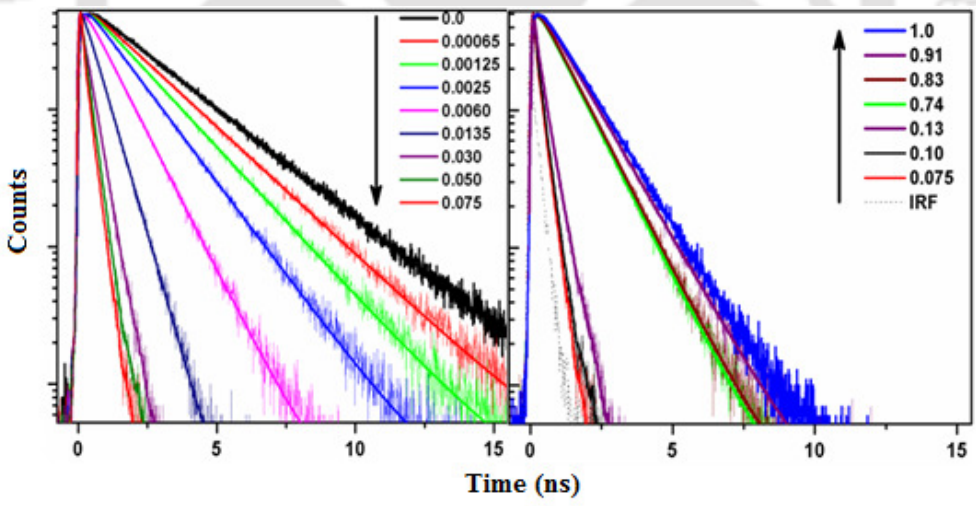

Figure 4.5: Fluorescence decays of C102 in the cyclohexane-aniline mixture at different mole fractions of aniline, X_{AN}. Left panel represents the decay of C102 upto 0.075 mole fraction of aniline which becomes gradually faster. Right panel represents the decay of C102 from 0.075 to 1.0 mole fraction of aniline which becomes gradually slower with enrichment of aniline. Fluorescence decays were measured at corresponding emission maxima of C102.

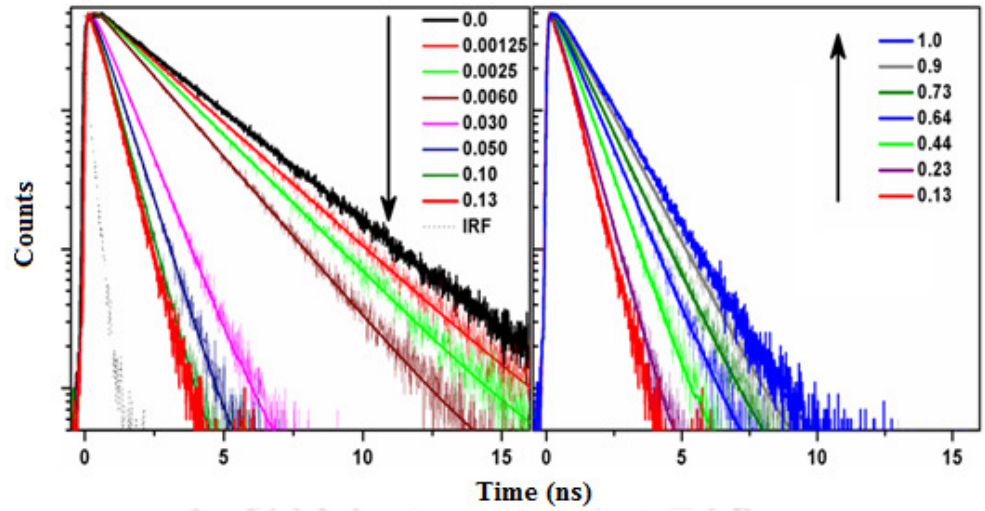

Figure 4.6: Fluorescence decays of C102 in the toluene-aniline mixture at different mole fractions of aniline, X_{AN}. Left panel represents the decay of C102 upto 0.13 mole fraction of aniline which becomes gradually faster. Right panel represents the decay of C102 from 0.13 to 1.0 mole fraction of aniline which becomes gradually slower with enrichment of aniline. Fluorescence decays were measured at corresponding emission maxima of C102.

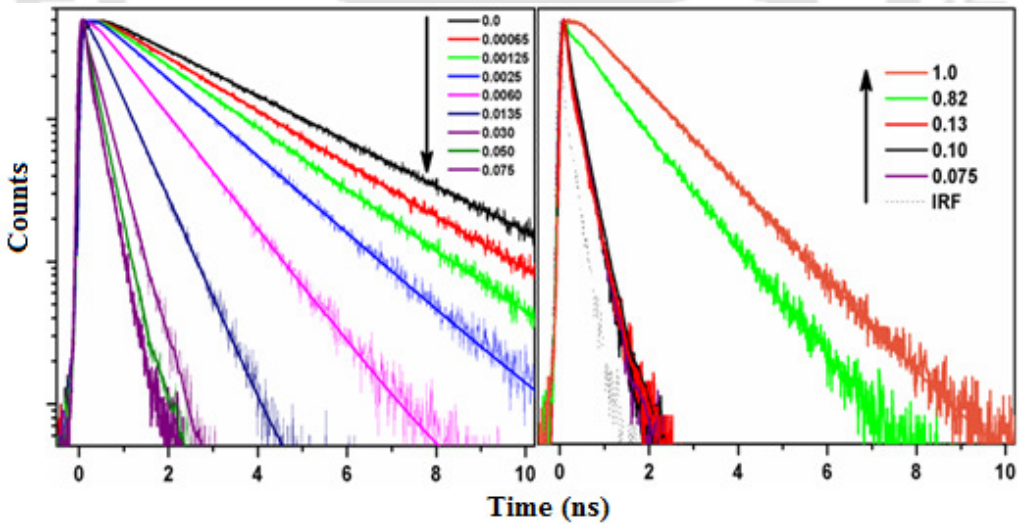

Figure 4.7: Fluorescence decays of C102 in the cyclohexane-aniline mixture at different mole fractions of aniline, X_{AN}. Arrows indicates mode of the lifetime variation with increase in X_{AN}. The decays were measured at 410 nm.

In addition, to understand if there exists any micro-heterogeneity or there is any influence of solvation dynamics, we have also measured the fluorescence decays at the wavelengths corresponding to the emission maxima of C102 in neat solvents (410 nm for cyclohexane; 460 nm for aniline) (**Figure 4.7** and **Figure 4.8**). We observed that the anomalous trend of the fluorescence lifetime remains invariant on the detection wavelengths. For all these three wavelengths, fluorescence decays become faster upon the addition of aniline to the non-interacting solvent (cyclohexane or toluene) up to the critical concentration and afterwards becomes gradually slower upon further addition.

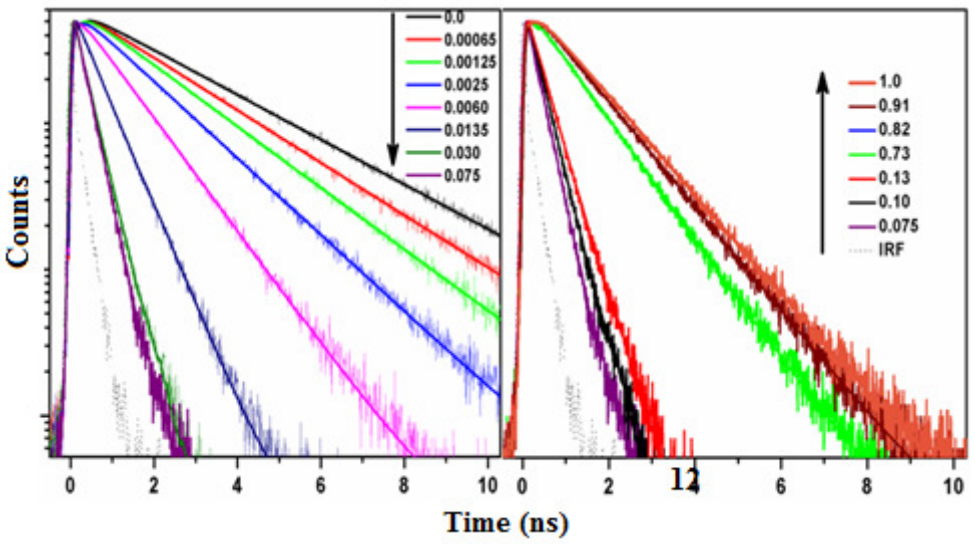

Figure 4.8: Fluorescence decays of C102 in the cyclohexane-aniline mixture at different mole fractions of aniline, X_{AN}. Arrows indicates mode of the lifetime variation with increase in X_{AN}. The decays were measured at 460 nm.

However, comparison of the decays at the critical mole fraction showed that at shorter wavelength decays are faster but progressively become slower at higher wavelengths (**Figure 4.9**). This wavelength dependence may be due to the solvation dynamics of C102 in the solvent mixture. For a mixture of non-polar and polar solvents, solvation dynamics is usually

much slower particularly at a low amount of polar component compared to a neat polar solvent.[161-162] Yoshihara and co-workers reported that the average solvation time in neat aniline is 13.2 ps.[84] We may expect that solvation dynamics in a cyclohexane–aniline or toluene–aniline mixture is much slower particularly at low aniline content.

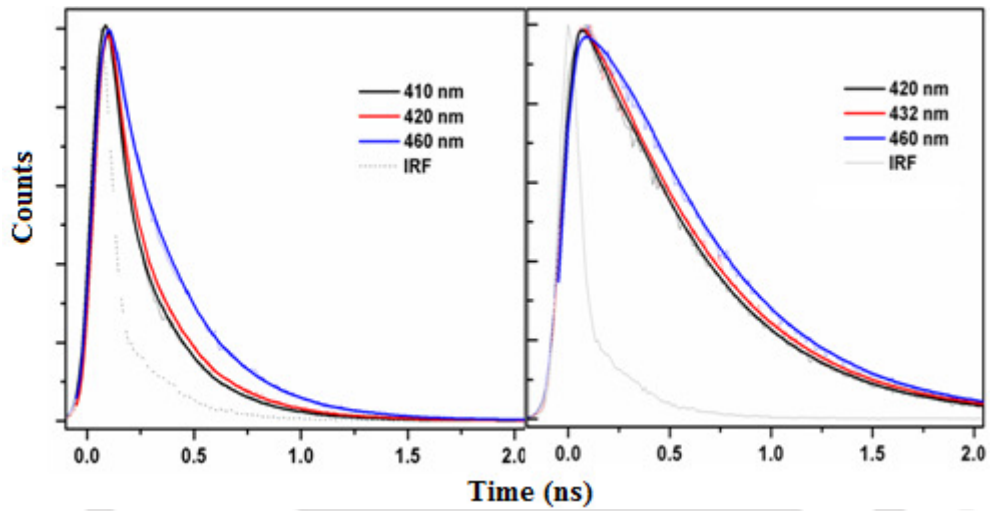

Figure 4.9: Fluorescence decays of C102 in the cyclohexane-aniline (left panel) and toluene-aniline (right panel) mixtures at three different emission wavelengths. Mole fractions of aniline, X_{AN} in cyclohexane-aniline and toluene-aniline mixtures are 0.075 and 0.13, respectively.

4.3. Discussion

4.3.1. Free energy of PET in the non-H-bonded complex

The feasibility of intermolecular electron transfer in a non-hydrogen bonded complex may be determined from the free energy of electron transfer (ΔG^0). For normal PET (i.e. for a non-H-bonded complex), ΔG^0 can be estimated using the Rehm–Weller equation (equation 1.3) [10] The radius of C102 and aniline (also for DMA) were taken as 5 Å and 1.5 Å,

respectively. Thus, r_0 i.e. the center to center distance between C^- and D^+ was assumed to be 6.5 Å.

The calculated values of the free energy of PET are summarised in **Table 4.4**. It is obvious that the free energy changes are positive for the PET from aniline to C102 in the non-polar medium, in neat aniline and in neat DMA. Note that PET in a nonpolar solvent is highly unfavourable because of very high solvation penalty of the generated ion pair as indicated by the very high value of the solvation factor. Hence, it may be concluded that normal PET (i.e. without activation by H-bonding) is not very feasible for C102. Note that other coumarins have negative free energy of PET and display ultrafast PET.[19]

Table 4.4: Energy gap between the ground and excited state of C102 (E_{00} in eV), oxidation potential of the donor (AN and DMA) and reduction potential of the acceptor C102 (in V vs SCE in acetonitrile), correction term for solvation energy with respect to acetonitrile (E_{sol}), ion pair stabilization energy (E_{IPS}) and free energy of electron transfer (ΔG^0).

Solvent	E_{00} (eV)	$E(D/D^+)^a$ (V)	$E(A/A^-)^b$ (V)	E_{sol} (eV)	E_{IPS} (eV)	ΔG^0 (eV)
Cyclohexane	3.23	0.93	2.1	2.378	1.17	1.01
Toluene	3.11	0.93	2.1	1.878	0.923	0.875
Aniline	2.89	0.93	2.1	0.364	0.323	0.178
DMA	3.03	0.76	2.1	0.705	0.434	0.097

[a] From ref 19.[b] From ref 163.

Calculations showed that the PET from AN to C102 is not favorable in neat solvents. However, such calculation of the free energy in the mixture is not straightforward, but possibly may be taken as intermediate between the two neat solvents. Nevertheless, we

observed fast PET in the binary mixture especially at the low mole fractions. The rate of electron transfer (k_{ET}) at various compositions of the liquid mixtures can be estimated as

$$k_{ET} = \frac{1}{\tau} - \frac{1}{\tau_0} \qquad (4.3)$$

where τ and τ_0 represent the fluorescence lifetime of C102 in the presence and in the absence of donor, respectively.

Figure 4.10 displays the variation of PET rate in the solvent mixture against mole fraction of AN. From the figure it is obvious that the PET rate is much higher for a diluted mixture of aniline than for neat aniline. Thus, the PET process in the mixture may be activated by some mechanism.

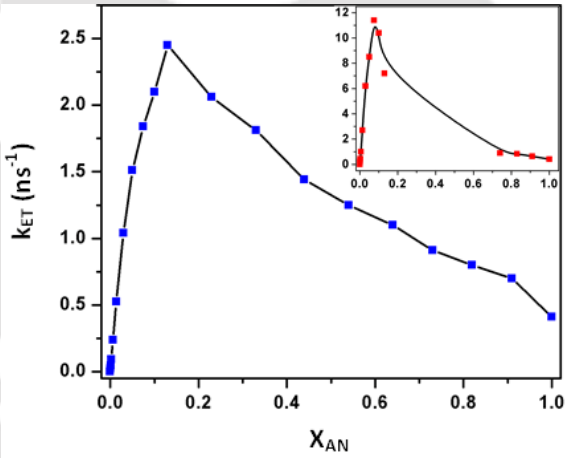

Figure 4.10: Variation of the photoinduced electron transfer rate constant, k_{ET} of C102 in the toluene-aniline mixture against the mole fraction of aniline, X_{AN}. The inset represents the same for the cyclohexane-aniline mixture.

4.3.2. Mechanism of PET in the H-bonded complex

The intermolecular PET between C102 and aniline may be aided by H-bonds. The possibility of PET within the H-bonded C102–aniline complex has been predicted earlier by

Liu et al. using TDDFT calculation.[83] According to their model, photo-excitation prepares the LE (S_2) state of the complex (**Scheme 4.2**). They also predicted that in addition to this there is a low-lying CT, (S_1) state which corresponds to the transfer of an electron from an orbital (HOMO) localized on AN to an orbital (LUMO) localized on C102. The LE state is fluorescence active but the CT state is non-emissive (dark) and the equilibrium between the fluorescent LE state and the non-fluorescent CT state may control the overall quenching.

Herbich et al. proposed a similar fluorescence quenching mechanism by intermolecular electron transfer for a H-bonded complex of pyridine with a heteroaromatic dye in hexane.[164] An activation mechanism of PET, by the intermolecular H-bond, was anticipated by Mataga and co-workers. According to them, H-bonding may lower the ionization potential of the acceptor while increasing the electron affinity of the acceptor. As a result, the PET between the two moieties may occur even if the standard thermodynamics estimates large positive ΔG values for the process.[14, 165] Any factor that can increase the H-bonding strength, in principle, favors the PET. The strengthening of the H-bonding in the excited state should have an important effect in facilitating the PET. Liu et al. showed that the H-bond energy of the 1:1 C102–aniline complex increases from 25.96 kJ mol^{-1} in the ground state to 37.27 kJ mol^{-1} in the electronically excited state.[83] In the H-bonded complex, a change in the redox potentials in the excited state induced by the H-bond strengthening effect facilitates the PET process.

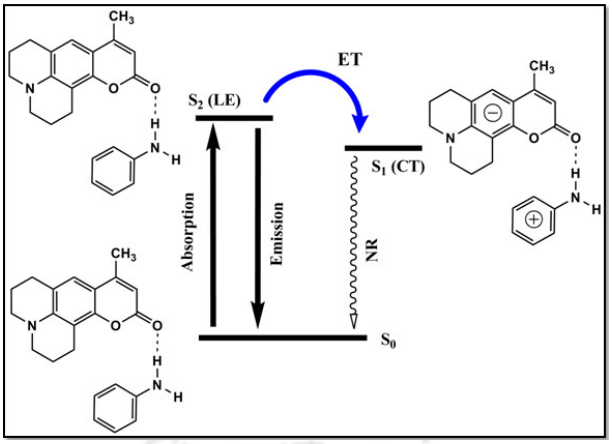

Scheme 4.2: Relaxation scheme of the H-bonded complex – absorption and emission are indicated by upward and downward solid arrows respectively; electron transfer (ET) from the S_2 (LE) state to the S_1 (CT) state is shown by a blue curved arrow; and non-radiative (NR) transition is represented as wavy arrow.

4.3.3. Unusual modulation of PET

Since the H-bond assisted PET is much more effective compared to non-H-bonded PET, the strength of the H-bonding may be the major factor in controlling the PET rate. It is important to know how solvent property affect on the H-bonding strength i.e., whether H-bonding is stronger in the nonpolar solvent, the solvent mixture or in neat aniline? FTIR investigation of Palit et al. on a similar system – C102 – in non interacting solvent TCE, neat aniline and in a TCE–aniline mixture, however, could not provide a conclusive answer.[84] In the region of the C=O stretching frequency of C102, another band due to self associated aniline complicates their result. Hence, determination of the association constant for the C102–aniline complex was not possible.

However, it is assumed that H-bonding in a non-polar medium is much stronger than in polar solvents due to solvation of the donor and the acceptor. For a C102–phenol H-bonded complex, we observed fast PET in cyclohexane but no PET in polar acetonitrile. With

increase in the aniline content the polarity of the mixture increases. The stronger H-bonding at low mole fractions is consistent with the higher emission shift observed at low mole fractions of aniline than at a higher aniline content. Hence, it can be assumed that H-bonding association is stronger at low mole fractions than at higher mole fractions.

The anomalous fluorescence modulation i.e. quenching followed by enhancement can be explained based on the relative stability of the LE and the CT excited states in addition to the dependence of the H-bonding strength on the solvent medium. It is understandable that due to a larger dipole moment, the CT state may be stabilized in polar solvents to a much higher degree than the LE state. At very low mole fractions, due to low polarity, H-bonding is strong but the CT state is not stabilized. Hence, at low mole fraction fluorescence from the LE state is dominant. However, at very high mole fractions, due to higher polarity the CT state is stabilized but the H-bonding is weak and hence, PET occurred mostly via a non-H-bonding pathway. Thus at a critical mole fraction, both the factors may have an optimum influence and the PET rate is the highest.

The faster PET in the solvent mixture than in neat aniline may also be explained on the basis of the competitive vs. non-competitive H-bonding in neat and mixture respectively. **Scheme 4.1** displays the probable compositions of the first solvation layer of the acceptor (C102) in neat aniline and in the solvent mixture. Note that for C102 dissolved in neat aniline, H-bonding is competitive, both C102–AN and AN-AN H-bonds may coexist. However, at low mole fractions of AN, the presence of a large number of the non-interacting component (cyclohexane or toluene) may disrupt the AN–AN H-bond. Subsequently, the key H-bonding between C102 and AN may strengthen or realign for facile electron transfer.

4.4. Conclusion

In summary, we observed unusual fluorescence modulation when an electron donating solvent aniline was gradually added to a non-interacting solvent (cyclohexane and toluene) containing the acceptor fluorophore C102. Both the fluorescence quantum yield and the fluorescence lifetime first quench up to a particular mole fraction of aniline, thereafter increase upon further increasing the mole fraction of aniline. The observed fluorescence quenching is in accordance with PET assisted by excited state H-bond strengthening of the H-bonded donor–acceptor (aniline–C102) complex as predicted in a theoretical study. The reversal of quenching was rationalized by the dependence of the H-bond strength, and the stability of the CT state in the medium. The study emphasized that the importance of H-bonding for an isolated H-bonded complex is much greater than expected for the same molecule in neat H-bonding solvents. Thus we may conclude that the effect of H-bonding on the photo-physics of a H-bonded complex may be widely different under different circumstances.

Chapter 5

Anomalous photoinduced electron transfer of coumarin 102 in aniline-*N,N*-dimethylaniline mixture*

5.1. Introduction

In the previous chapter (**chapter 4**), we have demonstrated an unusual observation that PET from AN to photoexcited C102 can be accelerated by introducing a non-interacting component (cyclohexane or toluene) to the neat electron donating solvent AN. It was proposed that the H-bond linking the electron donor (D, AN) and the acceptor (A, C102) dictate the PET process. The unusual PET modulation of C102 with X_{AN} was ascribed two possibilities: (1) the D-A (AN-C102) H-bonding itself may be modulated due to change in polarity of the medium as the donor and the inert solvent may have very different polarity or (2) the additional D-D (AN-AN) H-bonding may restrain the D-A H-bonding to adjust optimally for the PET. To distinguish these two effects, in this chapter, we have investigated the PET of C102 in AN-DMA mixture. Both AN and DMA have similar polarity as evident from the Kamlet-Taft parameters of the two solvents (**Table 4.1**), hence, the effect of polarity change in the mixture may be eliminated.

Interestingly, we still observed anomalous PET modulation for C102 in the mixture. The PET rate increases with increase in the X_{AN} upto a particular mole fraction, followed by a decrease of the rate with further increase in X_{AN}. The observed anomalous PET modulation may be due rationalized by considering efficient PET in the 1:1 H-bonded C102-AN complex (only D-A H-bond , non-competitive H-bonding) but less efficient in higher order C102-$(AN)_{n\geq 2}$ complexes (both D-A and D-D H-bonding, competitive H-bonding) where additional

*This work has been published in *Physical Chemistry Chemical Physics* **2014,** *16*, 27096-27103.

D-D (AN-AN) H-bonding may influence the key C102-AN H-bonding and thus retard the PET process.

5.2. Results

5.2.1. Steady-state fluorescence measurement

Figure 5.1 displays the emission spectrum of C102 in AN-DMA mixture at different mole fractions of AN. The emission maximum (λ_{em}^{max}) of C102 in neat AN and DMA were at 438 nm and 463 nm respectively. In the neat solvents the spectrum has two different features. First, the emission maximum in neat AN is markedly red-shifted (~25 nm) compared to that in neat DMA. Second, the emission intensity of C102 in neat AN is about half of the emission intensity in neat DMA. It is already mentioned in the chapter 4 (**see section 4.2.1**) that we have calculated the probable emission maxima of C102 in AN and DMA based on the Kamlet–Taft parameters of the solvents and the empirical emission correlation parameters of C102 obtained by Moog et al. (**Table 4.1**).[160] The experimentally observed emission maxima of C102 in AN and DMA showed good correlation with the calculated emission maxima. The marked red-shift of the emission maximum of C102 in AN compared to neat DMA should be accredited to the additional ability of AN to form H-bonds with C102. The decreased emission intensity (or the quantum yield) in AN may be due to H-bond assisted PET. Note that simple free energy calculation aided by the Rehm–Weller equation predicts unfavourable PET in either of the solvents.[10, 30]

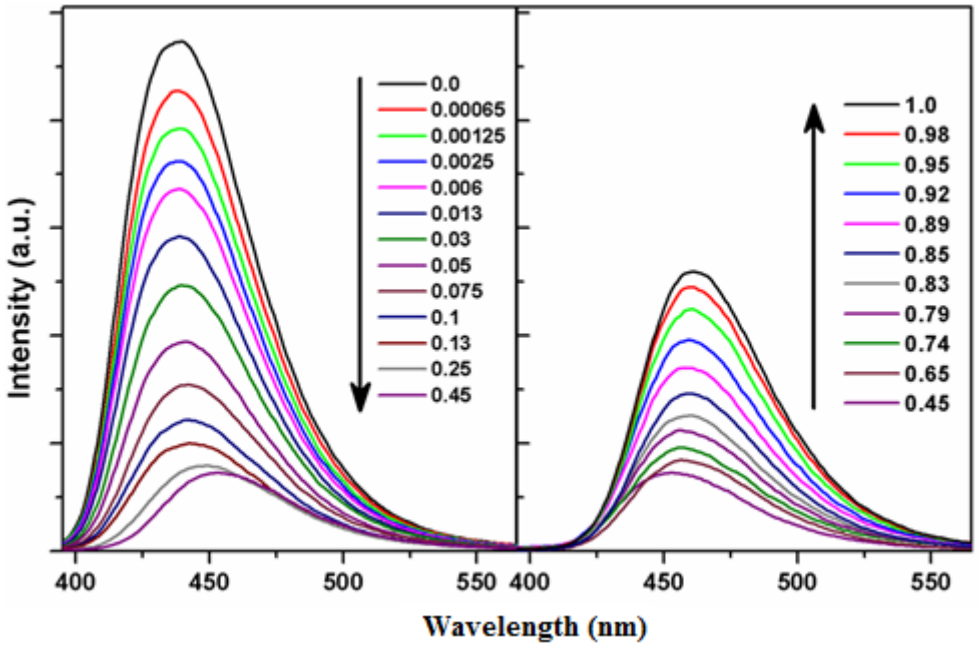

Figure 5.1: Emission spectra of C102 (λ_{ex} = 390 nm) in DMA-aniline mixture at different mole fractions of aniline, X_{AN}. The left panel represents the emission spectra at lower X_{AN} (0.0 to 0.45) whereas, the right panel shows the emission spectra at higher mole fractions (from 0.45 to 1.0). For ease of comparison, the spectrum at X_{AN}=0.45 is retained in both the panels.

In the case of the AN–DMA mixture, it can be expected that a gradual variation of the two parameters – the emission maximum and the emission quantum yield for an ideal behaviour of the mixture. **Figure 5.2** displays the variation of emission maximum of C102 in AN-DMA mixture with increase the mole fraction of AN. Although a gradual shift of the emission maximum was obtained as the mole fraction of AN was increased, there was a distinct slope change at X_{AN} ~ 0.45. At lower mole fractions the extent of spectral shift was higher than at higher mole fractions of AN. A linear fitting using equation 4.2 up to 0.45 mole fraction of AN gave a steeper slope of 36 ± 1 nm per mole fraction but a lower slope of 13 ± 0.5 nm per mole fraction from 0.45 to 1.0 mole fraction of AN. If the spectral shift was assigned to H-bonding, it is possible that two different types of H-bonding are present at AN deficient and AN-rich regions.

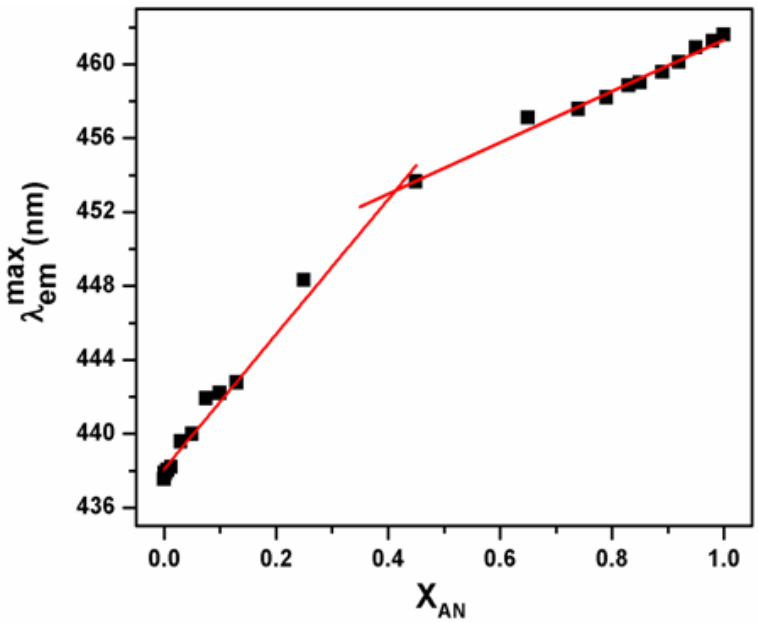

Figure 5.2: Variation of emission maxima of C102 in DMA-aniline mixture with the increasing mole fraction of aniline, $X_{AN.}$

The quantum yield of C102 in the AN–DMA mixture exhibited a strong deviation from ideal behaviour, first there was an abrupt decrease up to a certain X_{AN} ~ 0.45 and thereafter slowly increased to the value of neat AN with increase in the AN mole fraction (**Figure 5.3**). Note that the quantum yield at critical mole fraction (X_{AN} = 0.45) was ~6 times lower than in neat DMA and ~3.5 times lower than in neat AN (**Table 5.2**). Hence, H-bond assisted PET at this mole fraction is much more active than in neat AN.

5.2.2. Time-resolved fluorescence measurement

Figure 5.4 displays fluorescence decays of C102 in AN-DMA mixture at different mole fraction of AN, X_{AN}. Fluorescence decays of C102 in neat AN and DMA were single exponential with time constants of 2.5 ns and 1.4 ns, respectively.

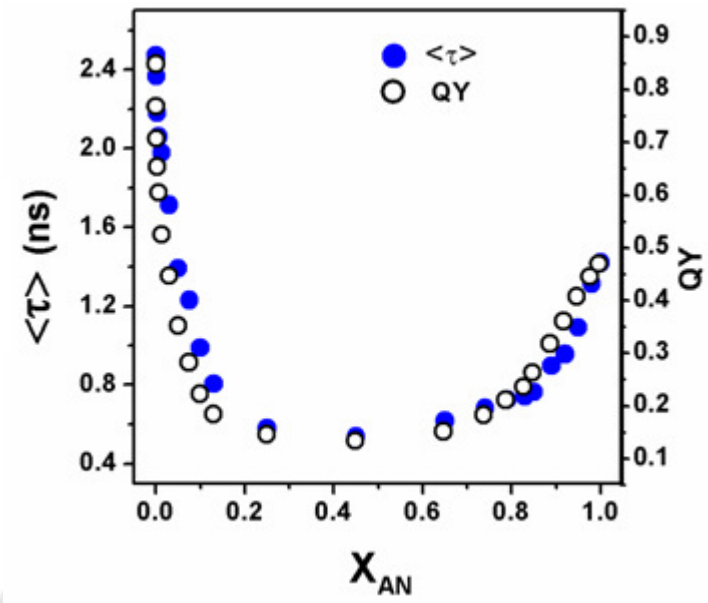

Figure 5.3: Variation of the average fluorescence life time (<τ>) and quantum yeild (QY) of C102 in the DMA–aniline mixture with the mole fraction of aniline, X_{AN}.

Note that the observed fluorescence lifetimes of C102 are much higher compared to the other coumarin dyes in these solvents which usually decay within a few picoseconds in these neat donor solvents.[19] Similar to the quantum yield variation, the fluorescence decays have become considerably faster with increase in the mole fraction of AN up to X_{AN} ~ 0.45. At this critical mole fraction the average fluorescence lifetime of C102 was decreased to 0.35 ns, which was about 4 times lower than the lifetime of C102 in neat AN. This proved that the PET at this mole fraction was much faster than in neat AN. After this mole fraction, with further enrichment of the AN content, the lifetime increased gradually and ultimately reached the bulk value of the lifetime in neat AN. The variation of the quantum yield and fluorescence lifetime showed good agreement (**Figure 5.3**). Although in neat solvent we observed single exponential decay, in the solvent mixture decays become bi-exponential with two distinct time components (**Table 5.2**). This may be ascribed to two different C102 states at different mole fractions. We observed that the contribution of the faster component (100–

550 ps) to the average fluorescence lifetime increased gradually up to the critical mole fraction and thereafter decreased at AN higher mole fraction of AN in the solvent mixture.

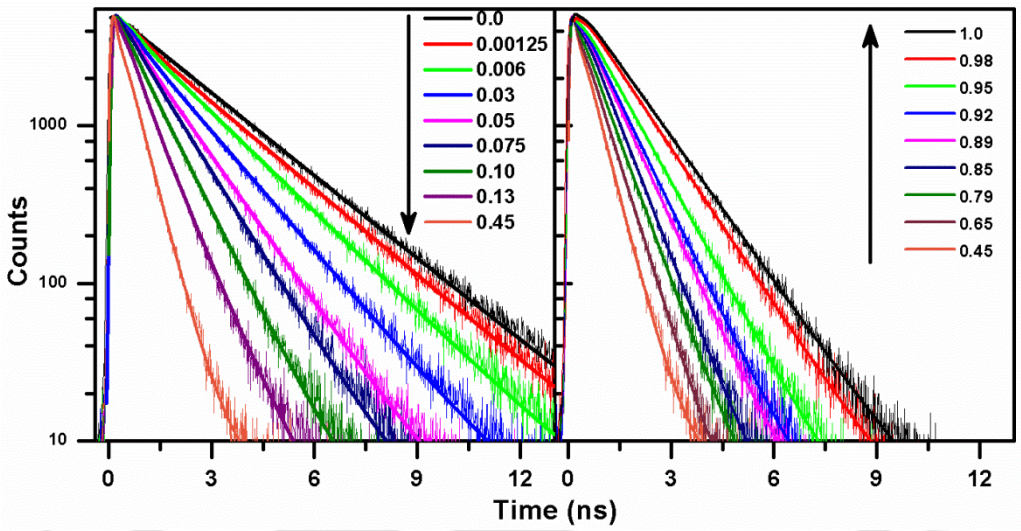

Figuer 5.4: Fluorescence decays of C102 in AN-DMA mixture at different mole fractions of aniline, X_{AN} Left panel represents the decays of C102 in the mixture from 0.0 to 0.45 whereas, right panel represents the same from 0.45 to 1.0. The decays were measured at wavelengths corresponding to the peak of steady-state emission (excitation wavelength was 375 nm).

PET rate for C102 at various AN-DMA compositions can be calculated by using equation 4.5 (**see section 4.3.1**). In that equation τ and τ_0 represent the lifetime of C102 in the presence and in the absence of donor. To estimate the τ_0, we have measured the fluorescence lifetime of C102 in ethylacetate whose polarity is similar to AN (or DMA). Note that in ethylacetate no PET takes place and lifetime was found to be 3.2 ns. The PET rates of C102 at different X_{AN} are given in **Table 5.1. Figure 5.5** displays the variation of PET rate against mole fraction. From the figure it was obvious that the PET rate increased first with increase in the X_{AN}, reached a maximum at X_{AN} ~ 0.45 and then falls off to attain the PET rate in AN. The PET rate at the critical mole fraction was ~6 times higher compared to that in neat AN.

Table 5.1: Emission maxima (λ_{em}^{max}), quantum yield (φ), fluorescence lifetimes (τ) and PET rate constant (k_{ET}) of C102 in the DMA-AN mixture at different mole fractions of aniline, (X_{AN}). Excitation wavelength was at 375 nm. Lifetimes were measured at corresponding emission maxima.

			Lifetimes (τ/ns)			
X_{AN}	λ_{em}^{max} (nm)	QY (φ)	$\tau_1(a_1)$	$\tau_2(a_2)$	<τ>	k_{ET} (ns^{-1})
0.0	437.5	0.85	–	2.50 (1.00)	2.50	0.10
0.00065	437.9	0.77	0.450 (0.26)	2.40 (0.74)	1.90	0.22
0.00125	437.8	0.71	0.420 (0.27)	2.40 (0.73)	1.82	0.24
0.0025	437.9	0.65	0.430 (0.28)	2.20 (0.72)	1.70	0.28
0.006	438.0	0.60	0.350 (0.29)	2.10 (0.71)	1.60	0.32
0.013	438.2	0.52	0.390 (0.28)	2.00 (0.72)	1.55	0.35
0.030	439.6	0.45	0.360 (0.29)	1.70 (0.71)	1.32	0.45
0.050	440.0	0.35	0.300 (0.29)	1.40 (0.71)	1.10	0.60
0.075	441.9	0.28	0.270 (0.29)	1.20 (0.71)	0.93	0.75
0.10	442.2	0.22	0.220 (0.31)	0.99 (0.69)	0.75	1.00
0.13	442.8	0.19	0.280 (0.40)	0.81 (0.60)	0.60	1.40
0.25	448.3	0.15	0.180 (0.49)	0.58 (0.51)	0.38	2.40
0.45	453.6	0.14	0.160 (0.50)	0.54 (0.50)	0.35	2.60
0.65	457.1	0.15	0.100 (0.41)	0.62 (0.59)	0.40	2.20
0.74	457.6	0.18	0.200 (0.31)	0.68 (0.69)	0.53	1.60
0.79	458.2	0.21	0.200 (0.27)	0.73 (0.73)	0.58	1.40
0.83	458.8	0.24	0.200 (0.22)	0.74 (0.78)	0.62	1.30
0.85	459.0	0.27	0.350 (0.19)	0.86 (0.81)	0.80	0.94
0.89	459.5	0.32	0.550 (0.22)	0.94 (0.78)	0.85	0.86
0.92	460.0	0.36	0.440 (0.21)	0.98 (0.79)	0.90	0.79
0.95	460.9	0.41	0.520 (0.06)	1.10 (0.94)	1.10	0.61
0.980	461.2	0.45	0.500 (0.02)	1.30 (0.98)	1.30	0.46
1.0	461.6	0.47	–	1.40 (1.00)	1.40	0.41

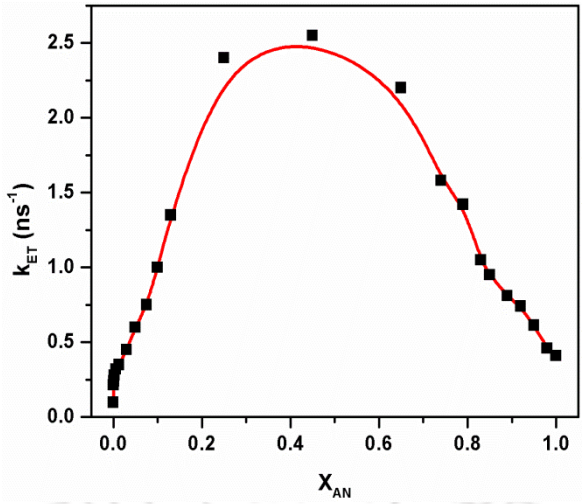

Figure 5.5: Variation of the photoinduced electron transfer rate constant, k_{ET}, of C102 in the DMA–aniline mixture against the mole fraction of aniline, X_{AN}.

5.2.3. Fourier transform infrared (FTIR) measurements

Figure 5.6 displays the FTIR spectra of C102 in C=O and N–H stretching frequency region in neat DMA as well as at various mole fractions of AN. In neat DMA, the C=O stretching frequency of C102 was found at 1731 cm^{-1}, which is characteristic of an unbound C=O group.[84] In the presence of 0.1 mole fraction of AN, a new band was appeared at 1701 cm^{-1}. However, in the presence of a 0.74 mole fraction of AN this new band (1703 cm^{-1}) became more prominent which indicated the formation of a C102–AN H-bonded complex. A similar red-shift of the C=O stretching frequency of C102 in the presence of different concentrations of AN in TCE was reported by Palit and co-workers.[84] At low concentration (0.1 mole fraction) of AN two strong bands appeared at 3376 and 3462 cm^{-1}, and these bands can be assigned to the symmetric and antisymmetric N–H stretching bands, respectively. These two bands resembled closely the N–H stretching bands of the AN–benzene cluster, where only π-stacking interaction could occur.[166-167] However, at a 0.74 mole fraction of AN the two bands exhibited red-shift to 3370 and 3451 cm^{-1}, respectively. This red-shift may be

due to the formation of AN–AN H-bond or a π-stacked dimer. We observed that the absorption bands at higher mole fraction were broader compared to at lower fractions and this indicate the presence of a higher H-bonding network.

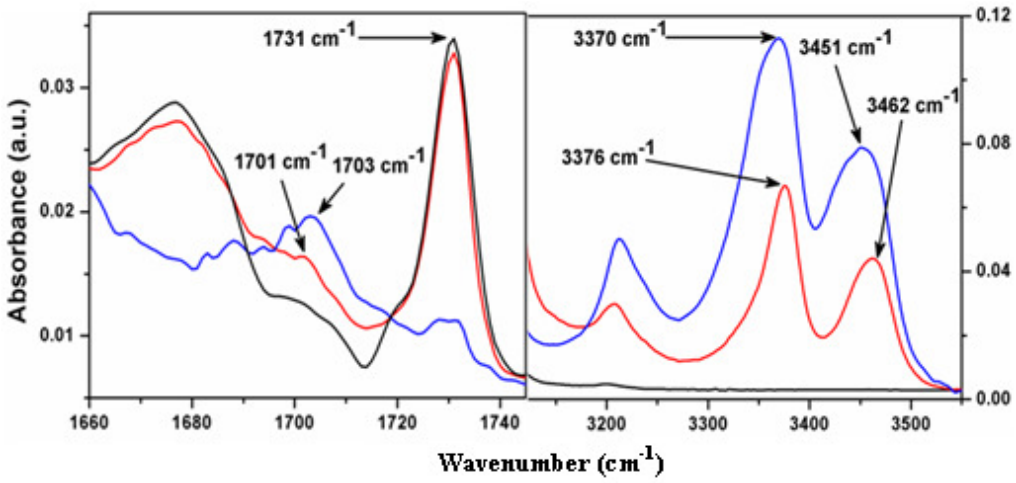

Figure 5.6: FTIR spectra of C102 in neat DMA, (black); in the presence of 0.1, (red) and 0.74 (blue) mole fractions of aniline in AN-DMA mixture. Left panel represents the C=O stretching frequency while right panel represents the N-H stretching frequency at different mole fraction of aniline in the mixture.

5.3. Discussion

The primary goal of this work is to understand the anomalous trend of PET observed for C102 in binary mixture where one component is the H-bonding electron donor AN and the other is an inert component (cyclohexane, toluene or DMA).[30] It was already mentioned that the inert component cannot involve directly in either H-bonding or PET, but it may change the system in two important ways.[30] First, the polarity of the mixture will be different at different compositions if the polarity of this inert component is different from AN. The polarity may also play a significant role on the H-bond assisted PET. The strength of the C102–AN H-bond also depends on the polarity. Also the stability of the LE and CT excited

states of the H-bonded complex may be different with change in the polarity of the medium. Second, the inert component may alter the nature of the H-bonded complex. In neat AN, C102 may form higher order complex C102–AN_n and in addition to the key C102–AN bond, the donor AN may be associated with more AN molecules ($n \geq 2$) by the formation of an AN–AN H-bond. However, in the mixture, particularly at lower AN content, formation of C102–AN 1 : 1 complex is more probable as the inert component may perturb the comparatively weaker AN–AN bond. The overall PET rate may be modulated if the two types of complexes show very different PET.

The propensity for PET without involvement of H-bond can be estimated from the Rehm–Weller equation.[10] In the previous chapter we have calculated the free energy for the PET of C102 in AN and DMA (**see section 4.3.1**) These calculated values in neat AN and DMA were 0.178 and 0.097 eV, respectively.[30] The high positive value shows that in neat AN or DMA non-H-bonded PET is not favourable. Thus in the AN-DMA the free energy will be of intermediate value in the absence of any strong interactions (like H-bond) between the components.

In this work, we have chosen DMA as the inert component. From the Kamlet-Taft parameters (**Table 4.1**) it is seen that AN and DMA have similar polarity hence, polarity of the mixture remains almost same in all the compositions. Thus, the PET modulation due to the variation of polarity in the mixture may be eliminated. Free energy calculations showed that PET from DMA to C102 is not favourable which was confirmed by the experiment that no PET occurs for C102 in neat DMA.[19] Hence, we can easily considered DMA as inert component with respect to PET. In addition to this DMA lacks the H-bond donating ability, hence, may be regarded as inert with respect to C102–AN H-bonding. However, DMA can act as a weak H-bond acceptor and may form H-bond with AN. Indeed, it may act as a better

AN–AN H-bond breaker compared to other inert components like the toluene or cyclohexane used in the previous chapter.[30]

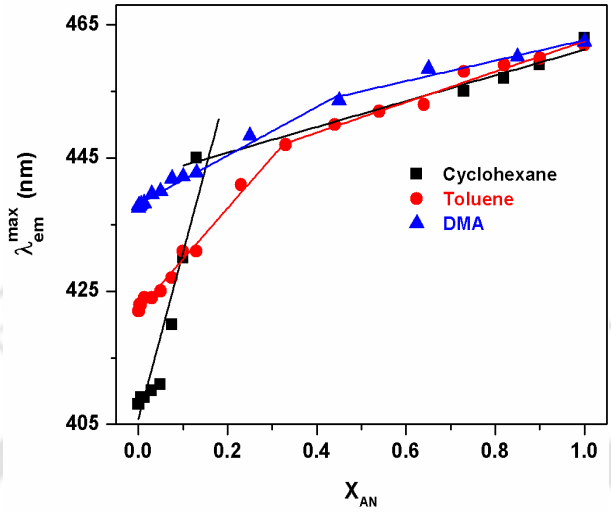

Figure 5.7: Variation of emission maxima of C102 with increasing mole fraction of aniline, X_{AN} in three different solvents.

Here we have observed anomalous trend of the PET modulation of C102 with X_{AN} in the AN-DMA mixture. The results showed that the overall trend of the PET modulation was similar to the AN-cyclohexane and AN-toluene mixtures discussed in the chapter 4.[30] A comparative analysis revealed several characteristic features. **Figure 5.7** displays the shift in emission maxima of C102 in all the three mixtures. From the figure it was observed that the shifting of the emission maxima with the X_{AN} follows two distinct slopes. At lower mole fraction the slope was much steeper than at higher mole fractions. The mole fraction at which the slope change occurs depends strongly on the nature of the non-interacting component. We observed this unique mole fraction at ~0.15, 0.33 and 0.45 in the case of cyclohexane, toluene and DMA, respectively. It is observed that the mole fraction shifted to higher values as the polarity of the solvent increased. **Figure 5.8** shows the variation of PET rate of C102 at various mole fraction of AN (X_C) in the all the three solvent mixtures. From the figure it is

observed that the variations of the PET rate with mole fraction of AN were similar. However, at the critical mole fraction (X_C) at which PET rate was the fastest, gradually shifted to a higher value from cyclohexane to DMA. Finally, we observed that the fastest fluorescence decay at the X_C in each mixture, in all cases the fluorescence decays were much faster than in neat AN (**Figure 5.9**). From the figure it is evident that for the cyclohexane–AN mixture the decay is the fastest whereas, the decay in the toluene–AN mixture is slightly faster than in the AN–DMA mixture.

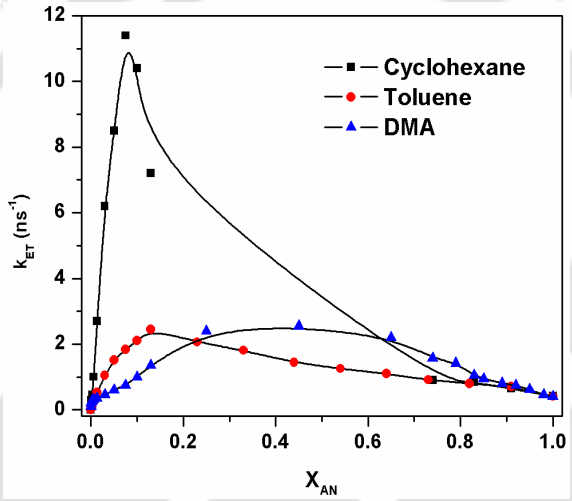

Figure 5.8: Variation of the photoinduced electron transfer (PET) rate constant, k_{ET} of C102 with mole fraction of aniline in cyclohexane, toluene and DMA.

To understand our results, we have considered the probable states of the donor (AN) and the acceptor (C102) in the mixture (**Scheme 5.1**). In the absence of AN, C102 would be solvated in the inert solvent (cyclohexane, toluene or DMA) by non-specific interactions only and hence remain in the free C102 state (no H-bond). On gradual addition of AN, some of the C102 molecule may be held by H-bond forming H-bonded complexes with AN. At lower mole fractions of aniline both 1 : 1 C102–AN complex and free C102 may present. Hence, the relative populations of the two forms will depend on the binding constant (related to the

of the H-bond) of the complex and the AN concentration. After that with further increase in the AN concentration may favour association of more AN molecules with the complex by forming AN–AN H-bonds and hence, higher order complex C102–$(AN)_{n\geq 2}$ may form.

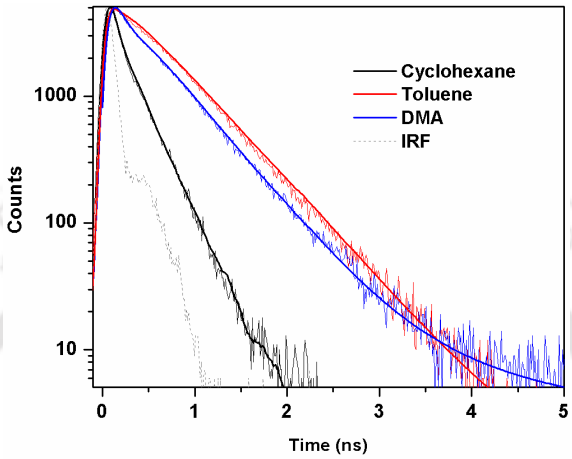

Figure 5.9: Fluorescence decays of C102 at critical mole fraction of aniline in three different solvents.

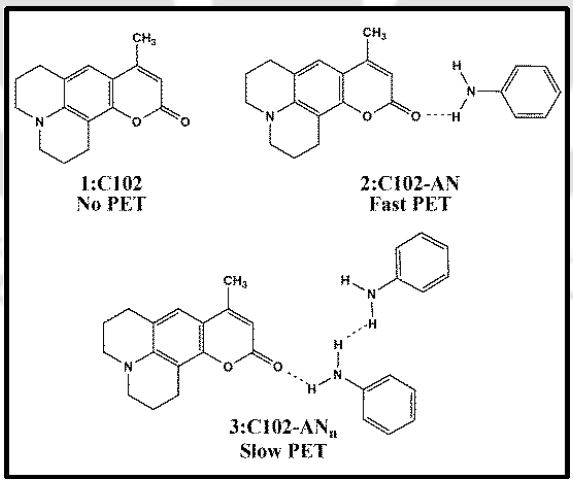

Scheme 5.1 The different states of the acceptor C102 and their assigned PET rates.

To explain the variations of the emission maxima against X_{AN}, we assumed that emission maxima of the 1 : 1 C102–AN complex exhibited significant red-shift compared to free C102. In contrast the higher order C102–$(AN)_{n\geq2}$ complex emitted at slightly higher wavelength than the 1 : 1 complex. On the other hand, the anomalous variations of the PET rate against X_{AN} indicated that the PET rate was much higher in the 1 : 1 complex than in the higher order complex. Hence, the quantum yield and lifetime of C102 should follow the order: C102 > C102–$(AN)_{n\geq2}$ > C102–AN.

At $X_{AN} < X_C$, both C102 and C102–AN complex were present and with increase in the mole fraction of AN the relative population of C102–AN increased. Hence, we observed sharp shift of the emission maximum to higher wavelength. In addition the quantum yield and lifetime decreased with increase in X_{AN}. At $X_{AN} < X_C$, 1 : 1 C102–AN and (C102–aniline)$_n$ complexes remain in the equilibrium. A fraction of the higher order complex increased with increase in the AN. Thus emission maxima exhibited slow increase along with an increase in the lifetime or quantum yield. Hence, PET may be much less favourable in the higher order complex compared to the 1 : 1 complex. In the higher order complex additional AN–AN H-bonding may affect the strength or relative orientation of the key C102–AN H-bonding. The competitive nature of the C102–AN and AN–AN H-bonding may hinder the donor and the acceptor from attaining optimum electronic coupling for the PET process and thus, reduce the PET probability.

The polarity may have a important role on the equilibrium between the free C102 and C102–AN H-bonded complex. In general, H-bond formation is more facile in a non-polar solvent than a polar solvent.[168-169] Cook et al. demonstrated that there is difference in the formation constant of a H-bonded complex between perfluoro-tertbutyl alcohol and tri-n-butylphosphine oxide by five times in magnitude as the solvent polarity was varied.[169] Similarly, we assumed that H-bonding association is the strongest in the least polar

cyclohexane, but varies from moderate-to-weak association in toluene and DMA, respectively. Thus if there is a decrease in association constant, more AN will be required to convert a significant fraction of the C102 molecules into a 1 : 1 H-bonded complex. This may be the reason for different values of X_C in different types of solvent mixture.

In bimolecular PET diffusion generally plays a significant role by controlling the relative distances of the reactants.[170-172] However, we have selected the system in such a manner that only the specific H-bonding interactions between the C102 and AN controlled PET and there is no PET without H-bonding. Since the H-bonding mediated PET is usually considered as direct unimolecular PET, diffusion may not play a key role in this case.

However, it is essential to understand whether the H-bonding modulation responsible for the anomalous PET trend actually occurs in the ground state or in the excited state. FTIR measurements may give important information in that regard. In neat DMA, the C=O stretching frequency of C102 appeared at 1731 cm^{-1}, which indicated that all of the C102 remains in the free form. In the presence of a 0.1 mole fraction of AN, in addition to the absorption peak at 1731 cm^{-1}, an additional band appeared at 1701 cm^{-1} in the mixture due to the formation of a C102–AN H-bond. At an AN rich mole fraction (0.74) the free C=O stretching frequency almost disappeared and the other band appeared at 1703 cm^{-1}. The extent of red-shift of the H-bonded C=O stretch decreased by 2 cm^{-1} at higher mole fraction compared to that at lower mole fraction. This indicated that the C102–AN H-bonding strength may be slightly reduced at higher mole fractions. However, the shift of the H-bonded C=O stretching frequency at different mole fractions of AN was not very large and the spectra was not well resolved enough to make any quantitative statement. The red-shift and broadening of the N–H stretching band at higher AN mole fraction compared to lower mole fraction may be due to the formation of AN–AN H-bond. Thus, we observed only a slight

variation of the C102–AN H-bonding strength with the mole fraction of AN. Hence, the anomalous fluorescence modulation may be governed by the excited state H-bonding effects.

Although, we have observed a dominant role of H-bonding in controlling PET, we cannot validate the H-bond dynamics at early times predicted by Chudoba et al.[65] (H-bond breaking) or Zhao et al.[75] (H-bond strengthening). This is due to the fact that our observations are at much slower time scales compared to them. But it may be affirmed that H-bonding should at least remain for significant moments of the excited state lifetime, i.e. H-bond, if broken at earlier time scales, should reappear at later times to exert an observable influence on fluorescence quenching.

5.4. Conclusion

The PET of the C102–AN system was found to be accelerated unusually at lower concentration of the donor (AN) in the mixture with a non-interacting component. The modulation appears surprising since the non-interacting component can not take part directly in either donor–acceptor H-bonding or in electron transfer. Addition, we have choosen the component in such a way that modulation due to the polarity change of the mixture can be neglected. Still, we observed similar anomalous modulation of PET in an AN–DMA mixture as in other (AN–cyclohexane or AN–toluene) mixtures. The anomalous modulation may be ascribed to the different types of H-bonding complexes present at different mole-fractions. In the 1 : 1 C102–AN complex PET is aided by the site-specific H-bonding between the C=O group of C102 with the $–NH_2$ group of AN. However, the activation may be decreased in the higher order C102–$(AN)_{n\geq2}$ complexes where an additional AN–AN hydrogen bond also exist. In the 1 : 1 complex (non-competitive, only D–A H-bonding) the D–A complex may easily attain optimum geometry in the excited state for facile PET. But in the higher order

complexes, due to competition between the D–A and D–D H-bonding the key D-A H-bond may not be fully effective for PET within the H-bonded complex.

Chapter 6

Reduced fluorescence quenching of coumarin 102 at higher phenol mole fractions in cyclohexane-phenol and anisole-phenol mixtures*

6.1. Introduction

In chapter 3, we have discussed that fluorescence of C102 is strongly quenched by the formation of H-bonding with phenol in a non-polar solvent cyclohexane. We attributed this quenching due to H-bond assisted PET within the H-bonded complex. Although that work gives an important demonstration of H-bond assisted PET but was deliberately restricted to very low concentration of phenol where only 1:1 C102-phenol complex predominantly exists. In this chapter, we have extended the work up to much fuller mole fractions of phenol to capture the complete modulation of fluorescence with the H-bonding environment.

Recall from chapter 4 that the H-bond assisted PET between C102 and AN displays an unusual modulation in aniline-cyclohexane and aniline-toluene mixtures. The C=O group of C102 forms H-bond with the $-NH_2$ group of AN. The AN molecule may also simultaneously linked with other AN molecules forming H-bond at high concentration in the mixture or in neat AN. Since C102 can involve in H-bond assisted PET quenching with phenol and as phenol can form self-associated H-bonding network at high concentrations, we may expect to observe a similar unusual pattern showing a minimum in the variation of quantum yield or lifetime with the mole fraction. In this chapter, we will establish that the prediction was indeed correct indicating the generality of our model of competitive H-bonding.

It is certain that H-bonding situation will modulate in a mixture of H-bonding and non-H-bonding constituents. However, in a solvent mixture, not only the H-bonding environment

*This work has been published in *RSC Advances* **2014,** *4*, 58299-58306.

modulates with mole fractions, other parameters like polarity, π-stacking interactions may also vary. In the case of cyclohexane-phenol mixture, since the polarity of phenol is much higher than cyclohexane it will increase with increase in the mole fraction of phenol (**Table 6.1**). Hence, in addition to the H-bonding modulation, the observed anomalous fluorescence modulation may be the outcome of polarity variation also. To verify the proposition, we have performed fluorescence measurements in phenol-anisole mixture as well. The chemical structures of phenol and anisole differ only by a methyl substitution. Kamlet-Taft parameter shows that both have similar polarity but anisole lacks the H-bonding ability (**Table 6.1**). It can be assumed that both anisole and phenol may have similar tendency to π-stacking interaction with C102. Thus, fluorescence study of C102 in anisole-phenol and cyclohexane-anisole mixtures will act as indicator to monitor the effect of π-stacking interaction and polarity on fluorescence modulation.

Table 6.1: Kamlet-Taft parameters of cyclohexane, anisole and phenol- α (hydrogen bond donor), β (hydrogen bond acceptor), and π^* (polarity).[159]

Solvent	α	β	π^*
Cyclohexane	0.0	0.0	0.0
Phenol	1.65	0.30	0.72
Anisole	0.00	0.32	0.73

6.2. Results

6.2.1. Steady-state measurements

The absorption spectra of C102 in three different mixtures viz. cyclohexane–phenol, anisole–phenol and cyclohexane–anisole at various mole fractions of phenol or anisole are

represented in **figure 6.1**. Absorption maxima of C102 in neat cyclohexane and anisole were found to be at 362 nm and 384 nm, respectively. In cyclohexane-phenol mixture, with increase in the mole fraction of phenol from 0.0 (i.e. neat cyclohexane) to 0.30, the absorption maximum of C102 exhibited red-shift with the development of an additional band at ~395 nm. Similar observation was also noticed for the C102–phenol in TCE.[146]

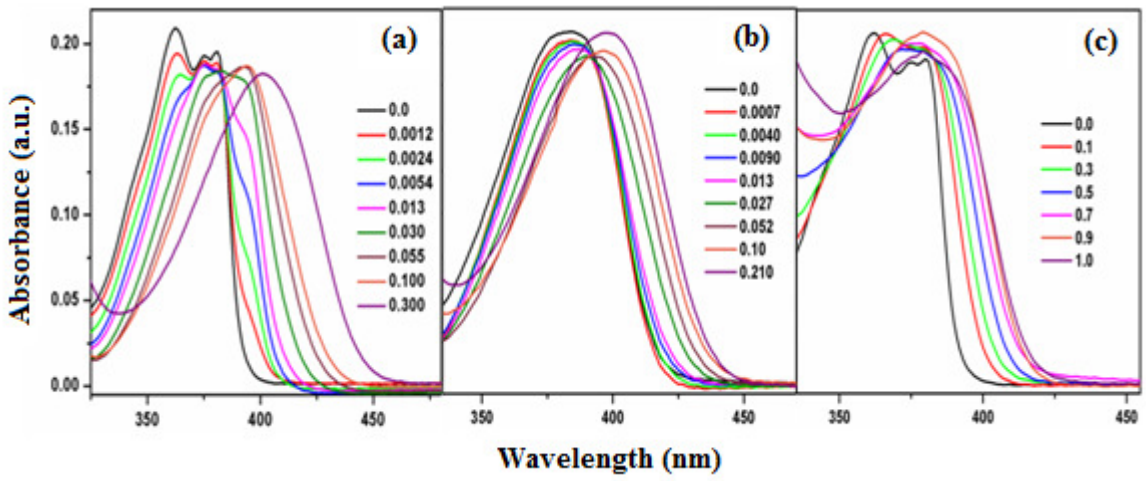

Figure 6.1: Absorption spectra of C102 in (a) cyclohexane-phenol, (b) anisole-phenol, and (c) cyclohexane-anisole mixtures at different mole fraction of phenol (a, b) or anisole (c).

At higher concentration of phenol the new band became more prominent with the subsequent reduction of the absorption band at 362 nm. This may be a due to the variation of polarity and H-bonding ability of the medium. Another important characteristic was that up to 0.030 mole fraction of phenol a clear isosbestic point was observed at 382 nm which may be an indication of the equilibrium between 1 : 1 C102–phenol complex and free C102. However, upon further enrichment of phenol the isosbestic region became defocused. This may be an indication of the formation of higher order C102–$(phenol)_n$ complex (n = 2, 3, etc.). Similarly, the absorption spectrum of C102 in anisole-phenol mixture modulated gradually in a manner that absorption of the higher wavelength side increased with a concomitant

decreased in the lower wavelength side maintaining an isosbestic point at 392 nm up to a high mole fraction (0.10) of phenol. The gradual red-shifts of absorption maximum may be due to the H-bond formation between C102 and phenol. This is because the polarity of the mixture remains similar at various compositions. However, absorption spectra of C102 in cyclohexane– anisole mixture exhibited red-shift with increase in the mole fraction of anisole without any isosbestic point. Since anisole lacks the H-bond formation ability with the C102 molecule, this red shift of absorption spectra may exclusively due to increase in the average polarity of the medium with increase in the mole fraction of anisole.

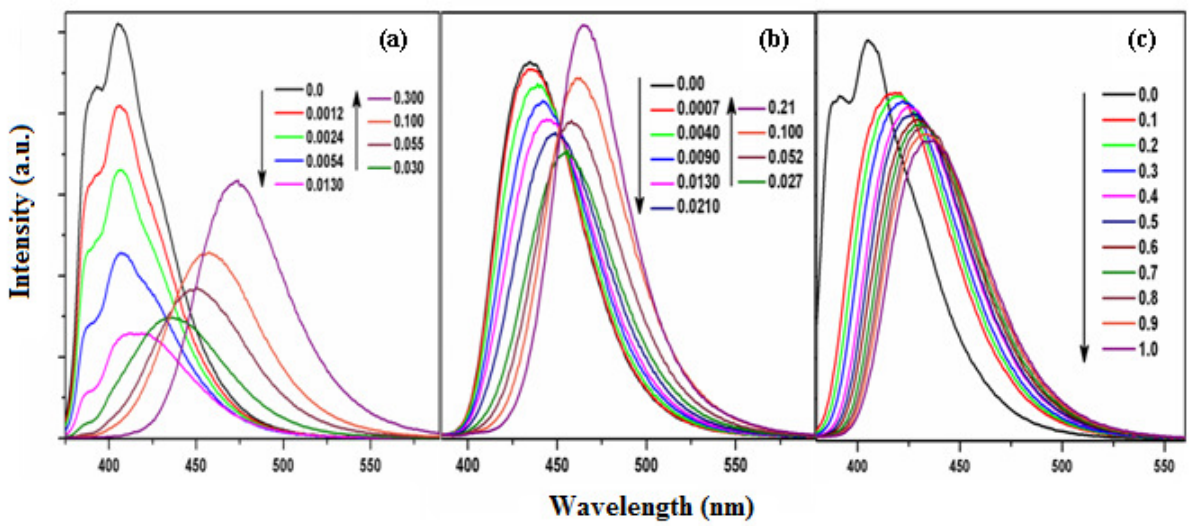

Figure 6.2: Emission spectra of C102 in (a) cyclohexane-phenol (λ_{ex} = 370 nm), (b) anisole-phenol (λ_{ex} = 375 nm) and (c) cyclohexane-anisole (λ_{ex} = 375 nm). In (a, b) fluorescence intensity of C102 decreases with increase in the mole fractions of phenol upto a certain mole fraction, thereafter increases with further enrichment of phenol. In (c) fluorescence intensity monotonically decreases with increase in the mole fraction of anisole.

Figure 6.2 displays the emission spectra of C102 the three solvent mixtures. The emission maximum (λ_{em}^{max}) of C102 is significantly affected by the polarity and H-bonding nature of the medium.[145, 160] The λ_{em}^{max} of C102 in neat cyclohexane and anisole were at 408 nm and 435 nm, respectively. In cyclohexane–phenol and anisole–phenol mixtures the

emission spectra of C102 exhibited gradual red-shift with increase in the mole fraction of phenol. However, the extent (i.e. slope) of the spectral shift was much higher at lower mole fraction of phenol compared to the higher mole fraction of the same. The variation of the emission maxima in frequency ν_{em}^{max} (in cm^{-1}) against mole fraction (x) can be conveniently fitted by the following equation-

$$\nu_{em}^{max}(x) = \nu_{em}^{max}(x=1) - \Delta\nu e^{-kx} \qquad (6.1)$$

where $\nu_{em}^{max}(x=1)$ is the emission frequency in neat phenol (or anisole) and $\Delta\nu$ is the total shift of the emission maxima and k is a constant. The equation can be easily derived as shown below if one assumes that the extent (i.e. slope) of energy lowering is proportional to the difference in energy of the mixture from that of the neat H-bonded or the polar solvent (i.e. at x =1).

$$\frac{d[\nu_{em}^{max}(x) - \nu_{em}^{max}(x=1)]}{dx} = -k[\nu_{em}^{max}(x) - \nu_{em}^{max}(x=1)] \qquad (6.2)$$

Or, $\frac{dy}{dx} = -ky$, where $y = \nu_{em}^{max}(x) - \nu_{em}^{max}(x=1)$ (6.3)

Integrating we obtain

$$y = y_0 e^{-kx} \qquad (6.4)$$

Or, $\nu_{em}^{max}(x) - \nu_{em}^{max}(x=1) = [\nu_{em}^{max}(0) - \nu_{em}^{max}(x=1)]e^{-kx}$ (6.5)

Or, $\nu_{em}^{max}(x) = \nu_{em}^{max}(x=1) + [\nu_{em}^{max}(0) - \nu_{em}^{max}(x=1)]e^{-kx}$ (6.6)

The details of the fitting parameters are given in the **table 6.2**. It is clear that when the H-bonding is involved (in cyclohexane–phenol and phenol–anisole mixtures), the frequency shift levels off at very low mole fraction (**Figure 6.3**). Conversely, when only polarity (in cyclohexane– anisole) is involved the frequency shift almost varies linearly with mole fraction (**Figure 6.2c and 6.3**).

Table 6.2: Fitting parameters of emission maxima against mole fractions in the three solvent mixtures using the equation 6.1. Within bracket represents the standard error.

Solvent Mixture	ν_{em}^{max} $(x = 1)$ (cm^{-1})	$\Delta\nu$ (cm^{-1})	k
Cyclohexane-phenol	21320 (87)	3521 (94)	25.0 (2.0)
Anisole-phenol	21353 (77)	1606 (96)	27.0 (4.5)
Cyclohexane-anisole	22998 (106)	1709 (123)	3.3 (0.06)

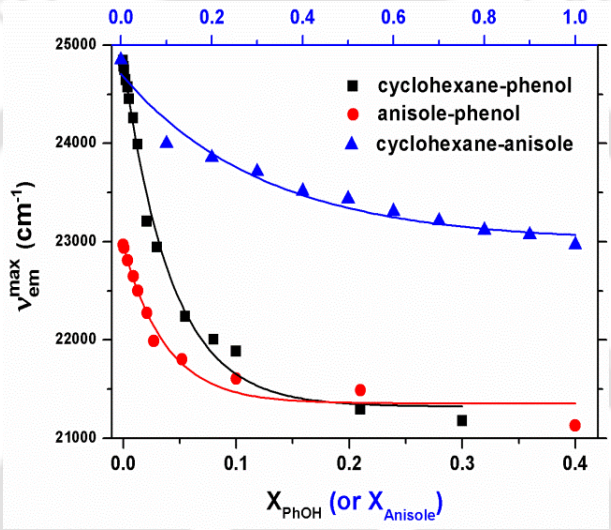

Figure 6.3: Variation of the emission maxima, ν_{em}^{max} (cm^{-1}), of C102 in the three different solvent mixtures against the mole fraction of phenol, X_{PhOH} (or anisole, $X_{Anisole}$).

With increase in the mole fraction of phenol, the emission intensity or quantum yield of C102 displayed the anomalous trend-first decreased up to a certain mole fraction of phenol and thereafter increased with further increase in the mole fraction of phenol (**Figure 6.4**). For the cyclohexane–phenol and anisole–phenol mixtures, the critical mole fractions of phenol were found at 0.013 and 0.027, respectively. However, fluorescence intensity of C102 in the cyclohexane–anisole mixture decreased linearly with increase in the mole fraction of anisole (**Figure 6.4**). This regular trend of fluorescence intensity change may be attributed to the

change in the polarity of the medium with increase in the mole fraction of anisole. Since anisole lacks the H-bonding ability, the anomalous fluorescence modulation of C102 in cyclohexane–phenol and anisole–phenol mixtures may be associated with the H-bonding modulation in the mixture.

6.2.2. Time-resolved measurements

The anomalous trend of steady-state fluorescence variation was also observed from the fluorescence lifetime measurements. **Figure 6.5** and **figure 6.6** show the fluorescence decays of C102 in the three mixtures– cyclohexane–phenol, anisole–phenol and cyclohexane–anisole measured at the respective emission maxima at different mole fractions of phenol (or anisole). In neat solvent fluorescence decays of C102 were found to be single exponential. The flourescence lifetimes of C102 in cyclohexane and anisole were 2.72 ns and 3.3 ns, respectively.

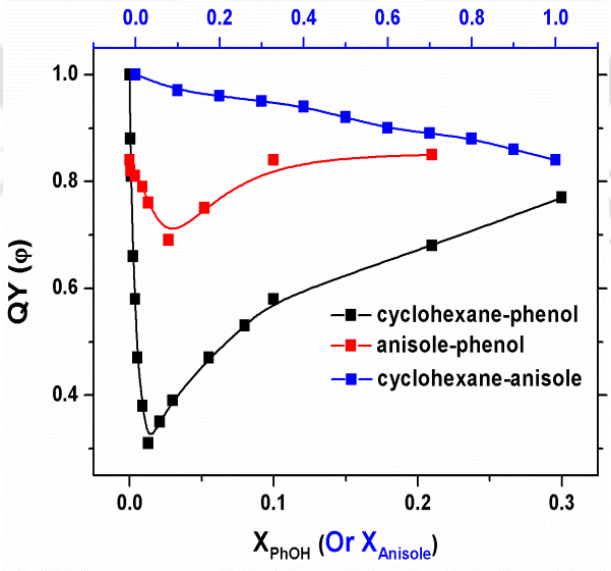

Figure 6.4: Variation of the quantum yield, (QY) of C102 in different mixtures with mole fraction of phenol (or anisole).

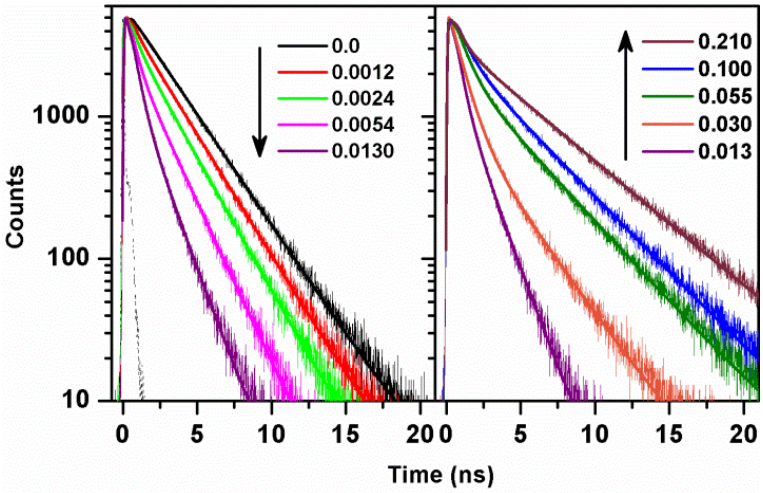

Figure 6.5: Fluorescence decays of C102 in cyclohexane-phenol mixture at λ_{ex} = 375 nm at different mole fractions of phenol. Left panel represents the fluorescence decay in lower mole fraction (0.0 to 0.013), whereas the right panel represents the decay in higher mole fraction (0.013 to 0.21). Fluorescence decays become faster at low concentration region but the trend reverse in the higher region.

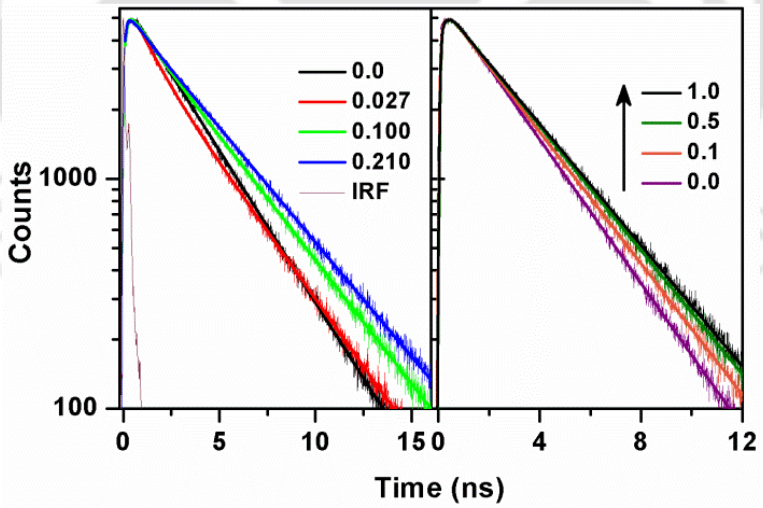

Figure 6.6: Fluorescence decays of C102 in anisole-phenol (left panel) and cyclohexane-anisole (right panel) mixtures at λ_{ex} = 375 nm at different mole fractions of phenol and anisole, respectively.

Table 6.3: Emission maxima (λ_{em}^{max}), quantum yield (φ) and lifetimes (τ) of C102 in the cyclohexane-phenol mixture at different mole fractions of phenol. Excitation wavelength was at 370 nm. Lifetime measuremnts were done at corresponding emission maxima (λ_{em}^{max}).

			Lifetimes (τ/ns)		
X_{PhOH}	λ_{em}^{max} (nm)	QY (φ)	τ_1 (a_1)	τ_2 (a_2)	<τ>
0.0	408	1.0	–	2.72 (1.0)	2.72
0.0005	409	0.88	0.38 (0.24)	2.66 (0.76)	2.10
0.0012	409	0.81	0.37 (0.33)	2.50 (0.67)	1.83
0.0024	409	0.66	0.46 (0.43)	2.30 (0.57)	1.52
0.0040	409	0.58	0.45 (0.51)	2.20 (0.49)	1.27
0.0054	410	0.47	0.42 (0.61)	1.90 (0.39)	1.00
0.009	411	0.38	0.40 (0.68)	1.60 (0.32)	0.79
0.013	423	0.31	0.44 (0.74)	1.50 (0.26)	0.72
0.021	432	0.35	0.77 (0.87)	2.50 (0.13)	0.98
0.030	436	0.39	0.83 (0.84)	2.90 (0.16)	1.16
0.055	449	0.47	0.83 (0.65)	3.80 (0.35)	1.88
0.080	454	0.53	0.86 (0.57)	3.90 (0.43)	2.18
0.10	459	0.58	0.88 (0.53)	4.00 (0.47)	2.36
0.21	460	0.68	0.58 (0.49)	4.90 (0.51)	2.77
0.30	472	0.77	0.58 (0.48)	5.10 (0.52)	2.87

However, in the mixture i.e. cyclohexane-phenol and anisole-phenol fluorescence decays of C102 were found to be bi-exponential with two distinct time components (**Table 6.3 and Table 6.4**). With increase in the mole fraction of phenol the average decay time of C102 gradually decreases up to the same (X_{PhOH} = 0.013) mole fraction at which quantum yield was minimum (**Figure. 6.7**). In the case of cyclohexane–phenol mixture the amplitude

of the faster component (370–860 ps) gradually increases up to this critical mole fraction and thereafter decreases with increase in the concentration of phenol (**Table 6.3**). For anisole–phenol mixture similar trend is observed (**Table 6.4**). It is already mentioned in chapter 3 that the fast component may be due the PET of the H-bonded complex whereas the slower component may be due to either an improperly oriented H-bonded complex or a non-H-bonded complex. However, no significant change of the average fluorescence lifetime of C102 is observed in case of cyclohexane–anisole mixture with increasing the mole fraction of anisole (**Table 6.5**)

Table 6.4: Emission maxima (λ_{em}^{max}), quantum yield (φ) and lifetimes (τ) of C102 in the anisole-phenol mixture at different mole fractions of phenol. Excitation wavelength was at 375 nm. Lifetime measuremnts were done at corresponding emission maxima (λ_{em}^{max}).

			Lifetimes (τ/ns)		
X_{PhOH}	λ_{em}^{max} (nm)	QY (φ)	τ_1 (a_1)	τ_2 (a_2)	<τ>
0.0	435	0.84	-	3.3 (1.00)	3.30
0.0007	436	0.82	0.97 (0.05)	3.2 (0.95)	3.16
0.0040	439	0.81	0.86 (0.09)	3.1 (0.91)	2.97
0.009	442	0.79	1.70 (0.14)	3.2 (0.86)	2.96
0.013	446	0.76	1.90 (0.28)	3.6 (0.72)	2.94
0.027	452	0.69	1.10 (0.32)	3.7 (0.68)	2.84
0.052	455	0.75	0.85 (0.30)	3.8 (0.70)	2.92
0.10	462	0.84	0.74 (0.18)	4.0 (0.82)	3.42
0.21	466	0.85	0.54 (0.18)	4.3 (0.82)	3.65

Table 6.5: Emission maxima (λ_{em}^{max}), quantum yield (φ) and lifetimes (τ) of C102 in the cyclohexane-anisole mixture at different mole fractions of anisole. Excitation wavelength was at 375 nm. Lifetime measuremnts were done at corresponding emission maxima (λ_{em}^{max}).

			Lifetimes (τ/ns)		
$X_{Anisole}$	λ_{em}^{max} (nm)	QY (φ)	τ_1 (a_1)	τ_2 (a_2)	<τ>
0.0	408	1.00	-	2.72 (1.00)	2.72
0.1	415	0.97	0.29 (0.20)	3.00 (0.80)	2.60
0.2	418	0.96	0.23 (0.18)	3.10 (0.82)	2.54
0.3	420	0.95	0.31 (0.18)	3.10 (0.82)	2.60
0.4	422	0.94	0.37 (0.20)	3.20 (0.80)	2.60
0.5	425	0.92	0.34 (0.19)	3.20 (0.79)	2.64
0.6	429	0.90	0.34 (0.23)	3.20 (0.77)	2.55
0.7	431	0.89	0.39 (0.23)	3.20 (0.77)	2.58
0.8	432	0.88	0.31 (0.18)	3.30 (0.82)	2.70
0.9	433	0.86	0.34 (0.17)	3.30 (0.83)	2.80
1.0	435	0.84	-	3.30 (1.00)	3.30

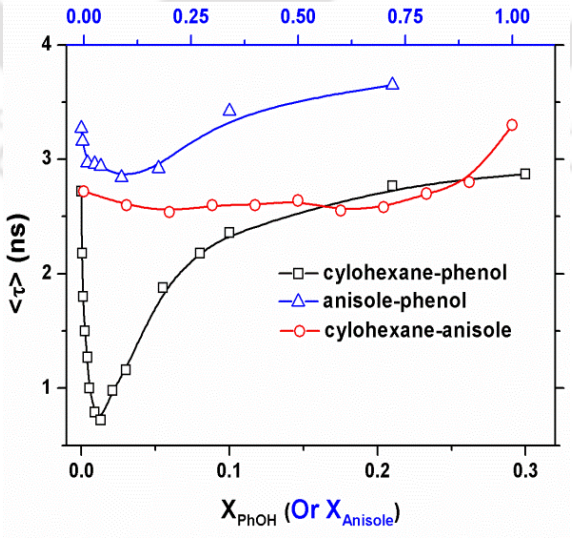

Figure 6.7: Variation of the average fluorescence lifetime, (<τ>) of C102 in different mixtures with mole fraction of phenol (or anisole).

6.2.3. Fourier transform infrared (FTIR) measurements

To investigate the nature of the H-bonding in the ground state, we have measured FT-IR spectra of C102 in the C=O stretching frequency region at several mole fractions of phenol (**Figure 6.8**). In cyclohexane, the C=O stretching frequency of C102 was observed at 1739 cm^{-1} which is the characteristics of free C=O group.[84, 123] On the addition of 50 mM (mole fraction 0.0055) of phenol, the C=O stretching frequency exhibited significant red-shift to 1697 cm^{-1}. The marked red-shift by 42 cm^{-1} may be due to the formation of H-bond with phenol. However, with increase in the phenol content, the extent of red-shift of C=O stretching frequency was decreased by 4–5 cm^{-1}. This may be due to the weakening of the H-bond strength at higher mole fractions. However, due to change in the spectral shape and possible effect of π-stacking interaction on the carbonyl stretching frequency, we were unable to do any quantitative estimation of H-bonding energy or binding constant.

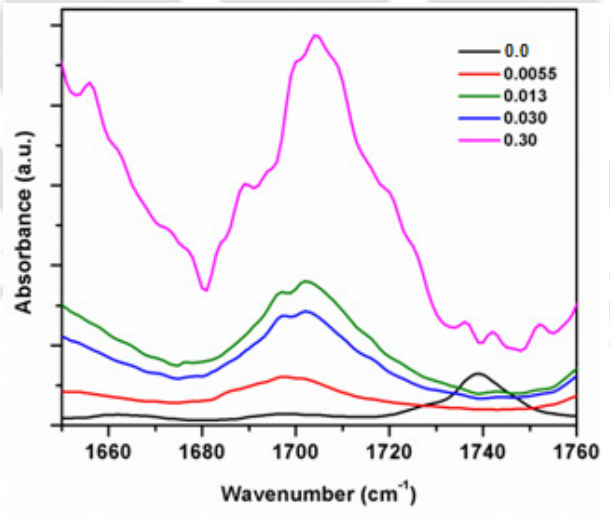

Figure 6.8 FTIR spectra of C102 in the presence of different mole fractions of phenol in cyclohexane. The C=O stretching frequencies were 1739 cm^{-1}, 1697 cm^{-1}, 1702 cm^{-1}, 1702 cm^{-1} and 1704 cm^{-1} at 2 mM of C102, 0.0055, 0.013, 0.030 and 0.30 mole fraction of phenol, respectively.

6.3. Discussion

We have already demonstrated that phenol acts as a potential PET quencher to C102 fluorescence. Generally, it is assumed that addition of more quencher should enhance quenching, however, we have obsevered that at higher phenol region fluorescence quenching of C102 reduced was reduced significantly in cyclohexane–phenol (or anisole–phenol) solvent mixture. This can explained by the mechanism of the H-bond controlled relaxation pathways of the C102–phenol H-bonded complex.

As predicted by the TDDFT calculations of Zhao et al.[75] and also supported by our study,[152] the PET within the H-bonded complex occurs *via* a transition from a LE, (S_2) state to a low-lying CT (S_1) state. The gap between the LE and the CT state depends on the strength of H-bonding. Similar H-bond induced PET was also proposed for C102–aniline complex by Liu et al.[83] which was experimentally verified by us.[30] Note that anisole and DMA are analogues of phenol and aniline respectively, lacking the H-bonding ability and thus, both are unable to quench the C102 fluorescence.

At the lower concentration region, it may be assumed that C102 exist either as 1 : 1 H-bonded complex or as free. Since only the H-bonded complex undergoes PET, with increase of phenol, the fraction of the C102–phenol increases resulting in higher quenching. We have shown that for initial few mole fractions, the quenching behaviour follows a linear Stern– Volmer trend.[152] The slope of the plot was found to depend on the strength of intermolecular H-bonding indicating the importance of H-boning in activating the PET. Here, we found that the linear quenching trend was only valid over initial few mole fractions. At higher mole fractions, the quenching markedly reduced. Several possible explanations may be discussed to account for the observation.

It is reasonable to assume that at higher concentration, a phenol donor that is linked with the C102, additionally coordinate to other phenols forming a H-bonded cluster, C102–$(phenol)_{n\geq2}$. These phenol–phenol H-bonding may weaken or hinder the key C102–phenol H-bonding to reach optimum condition required for PET. Hence, the key C102–phenol H-bonding may be less efficient in guiding electron transfer. Hence, the competitive nature of the C102–phenol and phenol– phenol H-bonding may reduce the PET quenching. The non-H-bonding component may assist to perturb or weaken the phenol–phenol H-bond. At the critical mole fraction where we observed the strongest fluorescence quenching the C102–phenol, H-bond may be the most efficient to undergo PET. Similar competitive H-bonding model has been introduced by us to explain the quenching anomaly of C102 in cyclohexane–aniline[30] and aniline–DMA[8] mixture.

Another important concern is possible modulation of polarity in a mixture of phenol–cyclohexane because phenol is more polar than cyclohexane. Polarity may have important effect over the PET energy and on the C102–phenol H-bonding. It is generally considered that H-bonding in a nonpolar medium is much stronger than in polar solvents due to solvation.[14] The polarity of the phenol-rich mixture may be higher and hence the H-bonding between coumarin and phenol may be weaker. Stronger H-bonding in a less polar medium compared to the high polar medium is consistent with the higher emission shift observed at lower mole fraction. Additionally, the relative stability of the LE and CT excited states may also depends on polarity. The CT state may be stabilized in polar mediumto amuch higher degree compared to the LE state due to larger dipole moment of the CT state. At lower mole fraction region i.e. in low polarity medium, H-bonding is strong but the CT state may not be energetically favourable and hence, fluorescence from the LE state is dominant. At higher mole fraction, due to higher polarity, the CT state is stabilized but the H-bonding is weak and

hence, PET may occur mostly via a non-H-bonding pathway, if allowed. At a critical mole fraction, both the factors may have an optimum influence and the PET rate is the highest.

To distinguish between the two possibilities (competitive H-bonding vs. polarity induced H-bonding modulation), we have chosen anisole–phenol solvent mixture. Due to similar polarity of anisole and phenol, the polarity of the mixture remains almost similar throughout all the compositions. Hence, the PET modulation due to change in the polarity of the mixture can be ignored. Since anisole does not posses H-bond donating ability, it can not compete with the C102–phenol H-bond but it may form H-bond with phenol and thus, reduce phenol–phenol H-bonding networking when present in large quantities. We observed similar reduced quenching as higher mole fraction for phenol–anisole mixture. Both the fluorescence quantum yield and average fluorescence lifetime gradually decreased up to the critical mole fraction and thereafter increased. As polarity remains invariant, it may be concluded that competitive H-bonding has an important role in the observed anomalous quenching behaviour. Very recently, we have also observed such unusual fluorescence quenching modulation of C102 in similar polarity aniline–DMA mixture discussed in chapter 5.[173]

To verify the effect of polarity only and to exclude H-bonding possibility, we have considered another solvent mixture –cyclohexane–anisole. In this case quantum yield of C102 decreased linearly with increase in the mole fraction of anisole. The slight linear decrease may be due to change in polarity of the medium. From this we can say that H-bond assisted PET has a pronounced effect on the anomalous fluorescence modulation of C102 in the two solvent mixtures – cyclohexane–phenol and anisole–phenol.

Now an important question is whether the fluorescence modulation is due to the H-bonding modulation in the ground state or in the excited state? The FT-IR spectroscopic investigation shows that H-bonding between C102–phenol is indeed modulated differentially at low-phenol and high-phenol regions in the ground state. At low mole fraction (0.0055) of

phenol in cyclohexane, the C=O stretching frequency of C102 exhibits a marked red shift of 42 cm^{-1} indicating a strong H-bond formation with phenol. However at higher phenol concentrations, the extent of red-shift was reduced by 4–5 cm^{-1}. Thus, it may be inferred that the C102–phenol H-bond becomes weaker at higher donor concentration because of self association of several donors. This result clearly illustrates that H-bonding strength is indeed depend on the mole fraction of phenol. However, for fluorescence modulation, we need to consider the H-bonding in the photoexcited state. We have shown that PET in the non-H-bonded complex is negligible and hence, significant PET in phenol containing mixtures implies that H-bonding should retain in the excited complex. Thus, we can indirectly infer that H-bonding between C102 and phenol may strengthening the excited state, which is consistent with the prediction by Han and co-workers.[75] Another minor possibility is that the H-bond may initially break within few hundreds of femtoseconds of excitation but subsequently, may recombine on a picosecond time scale to induce the PET process. Similar model of H-bond dynamics was proposed by Palit and co-workers for the case of C102–aniline H-bond dynamics.[84] Overall, our results show the dominant role of H-bonding between C102 and phenol for controlling the anomalous fluorescence quenching within the C102–phenol H-bonded complex.

6.4. Conclusion

The H-bond mediated PET between C102–phenol is found to be more activated at a lower mole fraction of the H-bond donor rather than at higher mole fraction of the donor (phenol). It is proposed that at higher mole fraction, C102 may form higher order C102–$(phenol)_{n\geq2}$ complex where, the phenol may associate with more phenol molecules through phenol–phenol H-bond. The phenol–phenol H-bond may perturb the H-bond between the

C=O group of C102 and the HO– group of phenol to attain optimum geometry for PET. This competitive nature of H-bonding that reduces the H-bonding strength between C102 and phenol makes the complex less effective to undergo PET. This was further complemented by the FTIR measurement, which shows higher red-shift of the C=O frequency at low phenol concentration compared to the higher phenol concentrations.

Chapter 7

An inert component mixed with donor solvent can make ultrafast H-bond assisted photoinduced electron transfer even faster*

7.1. Introduction

In all of the previous chapters, we have discussed PET for C102 in different solvent mixtures. However, C102 is not a very good representative to study ultrafast PET. Ultrafast PET has been observed for many other coumarins but not with C102. This is because C102 is reluctant to undergo PET in the absence of H-bonding.[18-21] This can be manifested from the fact that no PET occurs for C102 dissolved in neat DMA.

In this work, we have chosen C153 as an acceptor which is known to undergo ultrafast PET in both neat AN and DMA.[18-21] Structurally, C153 is similar to C102; only the methyl group is substituted by trifluoromethyl group (**scheme 1.1**). The $-CF_3$ substitution has a profound effect on the reduction potential and hence, the free energy of electron transfer becomes much more favorable. A brief account of substitution effect on PET has been presented earlier in **section 1.2.2**. Thus, for C153, normal (non-H-bonded) PET is also favorable as evident from ultrafast PET in DMA.[18-21] Here, we have studied PET of excited C153 in the cyclohexane-DMA and cyclohexane-AN mixtures. Similar to C102, the carbonyl group of C153 is expected to form H-bond with the amine hydrogen of AN. The central concept is that the inert component may activate the H-bonded PET channel while diminish the non-H-bonded PET probability (**Scheme 7.1**). Thus, the effect of H-bonding (if present), will be amplified. It is also interesting to see whether the H-bond mediated PET could be detectable from the simultaneous non-H-bonded ultrafast PET.

---

*This work has been communicated

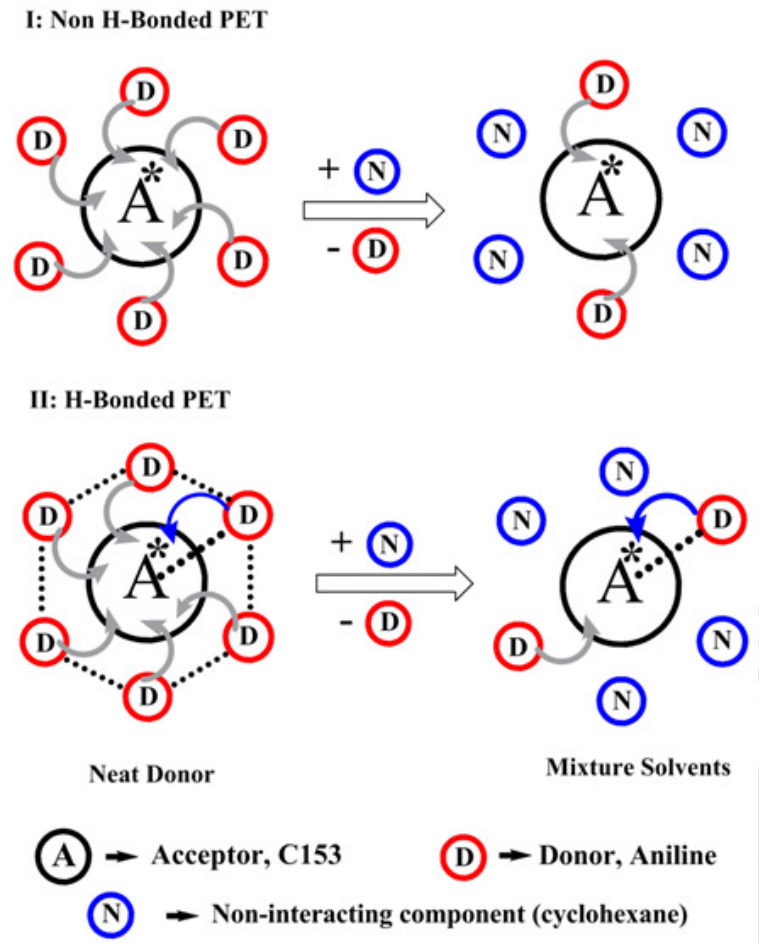

Scheme 7.1: Addition of inert co-solvent leads to different modulation of PET depending on the H-bonding ability of the donor. Gray and blue arrows indicate non-H-bonded and H-bonded PET, respectively. In the mixture, H-bonded PET dominates while non-H-bonded PET diminishes.

7.2. Results

7.2.1. Steady-state fluorescence measurements

Figure 7.1 displays the emission spectra of C153 in cyclohexane-DMA and cyclohexane-AN mixtures. C153 shows a very intense emission in cyclohexane (QY close to unity and its value is ~ 0.90[145]) but becomes strongly quenched in AN or DMA. The extent of reduction of emission intensity was more severe in DMA than in AN. This was in accordance

with the better electron donating ability of DMA compared to AN (oxidation potentials of AN and DMA in acetonitrile are 0.93 and 0.76V vs. SCE, respectively[19]). Addition of DMA to C153 dissolved in cyclohexane results in a continuous decrease of the emission intensity and gradual shifts of emission maxima (**Figure 7.1a**). The shift in the emission maximum of C153 is indicative of the polarity modulation in mixture while the quenching of the fluorescence is due to PET from the donor solvent to the excited C153. However, in cyclohexane-AN mixture, the variation of quantum yield was anomalous (**Figure 7.1b**). The QY first decreased with increase in the mole fraction of AN (X_{AN}). The QY was similar at mole fractions 0.13 and 0.74. Note that we could not perform experiment in between this range due to insolubility of the mixtures. Thereafter, QY increased as the amount of AN exceeded further. The QY at X_{AN} = 0.13 was found to be ~120 times lower than that in neat cyclohexane and nearly two times less compared to neat AN (**Table 7.1**).

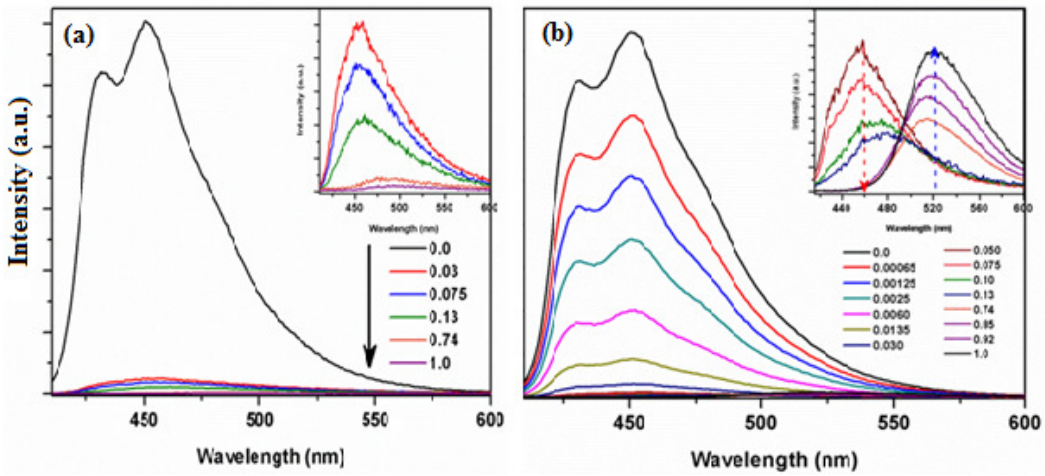

Figure 7.1: Steady-state emission spectra of C153 in (a) cyclohexane-DMA and (b) cyclohexane-AN mixtures at different mole fractions of the electron donor (DMA or AN). Strongly quenched emission spectra are displayed further in the inset for clarity. It is evident that quantum yield of C153 gradually diminishes on addition of DMA solvent but shows an anomalous trend in the case of aniline.

7.2.2. Time-resolved fluorescence measurements

To probe the ultrafast decays of the fluorescent acceptor, fluorescence up-conversion measurements were carried out at different mole fractions of the donor in the donor-inert solvent mixtures (**Figure 7.2**). All the decay components were found to be bi-exponential (**Table 7.1 and Table 7.2**). In cyclohexane-DMA mixture, the fast (2-3ps) component remains almost invariant to the amount of donor while the other component becomes faster with increase in mole fraction of the donor. The fast component may be due to PET from donors in the vicinity of the excited acceptor, while the slower component may arise due to diffusion of the donor within the excited state lifetime of C153. In cyclohexane-DMA mixture, the average fluorescence lifetime of C153 decreases regularly with increase in the mole fraction of DMA (**Table 7.1**). However, in cyclohexane-AN mixture the average fluorescence lifetime initially decreased with increase in X_{AN} (shortest lifetime at $X_{AN} = 0.74$) and thereafter, increased with further increase in X_{AN}. The fast component (6-35ps) may be assigned to PET within the C153-AN H-bonded complex and its contribution is found to be maximum at $X_{AN} = 0.74$ (**Table 7.2**). Thus, both steady-state and time-resolved fluorescence results indicate more facile H-bonded PET at an intermediate mole fraction ($X_{AN} = 0.74$) rather than in neat AN.

7.2.3. Fourier transform infrared (FTIR) measurements

To understand the H-bonding nature of C153 in aniline-cyclohexane mixtures, FTIR spectra were recorded (**Figure 7.3**) for the C=O stretching region of C153. In neat cyclohexane, the C=O stretch of C153 was found to be at 1748 cm^{-1}, which is characteristics of an unbound C=O group. However, with increase in X_{AN}, the strength of the absorption band at 1748 cm^{-1} decreases with the development of an additional band at 1736 cm^{-1}. This

new band may be due to lowering of the stretching frequency of the carbonyl group of C153 in the H-bonded complex. The intensity of the band at 1736 cm^{-1} gradually increases with increase in the mole fraction of aniline. However, the C=O stretching vibration (mainly at X_{AN} = 0.74 and in neat AN) is overlapped with some other vibration mode of aniline (possibly arising due to aniline-aniline association[84]). Hence, a very conclusive remark about the H-bonding condition at higher mole fractions may not be inferred from the FTIR measurement.

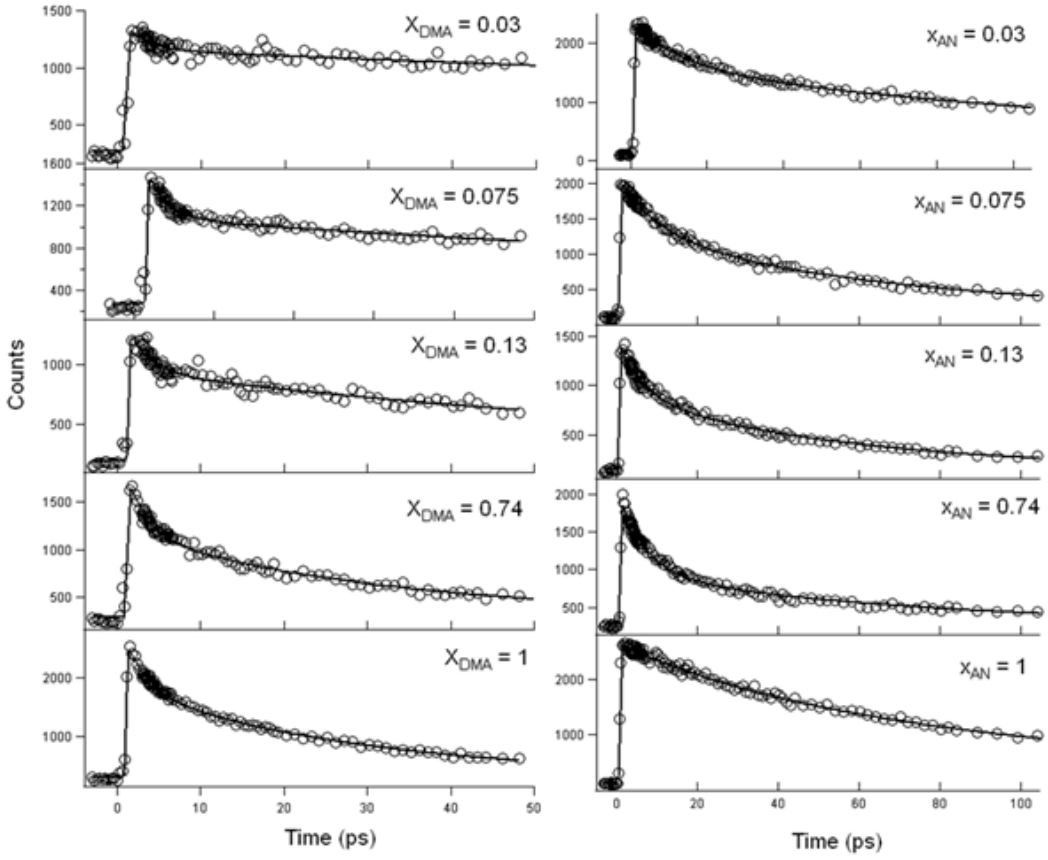

Figure 7.2: The fluorescence decays of C153 in cyclohexane-DMA (left panel) and cyclohexane-AN (right panel) mixtures at different mole fractions of the electron donor (DMA/AN). Clearly as the amount of DMA increases, PET becomes faster and reaches the optimum value in neat DMA. Interestingly, for cyclohexane-AN mixture, PET becomes faster at intermediate X_{AN} compared to neat AN.

Table 7.1: Fluorescence decay components of coumarin 153 (C153) in the cyclohexane-DMA mixture at different mole fractions of the DMA, X_{DMA}. Excitation wavelength was at 405 nm and decays were measured at corresponding emission maxima.

X_{DMA}	QY (φ)	τ_1 (a_1) (ps)	τ_2 (a_2) (ps)	<τ> (ps)
0.03	0.055	2.6 (0.19)	285 (0.81)	232
0.075	0.040	2.5 (0.36)	147 (0.64)	95
0.13	0.027	2.7 (0.34)	90 (0.66)	60
0.74	0.006	2.4 (0.40)	31 (0.60)	20
1.00	0.003	2.8 (0.36)	28 (0.64)	19

Table 7.2: Fluorescence decay components of coumarin 153 (C153) in the cyclohexane-AN mixture at different mole fractions of the AN, X_{AN}. Excitation wavelength was at 405 nm and decays were measured at corresponding emission maxima.

X_{AN}	QY (φ)	τ_1 (a_1) (ps)	τ_2 (a_2) (ps)	<τ> (ps)
0.03	0.040	13 (0.33)	165 (0.67)	115
0.075	0.023	10 (0.40)	75 (0.60)	49
0.13	0.007	6 (0.40)	53 (0.60)	34
0.74	0.008	7 (0.58)	67 (0.42)	32
1.00	0.015	35 (0.26)	120 (0.74)	96

Very recently MD simulations from our group showed that the H-bonding at X_{AN} = 0.74 is more favorable compared to neat aniline and is also better oriented (more collinear).[174] Although, we have speculated that D-A H-bonding becomes favorable at some intermediate

mole fractions in the presence of a non-interacting co-solvent in previous chapters[173, 175] but it is for the first time, we have explicitly shown it. These H-bonded pairs undergo much faster PET than non-H-bonded donors, thus, surpasses the rate observed at neat condition. In fact a simulation with excited-state charge densities on C153 may give a better insight. However, if we take the view of Zhao and Han[75] that H-bonding becomes stronger in the excited state, we could expect an even more preferable distribution of the H-bonded species in the mixture compared to neat aniline.

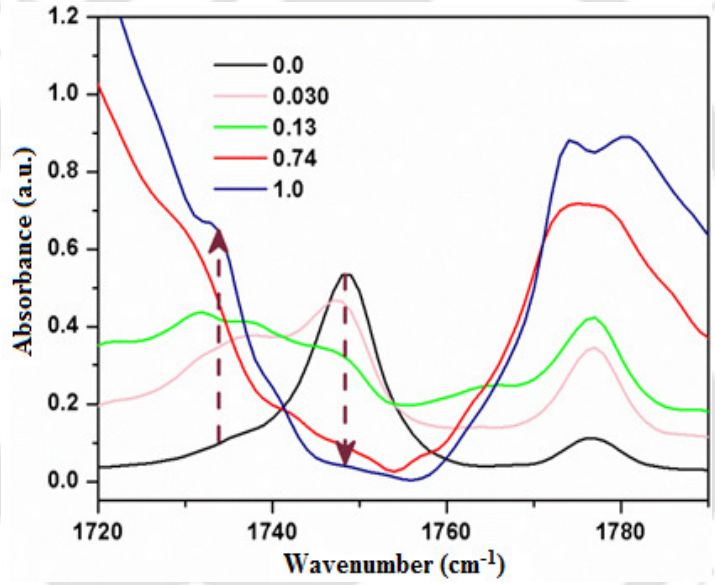

Figure 7.3: The FTIR spectra of 20 mM coumarin 153 in the carbonyl stretching region in the cyclohexane-AN mixtures at different mole fractions of the electron donor (AN). Gradual disappearance of the free C=O stretching frequency (at 1748 cm^{-1}) and appearance of a new peak at 1736 may be due to H-bonding.

7.3. Summary and conclusion

In summary, using steady-state and ultrafast fluorescence measurements, we have demonstrated that the PET behavior of an acceptor (C153) dissolved in mixture of electron

donor and a non-interacting solvent may be drastically different in nature depending on the possibility of H-bond formation with the acceptor. In the case of DMA, the co-solvent retards PET while the same co-solvent assists PET from aniline to C153 at some particular composition of the mixture. FTIR measurements indicated the evidence of H-bond formation between C153 and aniline in the cyclohexane-aniline mixtures at all mole fractions. The speculation that H-bonding indeed assists the PET in aniline containing mixtures, was further rationalized from MD simulations studies performed in our group. MD simulation revealed the presence of highest number of aniline molecules H-bonded to the acceptor at the same mole fraction where PET rate was found to be the fastest. This remarkable agreement between the experiments and theory confirms the theoretical predication that H-bonding should favor PET within the coumarin-aniline complex. Here, for the first time, we provide the evidence that D-A H-bonding is indeed better oriented in a mixture at some definite mole fraction in comparison to neat aniline.

Hence, we conclude that a non-interacting co-solvent can effectively amplify the effect of H-bonding to such an extent that it can be observed distinctly from non-H-bonded PET. Thus, a direct correlation between H-bonding and PET has been demonstrated through this study.

References

1. Valeur, B., Molecular Fluorescence: Principles and Applications. Wiely - VCH Verlag GmbH: 2001.
2. V. May, O. K., Charge and Energy Transfer Dynamics in Molecular Systems. Wiely - VCH Verlag GmbH: 2000.
3. Suppan, P., In *Chemistry and Light*, The Royal Society of Chemistry: 1994; pp 27-86.
4. Giese, B.; Amaudrut, J.; Kohler, A.-K.; Spormann, M.; Wessely, S., Direct Observation of Hole Transfer through DNA by Hopping between Adenine Bases and by Tunnelling. *Nature* **2001,** *412*, 318-320.
5. de Rege, P.; Williams, S.; Therien, M., Direct Evaluation of Electronic Coupling Mediated by Hydrogen Bonds: Implications for Biological Electron Transfer. *Science* **1995,** *269*, 1409-1413.
6. Marcus, R. A., Chemical and Electrochemical Electron-Transfer Theory. *Annu. Rev. Phys. Chem.* **1964,** *15*, 155-196.
7. Barbara, P. F.; Meyer, T. J.; Ratner, M. A., Contemporary Issues in Electron Transfer Research. *J. Phys. Chem.* **1996,** *100*, 13148-13168.
8. Weaver, M. J.; McManis, G. E., Dynamical Solvent Effects on Electron-Transfer Processes: Recent Progress and Perspectives. *Acc. Chem. Res.* **1990,** *23*, 294-300.
9. Marcus, R. A., On the Theory of Oxidation-Reduction Reactions Involving Electron Transfer. I. *J. Chem. Phys.* **1956,** *24*, 966-978.
10. Rehm, D.; Weller, A., Kinetics of Fluorescence Quenching by Electron and H-Atom Transfer. *Isr. J. Chem.* **1970,** *8*, 259-271.
11. Fox, M. A., Introduction - Electron Transfer: A Critical Link between Subdisciplines in Chemistry. *Chem. Rev.* **1992,** *92*, 365-368.
12. Calef, D. F.; Wolynes, P. G., Classical Solvent Dynamics and Electron Transfer. 1. Continuum Theory. *J. Phys. Chem.* **1983,** *87*, 3387-3400.
13. Hynes, J. T., Outer-Sphere Electron-Transfer Reactions and Frequency-Dependent Friction. *J. Phys. Chem.* **1986,** *90*, 3701-3706.
14. Ikeda, N.; Miyasaka, H.; Okada, T.; Mataga, N., Picosecond Laser Photolysis Studies of Deactivation Processes of Excited Hydrogen Bonding Complexes. 3. Detection of the Nonfluorescent Charge-Transfer State in the Excited 1-Aminopyrene-Pyridine Hydrogen Bonded Pair and Related Systems. *J. Am. Chem. Soc.* **1983,** *105*, 5206-5211.
15. Roy, S.; Bagchi, B., Adiabatic and Nonadiabatic Outersphere Electron Transfer Reactions in Methanol: Effects of the Ultrafast Solvent Polarization Modes. *J. Chem. Phys.* **1995,** *102*, 6719-6726.
16. Nagasawa, Y.; Yartsev, A. P.; Tominaga, K.; Johnson, A. E.; Yoshihara, K., Substituent Effects on Intermolecular Electron Transfer: Coumarins in Electron-Donating Solvents. *J. Am. Chem. Soc.* **1993,** *115*, 7922-7923.
17. Nagasawa, Y.; Yartsev, A. P.; Tominaga, K.; Johnson, A. E.; Yoshihara, K., Temperature Dependence of Ultrafast Intermolecular Electron Transfer Faster Than Solvation Process. *J. Chem. Phys.* **1994,** *101*, 5717-5726.
18. Nagasawa, Y.; Yartsev, A. P.; Tominaga, K.; Bisht, P. B.; Johnson, A. E.; Yoshihara, K., Dynamic Aspects of Ultrafast Intermolecular Electron Transfer Faster Than Solvation Process: Substituent Effects and Energy Gap Dependence. *J. Phys. Chem.* **1995,** *99*, 653-662.
19. Shirota, H.; Pal, H.; Tominaga, K.; Yoshihara, K., Substituent Effect and Deuterium Isotope Effect of Ultrafast Intermolecular Electron Transfer: Coumarin in Electron-Donating Solvent. *J. Phys. Chem. A* **1998,** *102*, 3089-3102.
20. Pal, H.; Shirota, H.; Tominaga, K.; Yoshihara, K., Ultrafast Intermolecular Electron Transfer from Orthomethoxyaniline to Excited Coumarin Dyes. *J. Chem. Phys.* **1999,** *110*, 11454-11465.
21. Pal, H.; Nagasawa, Y.; Tominaga, K.; Yoshihara, K., Deuterium Isotope Effect on Ultrafast Intermolecular Electron Transfer. *J. Phys. Chem.* **1996,** *100*, 11964-11974.
22. Yoshihara, K., Ultrafast Intermolecular Electron Trasnfer in Solution. In *Adv. Chem. Phys.*, 1999; Vol. 107, p 37.

23. Kumar, K.; Tepper, R. J.; Zeng, Y.; Zimmt, M. B., Syntheses of Rigid and Semirigid Molecules for Investigations of Photoinduced Electron Transfer Reactions. *J. Org. Chem.* **1995,** *60*, 4051-4066.
24. Maruyama, K.; Otsuki, T.; Tai, S., Photoinduced Electron-Transfer-Initiated Aromatic Cyclization. *J. Org. Chem.* **1985,** *50*, 52-60.
25. Wong, K.-T.; Ku, S.-Y.; Cheng, Y.-M.; Lin, X.-Y.; Hung, Y.-Y.; Pu, S.-C.; Chou, P.-T.; Lee, G.-H.; Peng, S.-M., Synthesis, Structures, and Photoinduced Electron Transfer Reaction in the 9,9'-Spirobifluorene-Bridged Bipolar Systems. *J. Org. Chem.* **2005,** *71*, 456-465.
26. Marcus, R. A., Electrostatic Free Energy and Other Properties of States Having Nonequilibrium Polarization. I. *J. Chem. Phys.* **1956,** *24*, 979-989.
27. Marcus, Y., The Effectivity of Solvents as Electron Pair Donors. *J Solution Chem* **1984,** *13*, 599-624.
28. Zhao, G.-J.; Han, K.-L., Hydrogen Bonding in the Electronic Excited State. *Acc. Chem. Res.* **2011,** *45*, 404-413.
29. Zhao, G.-J.; Liu, J.-Y.; Zhou, L.-C.; Han, K.-L., Site-Selective Photoinduced Electron Transfer from Alcoholic Solvents to the Chromophore Facilitated by Hydrogen Bonding: A New Fluorescence Quenching Mechanism. *J. Phys. Chem. B* **2007,** *111*, 8940-8945.
30. Barman, N.; Singha, D.; Sahu, K., Faster Photoinduced Electron Transfer in a Diluted Mixture Than in a Neat Donor Solvent: Effect of Excited-State H-Bonding. *Phys. Chem. Chem. Phys.* **2014,** *16*, 6159-6166.
31. Dimroth, K.; Reichardt, C.; Siepmann, T.; Bohlmann, F., Über Pyridinium-N-Phenol-Betaine Und Ihre Verwendung Zur Charakterisierung Der Polarität Von Lösungsmitteln. *Liebigs Ann. Chem.* **1963,** *661*, 1-37.
32. Gutmann, V.; Wychera, E., Coordination Reactions in Non Aqueous Solutions - the Role of the Donor Strength. *Inorganic and Nuclear Chemistry Letters* **1966,** *2*, 257-260.
33. Suppan, P., Local Polarity of Solvent Mixtures in the Field of Electronically Excited Molecules and Exciplexes. *Journal of the Chemical Society, Faraday Transactions 1: Physical Chemistry in Condensed Phases* **1987,** *83*, 495-509.
34. Khajehpour, M.; Kauffman, J. F., Dielectric Enrichment of 1-(9-Anthryl)-3-(4-N,N-Dimethylaniline) Propane in Hexane−Ethanol Mixtures. *J. Phys. Chem. A* **2000,** *104*, 7151-7159.
35. Khajehpour, M.; Welch, C. M.; Kleiner, K. A.; Kauffman, J. F., Separation of Dielectric Nonideality from Preferential Solvation in Binary Solvent Systems: An Experimental Examination of the Relationship between Solvatochromism and Local Solvent Composition around a Dipolar Solute. *J. Phys. Chem. A* **2001,** *105*, 5372-5379.
36. Petrov, N. K.; Wiessner, A.; Fiebig, T.; Staerk, H., Study of Preferential Solvation in Binary Solvent Mixtures by the Spectro-Streak Picosecond Technique. *Chem. Phys. Lett.* **1995,** *241*, 127-132.
37. Cichos, F.; Willert, A.; Rempel, U.; von Borczyskowski, C., Solvation Dynamics in Mixtures of Polar and Nonpolar Solvents. *J. Phys. Chem. A* **1997,** *101*, 8179-8185.
38. Schatz, T. R.; Kobetic, R.; Piotrowiak, P., Probing Preferential Solvation and Ion Aggregation with Charge Transfer Triplet States of Aromatic Amino-Nitro Compounds. *J. Photochem. Photobiol., A* **1997,** *105*, 249-254.
39. Nishiyama, K.; Okada, T., Relaxation Dynamics of Inhomogeneous Spectral Width in Binary Solvents Studied by Transient Hole-Burning Spectroscopy. *J. Phys. Chem. A* **1998,** *102*, 9729-9733.
40. Bangar Raju, B.; M. B. Costa, S., Photophysical Properties of 7-Diethylaminocoumarin Dyes in Dioxane-Water Mixtures: Hydrogen Bonding, Dielectric Enrichment and Polarity Effects. *Phys. Chem. Chem. Phys.* **1999,** *1*, 3539-3547.
41. M. Andrade, S.; M. B. Costa, S., Hydrogen Bonding Effects in the Photophysics of a Drug, Piroxicam, in Homogeneous Media and Dioxane-Water Mixtures. *Phys. Chem. Chem. Phys.* **1999,** *1*, 4213-4218.
42. Nandi, N.; Bhattacharyya, K.; Bagchi, B., Dielectric Relaxation and Solvation Dynamics of Water in Complex Chemical and Biological Systems. *Chem. Rev.* **2000,** *100*, 2013-2046.
43. Bagchi, B., Water Dynamics in the Hydration Layer around Proteins and Micelles. *Chem. Rev.* **2005,** *105*, 3197-3219.
44. Bhattacharyya, K., Solvation Dynamics and Proton Transfer in Supramolecular Assemblies. *Acc. Chem. Res.* **2002,** *36*, 95-101.

45. Pal, S. K.; Zewail, A. H., Dynamics of Water in Biological Recognition. *Chem. Rev.* **2004,** *104*, 2099-2124.
46. Sahu, K.; Mondal, S. K.; Ghosh, S.; Bhattacharyya, K., Ultrafast Dynamics in Biological Systems and in Nano-Confined Environments. *Bull. Chem. Soc. Jpn.* **2007,** *80*, 1033-1043.
47. Maroncelli, M.; Fleming, G. R., Picosecond Solvation Dynamics of Coumarin 153: The Importance of Molecular Aspects of Solvation. *J. Chem. Phys.* **1987,** *86*, 6221-6239.
48. Cho, M.; Fleming, G. R.; Saito, S.; Ohmine, I.; Stratt, R. M., Instantaneous Normal Mode Analysis of Liquid Water. *J. Chem. Phys.* **1994,** *100*, 6672-6683.
49. Raineri, F. O.; Resat, H.; Perng, B. C.; Hirata, F.; Friedman, H. L., A Molecular Theory of Solvation Dynamics. *J. Chem. Phys.* **1994,** *100*, 1477-1491.
50. Schwartz, B. J.; Rossky, P. J., An Exploration of the Relationship between Solvation Dynamics and Spectrally Determined Solvent Response Functions by Computer Simulation. *J. Phys. Chem.* **1995,** *99*, 2953-2958.
51. Carter, E. A.; Hynes, J. T., Solvation Dynamics for an Ion Pair in a Polar Solvent: Time-Dependent Fluorescence and Photochemical Charge Transfer. *J. Chem. Phys.* **1991,** *94*, 5961-5979.
52. Ladanyi, B. M.; Stratt, R. M., Short-Time Dynamics of Solvation: Linear Solvation Theory for Polar Solvents. *J. Phys. Chem.* **1995,** *99*, 2502-2511.
53. Stratt, R. M., The Instantaneous Normal Modes of Liquids. *Acc. Chem. Res.* **1995,** *28*, 201-207.
54. Rips, I.; Jortner, J., Dynamic Solvent Effects on Outer-Sphere Electron Transfer. *J. Chem. Phys.* **1987,** *87*, 2090-2104.
55. Rips, I.; Jortner, J., Outer Sphere Electron Transfer in Polar Solvents. Activationless and Inverted Regimes. *J. Chem. Phys.* **1987,** *87*, 6513-6519.
56. Rips, I.; Jortner, J., The Effect of Solvent Relaxation Dynamics on Outer-Sphere Electron Transfer. *Chem. Phys. Lett.* **1987,** *133*, 411-414.
57. Wu, Y.-D.; Han, W.; Wang, D.-P.; Gao, Y.; Zhao, Y.-L., Theoretical Analysis of Secondary Structures of B-Peptides. *Acc. Chem. Res.* **2008,** *41*, 1418-1427.
58. Alexander, A. J.; Zare, R. N., Molecular Tennisflat Smashes and Wicked Cuts. *Acc. Chem. Res.* **2000,** *33*, 199-205.
59. Wu, Y. D.; Houk, K. N.; Valentine, J. S.; Nam, W., Is Intramolecular Hydrogen-Bonding Important for Bleomycin Reactivity? A Molecular Mechanics Study. *Inorganic Chemistry* **1992,** *31*, 718-720.
60. Wagner, B. D., Hydrogen Bonding of Excited States in Supramolecular Host-Guest Inclusion Complexes. *Phys. Chem. Chem. Phys.* **2012,** *14*, 8825-8835.
61. Zilberg, S.; Kahan, A.; Haas, Y., The Photo-Dissociation of the Pyrrole-Ammonia Complex-the Role of Hydrogen Bonding in Rydberg States Photochemistry. *Phys. Chem. Chem. Phys.* **2012,** *14*, 8836-8841.
62. Hardman, S. J. O.; Thompson, K. C., Influence of Base Stacking and Hydrogen Bonding on the Fluorescence of 2-Aminopurine and Pyrrolocytosine in Nucleic Acids†. *Biochemistry* **2006,** *45*, 9145-9155.
63. Perun, S.; Sobolewski, A. L.; Domcke, W., Role of Electron-Driven Proton-Transfer Processes in the Excited-State Deactivation of the Adenine–Thymine Base Pair. *J. Phys. Chem. A* **2006,** *110*, 9031-9038.
64. Catalán, J.; Kasha, M., Photophysics of 7-Azaindole, Its Doubly-H-Bonded Base-Pair, and Corresponding Proton-Transfer-Tautomer Dimeric Species, Via Defining Experimental and Theoretical Results. *J. Phys. Chem. A* **2000,** *104*, 10812-10820.
65. Chudoba, C.; Nibbering, E. T. J.; Elsaesser, T., Ultrafast Structural Response of Hydrogen Bonded Complexes to Electronic Excitation in the Liquid Phase. *J. Phys. Chem. A* **1999,** *103*, 5625-5628.
66. Zhao, G.-J.; Han, K.-L., Effects of Hydrogen Bonding on Tuning Photochemistry: Concerted Hydrogen-Bond Strengthening and Weakening. *ChemPhysChem* **2008,** *9*, 1842-1846.
67. Zhao, G.-J.; Han, K.-L., Hydrogen Bonding in the Electronic Excited State. *Acc. Chem. Res.* **2011,** *45*, 404-413.

68. Nibbering, E. T. J.; Elsaesser, T., Ultrafast Vibrational Dynamics of Hydrogen Bonds in the Condensed Phase. *Chem. Rev.* **2004,** *104*, 1887-1914.
69. Cramer, C. J.; Truhlar, D. G., A Universal Approach to Solvation Modeling. *Acc. Chem. Res.* **2008,** *41*, 760-768.
70. Olsen, S.; Smith, S. C., Bond Selection in the Photoisomerization Reaction of Anionic Green Fluorescent Protein and Kindling Fluorescent Protein Chromophore Models. *J. Am. Chem. Soc.* **2008,** *130*, 8677-8689.
71. Schlücker, S.; Singh, R. K.; Asthana, B. P.; Popp, J.; Kiefer, W., Hydrogen-Bonded Pyridine−Water Complexes Studied by Density Functional Theory and Raman Spectroscopy. *J. Phys. Chem. A* **2001,** *105*, 9983-9989.
72. Neela, Y. I.; Mahadevi, A. S.; Sastry, G. N., Hydrogen Bonding in Water Clusters and Their Ionized Counterparts. *J. Phys. Chem. B* **2010,** *114*, 17162-17171.
73. Alabugin, I. V.; Manoharan, M.; Peabody, S.; Weinhold, F., Electronic Basis of Improper Hydrogen Bonding: A Subtle Balance of Hyperconjugation and Rehybridization. *J. Am. Chem. Soc.* **2003,** *125*, 5973-5987.
74. Stoner-Ma, D.; Jaye, A. A.; Matousek, P.; Towrie, M.; Meech, S. R.; Tonge, P. J., Observation of Excited-State Proton Transfer in Green Fluorescent Protein Using Ultrafast Vibrational Spectroscopy. *J. Am. Chem. Soc.* **2005,** *127*, 2864-2865.
75. Zhao, G.-J.; Han, K.-L., Early Time Hydrogen-Bonding Dynamics of Photoexcited Coumarin 102 in Hydrogen-Donating Solvents: Theoretical Study. *J. Phys. Chem. A* **2007,** *111*, 2469-2474.
76. Chudoba, C.; Nibbering, E. T. J.; Elsaesser, T., Ultrafast Structural Response of Hydrogen Bonded Complexes to Electronic Excitation in the Liquid Phase. *J. Phys. Chem. A* **1999,** *103*, 5625-5628.
77. Nibbering, E. T. J.; Tschirschwitz, F.; Chudoba, C.; Elsaesser, T., Femtochemistry of Hydrogen Bonded Complexes after Electronic Excitation in the Liquid Phase: The Case of Coumarin 102. *J. Phys. Chem. A* **2000,** *104*, 4236-4246.
78. Palit, D. K.; Zhang, T.; Kumazaki, S.; Yoshihara, K., Hydrogen-Bond Dynamics in the Excited State of Coumarin 102−Aniline Hydrogen-Bonded Complex. *J. Phys. Chem. A* **2003,** *107*, 10798-10804.
79. Samant, V.; Singh, A. K.; Ramakrishna, G.; Ghosh, H. N.; Ghanty, T. K.; Palit, D. K., Ultrafast Intermolecular Hydrogen Bond Dynamics in the Excited State of Fluorenone. *J. Phys. Chem. A* **2005,** *109*, 8693-8704.
80. Zhao, G.-J.; Han, K.-L., Ultrafast Hydrogen Bond Strengthening of the Photoexcited Fluorenone in Alcohols for Facilitating the Fluorescence Quenching†. *J. Phys. Chem. A* **2007,** *111*, 9218-9223.
81. Zhao, G.-J.; Han, K.-L., Role of Intramolecular and Intermolecular Hydrogen Bonding in Both Singlet and Triplet Excited States of Aminofluorenones on Internal Conversion, Intersystem Crossing, and Twisted Intramolecular Charge Transfer†. *J. Phys. Chem. A* **2009,** *113*, 14329-14335.
82. Zhao, G.-J.; Liu, J.-Y.; Zhou, L.-C.; Han, K.-L., Site-Selective Photoinduced Electron Transfer from Alcoholic Solvents to the Chromophore Facilitated by Hydrogen Bonding: A New Fluorescence Quenching Mechanism. *J. Phys. Chem. B* **2007,** *111*, 8940-8945.
83. Liu, Y.; Ding, J.; Shi, D.; Sun, J., Time-Dependent Density Functional Theory Study on Electronically Excited States of Coumarin 102 Chromophore in Aniline Solvent: Reconsideration of the Electronic Excited-State Hydrogen-Bonding Dynamics. *J. Phys. Chem. A* **2008,** *112*, 6244-6248.
84. Palit, D. K.; Zhang, T.; Kumazaki, S.; Yoshihara, K., Hydrogen-Bond Dynamics in the Excited State of Coumarin 102−Aniline Hydrogen-Bonded Complex†. *J. Phys. Chem. A* **2003,** *107*, 10798-10804.
85. Sobolewski, A. L.; Domcke, W., Photophysics of Malonaldehyde: An Ab Initio Study. *J. Phys. Chem. A* **1999,** *103*, 4494-4504.
86. Sobolewski, A. L.; Domcke, W., Intramolecular Hydrogen Bonding in the S1(Ππ*) Excited State of Anthranilic Acid and Salicylic Acid: Tddft Calculation of Excited-State Geometries and Infrared Spectra. *J. Phys. Chem. A* **2004,** *108*, 10917-10922.
87. Southern, C. A.; Levy, D. H.; Florio, G. M.; Longarte, A.; Zwier, T. S., Electronic and Infrared Spectroscopy of Anthranilic Acid in a Supersonic Jet. *J. Phys. Chem. A* **2003,** *107*, 4032-4040.

88. Sobolewski, A. L.; Domcke, W., Ab Initio Studies on the Photophysics of the Guanine-Cytosine Base Pair. *Phys. Chem. Chem. Phys.* **2004,** *6*, 2763-2771.
89. Hieringer, W.; Görling, A., Failure of Time-Dependent Density Functional Methods for Excitations in Spatially Separated Systems. *Chem. Phys. Lett.* **2006,** *419*, 557-562.
90. Han, K.-L.; He, G.-Z., Photochemistry of Aryl Halides: Photodissociation Dynamics. *J. Photochem. Photobiol. C* **2007,** *8*, 55-66.
91. Yu, F.; Li, P.; Li, G.; Zhao, G.; Chu, T.; Han, K., A near-Ir Reversible Fluorescent Probe Modulated by Selenium for Monitoring Peroxynitrite and Imaging in Living Cells. *J. Am. Chem. Soc.* **2011,** *133*, 11030-11033.
92. Zhang, M.-X.; Zhao, G.-J., Modification of N-Type Organic Semiconductor Performance of Perylene Diimides by Substitution in Different Positions: Two-Dimensional Π-Stacking and Hydrogen Bonding. *ChemSusChem* **2012,** *5*, 879-887.
93. Zhao, G.-J.; Han, K.-L., Site-Specific Solvation of the Photoexcited Protochlorophyllide a in Methanol: Formation of the Hydrogen-Bonded Intermediate State Induced by Hydrogen-Bond Strengthening. *Biophys. J.* **2008,** *94*, 38-46.
94. Chai, S.; Zhao, G.-J.; Song, P.; Yang, S.-Q.; Liu, J.-Y.; Han, K.-L., Reconsideration of the Excited-State Double Proton Transfer (Esdpt) in 2-Aminopyridine/Acid Systems: Role of the Intermolecular Hydrogen Bonding in Excited States. *Phys. Chem. Chem. Phys.* **2009,** *11*, 4385-4390.
95. Zhao, G.-J.; Han, K.-L., Novel Infrared Spectra for Intermolecular Dihydrogen Bonding of the Phenol-Borane-Trimethylamine Complex in Electronically Excited State. *J. Chem. Phys.* **2007,** *127*, 024306-6.
96. Zhao, G.-J.; Han, K.-L., Time-Dependent Density Functional Theory Study on Hydrogen-Bonded Intramolecular Charge-Transfer Excited State of 4-Dimethylamino-Benzonitrile in Methanol. *J. Comput. Chem.* **2008,** *29*, 2010-2017.
97. Zhao, G.-J.; Han, K.-L.; Stang, P. J., Theoretical Insights into Hydrogen Bonding and Its Influence on the Structural and Spectral Properties of Aquo Palladium(Ii) Complexes: Cis-[(Dppp)Pd(H2o)2]2+, Cis-[(Dppp)Pd(H2o)(Oso2cf3)]+(Oso2cf3)−, and Cis-[(Dppp)Pd(H2o)2]2+(Oso2cf3)−2. *J. Chem. Theory Comput.* **2009,** *5*, 1955-1958.
98. Zhao, G.-J.; Northrop, B. H.; Han, K.-L.; Stang, P. J., The Effect of Intermolecular Hydrogen Bonding on the Fluorescence of a Bimetallic Platinum Complex. *J. Phys. Chem. A* **2010,** *114*, 9007-9013.
99. Zhao, G.-J.; Han, K.-L., Ultrafast Hydrogen Bond Strengthening of the Photoexcited Fluorenone in Alcohols for Facilitating the Fluorescence Quenching. *J. Phys. Chem. A* **2007,** *111*, 9218-9223.
100. Palit, D. K., Ultrafast Dynamics of the Excited States of Hydrogen-Bonded Complexes and Solvation. In *Hydrogen Bonding and Transfer in the Excited State*, John Wiley & Sons, Ltd: 2010; pp 761-795.
101. Hirai, S.; Banno, M.; Ohta, K.; Palit, D. K.; Tominaga, K., Subpicosecond Uv-Pump and Ir-Probe Spectroscopy of 9-Fluorenone in Deuterated Acetonitrile and Methanol. *Chemistry Letters* **2010,** *39*, 932-934.
102. Mondal, J. A.; Samant, V.; Varne, M.; Singh, A. K.; Ghanty, T. K.; Ghosh, H. N.; Palit, D. K., The Role of Hydrogen-Bonding Interactions in the Ultrafast Relaxation Dynamics of the Excited States of 3- and 4-Aminofluoren-9-Ones. *ChemPhysChem* **2009,** *10*, 2995-3012.
103. Underwood, D. F.; Blank, D. A., Ultrafast Solvation Dynamics: A View from the Solvent's Perspective Using a Novel Resonant-Pump, Nonresonant-Probe Technique. *J. Phys. Chem. A* **2003,** *107*, 956-961.
104. Underwood, D. F.; Blank, D. A., Measuring the Change in the Intermolecular Raman Spectrum During Dipolar Solvation. *J. Phys. Chem. A* **2005,** *109*, 3295-3306.
105. Wells, N. P.; McGrath, M. J.; Siepmann, J. I.; Underwood, D. F.; Blank, D. A., Excited State Hydrogen Bond Dynamics: Coumarin 102 in Acetonitrile−Water Binary Mixtures. *J. Phys. Chem. A* **2008,** *112*, 2511-2514.
106. Wells, N. P.; McGrath, M. J.; Siepmann, J. I.; Underwood, D. F.; Blank, D. A., Excited State Hydrogen Bond Dynamics: Coumarin 102 in Acetonitrile−Water Binary Mixtures. *J. Phys. Chem. A* **2008,** *112*, 2511-2514.

107. Cong, L.; Yin, H.; Shi, Y.; Jin, M.; Ding, D., Different Mechanisms of Ultrafast Excited State Deactivation of Coumarin 500 in Dioxane and Methanol Solvents: Experimental and Theoretical Study. *RSC Adv.* **2015,** *5*, 1205-1212.
108. Williamson, D. A.; Bowler, B. E., Electron Transfer through the Hydrogen-Bonded Interface of a B-Turn-Forming Depsipeptide. *J. Am. Chem. Soc.* **1998,** *120*, 10902-10911.
109. Mohammed, O. F.; Kwon, O.-H.; Othon, C. M.; Zewail, A. H., Charge Transfer Assisted by Collective Hydrogen-Bonding Dynamics. *Angew. Chem. Int. Ed.* **2009,** *48*, 6251-6256.
110. Trifonov, A.; Buchvarov, I.; Wagenknecht, H.-A.; Fiebig, T., Real-Time Observation of Hydrogen Bond-Assisted Electron Transfer to a DNA Base. *Chem. Phys. Lett.* **2005,** *409*, 277-280.
111. Pereira, R. V.; Gehlen, M. H., H-Bonding Assisted Intramolecular Charge Transfer in 1-Aminopyrene Derivatives. *Chem. Phys. Lett.* **2006,** *426*, 311-317.
112. Fonseca Guerra, C.; Bickelhaupt, F. M.; Snijders, J. G.; Baerends, E. J., The Nature of the Hydrogen Bond in DNA Base Pairs: The Role of Charge Transfer and Resonance Assistance. *Chem. Eur. J.* **1999,** *5*, 3581-3594.
113. Kirby, J. P.; Roberts, J. A.; Nocera, D. G., Significant Effect of Salt Bridges on Electron Transfer. *J. Am. Chem. Soc.* **1997,** *119*, 9230-9236.
114. Bowler, B. E.; Meade, T. J.; Mayo, S. L.; Richards, J. H.; Gray, H. B., Long-Range Electron Transfer in Structurally Engineered Pentaammineruthenium (Histidine-62)Cytochrome C. *J. Am. Chem. Soc.* **1989,** *111*, 8757-8759.
115. Therien, M. J.; Selman, M.; Gray, H. B.; Chang, I. J.; Winkler, J. R., Long-Range Electron Transfer in Ruthenium-Modified Cytochrome C: Evaluation of Porphyrin-Ruthenium Electronic Couplings in the Candida Krusei and Horse Heart Proteins. *J. Am. Chem. Soc.* **1990,** *112*, 2420-2422.
116. Turro, C.; Chang, C. K.; Leroi, G. E.; Cukier, R. I.; Nocera, D. G., Photoinduced Electron Transfer Mediated by a Hydrogen-Bonded Interface. *J. Am. Chem. Soc.* **1992,** *114*, 4013-4015.
117. Yoshihara, K.; Tominaga, K.; Nagasawa, Y., Effects of the Solvent Dynamics and Vibrational Motions in Electron Transfer. *Bull. Chem. Soc. Jpn.* **1995,** *68*, 696-712.
118. Ghosh, H. N.; Verma, S.; Nibbering, E. T. J., Ultrafast Forward and Backward Electron Transfer Dynamics of Coumarin 337 in Hydrogen-Bonded Anilines as Studied with Femtosecond Uv-Pump/Ir-Probe Spectroscopy. *J. Phys. Chem. A* **2010,** *115*, 664-670.
119. Yang, D.; Liu, Y.; Shi, D.; Sun, J., Theoretical Study on the Excited-State Photoinduced Electron Transfer Facilitated by Hydrogen Bonding Strengthening in the C337–an/Man Complexes. *Comp. Theor. Chem.* **2012,** *984*, 76-84.
120. Lemaur, V.; Steel, M.; Beljonne, D.; Brédas, J.-L.; Cornil, J., Photoinduced Charge Generation and Recombination Dynamics in Model Donor/Acceptor Pairs for Organic Solar Cell Applications: A Full Quantum-Chemical Treatment. *J. Am. Chem. Soc.* **2005,** *127*, 6077-6086.
121. Castner, E. W.; Kennedy, D.; Cave, R. J., Solvent as Electron Donor: Donor/Acceptor Electronic Coupling Is a Dynamical Variable. *J. Phys. Chem. A* **2000,** *104*, 2869-2885.
122. Chudoba, C.; Nibbering, E. T. J.; Elsaesser, T., Site-Specific Excited-State Solute-Solvent Interactions Probed by Femtosecond Vibrational Spectroscopy. *Physical Review Letters* **1998,** *81*, 3010-3013.
123. Nibbering, E. T. J.; Chudoba, C.; Elsaesser, T., Hydrogen-Bond Dynamics and Solvation of Electronically Excited States as Determined by Femtosecond Vibrational Spectroscopy. *Isr. J. Chem.* **1999,** *39*, 333-346.
124. Engleitner, S.; Seel, M.; Zinth, W., Nonexponentialities in the Ultrafast Electron-Transfer Dynamics in the System Oxazine 1 in N,N-Dimethylaniline. *J. Phys. Chem. A* **1999,** *103*, 3013-3019.
125. Weaver, M. J.; Nettles, S. M., Solvent Isotope Effects Upon the Thermodynamics of Some Transition-Metal Redox Couples in Aqueous Media. *Inorg. Chem.* **1980,** *19*, 1641-1646.
126. Siders, P.; Marcus, R. A., Quantum Effects in Electron-Transfer Reactions. *J. Am. Chem. Soc.* **1981,** *103*, 741-747.
127. Reid, P. J.; Silva, C.; Barbara, P. F.; Karki, L.; Hupp, J. T., Electronic Coherence, Vibrational Coherence, and Solvent Degrees of Freedom in the Femtosecond Spectroscopy of Mixed-Valence Metal Dimers in H2o and D2o. *J. Phys. Chem.* **1995,** *99*, 2609-2616.
128. Némethy, G.; Scheraga, H. A., Structure of Water and Hydrophobic Bonding in Proteins. Iv. The Thermodynamic Properties of Liquid Deuterium Oxide. *J. Chem. Phys.* **1964,** *41*, 680-689.

129. Kliner, D. A. V.; Tominaga, K.; Walker, G. C.; Barbara, P. F., Comparison of Experimental and Theoretical Absolute Rates for Intervalence Electron Transfer. *J. Am. Chem. Soc.* **1992,** *114*, 8323-8325.
130. Ghosh, H. N.; Adamczyk, K.; Verma, S.; Dreyer, J.; Nibbering, E. T. J., On the Role of Hydrogen Bonds in Photoinduced Electron-Transfer Dynamics between 9-Fluorenone and Amine Solvents. *Chem. Eur. J.* **2012,** *18*, 4930-4937.
131. Pugžlys, A.; den Hartog, H. P.; Baltuška, A.; Pshenichnikov, M. S.; Umapathy, S.; Wiersma, D. A., Solvent-Controlled Acceleration of Electron Transfer in Binary Mixtures. *J. Phys. Chem. A* **2001,** *105*, 11407-11413.
132. Saini, R. K.; Das, K., Picosecond Spectral Relaxation of Curcumin Excited State in a Binary Solvent Mixture of Toluene and Methanol. *J. Phys. Chem. B* **2012,** *116*, 10357-10363.
133. Saini, R. K.; Das, K., Picosecond Spectral Relaxation of Curcumin Excited State in Toluene–Alcohol Mixtures. *J. Lumin.* **2013,** *144*, 169-175.
134. Mandal, S.; Ghosh, S.; Banerjee, C.; Kuchlyan, J.; Sarkar, N., Unique Photophysical Behavior of 2,2′-Bipyridine-3,3′-Diol in Dmso–Water Binary Mixtures: Potential Application for Fluorescence Sensing of Zn2+ Based on the Inhibition of Excited-State Intramolecular Double Proton Transfer. *J. Phys. Chem. B* **2013,** *117*, 12212-12223.
135. Hohenberg, P.; Kohn, W., Inhomogeneous Electron Gas. *Physical Review* **1964,** *136*, B864-B871.
136. Kohn, W.; Sham, L. J., Self-Consistent Equations Including Exchange and Correlation Effects. *Physical Review* **1965,** *140*, A1133-A1138.
137. Marques, M. A. L.; Gross, E. K. U., Time-Dependent Density Functional Theory. *Annu. Rev. Phys. Chem.* **2004,** *55*, 427-455.
138. Casida, M. E.; Huix-Rotllant, M., Progress in Time-Dependent Density-Functional Theory. *Annu. Rev. Phys. Chem.* **2012,** *63*, 287-323.
139. Burke, K.; Werschnik, J.; Gross, E. K. U., Time-Dependent Density Functional Theory: Past, Present, and Future. *J. Chem. Phys.* **2005,** *123*, 062206.
140. Tsai, H.-H. G.; Sun, H.-L. S.; Tan, C.-J., Td-Dft Study of the Excited-State Potential Energy Surfaces of 2-(2′-Hydroxyphenyl)Benzimidazole and Its Amino Derivatives. *J. Phys. Chem. A* **2010,** *114*, 4065-4079.
141. Jamorski, C.; Foresman, J. B.; Thilgen, C.; Lüthi, H.-P., Assessment of Time-Dependent Density-Functional Theory for the Calculation of Critical Features in the Absorption Spectra of a Series of Aromatic Donor–Acceptor Systems. *J. Chem. Phys.* **2002,** *116*, 8761-8771.
142. M. J. Frisch, G. W. T., H. B. Schlegel, G. E. Scuseria, M. A. Robb, J. R. Cheeseman, J. A. Montgomery, Jr., T. Vreven, K. N. Kudin, J. C. Burant, J. M. Millam, S. S. Iyengar, J. Tomasi, V. Barone, B. Mennucci, M. Cossi, G. Scalmani, N. Rega, G. A. Petersson, H. Nakatsuji, M. Hada, M. Ehara, K. Toyota, R. Fukuda, J. Hasegawa, M. Ishida, T. Nakajima, Y. Honda, O. Kitao, H. Nakai, M. Klene, X. Li, J. E. Knox, H. P. Hratchian, J. B. Cross, V. Bakken, C. Adamo, J. Jaramillo, R. Gomperts, R. E. Stratmann, O. Yazyev, A. J. Austin, R. Cammi, C. Pomelli, J. W. Ochterski, P. Y. Ayala, K. Morokuma, G. A. Voth, P. Salvador, J. J. Dannenberg, V. G. Zakrzewski, S. Dapprich, A. D. Daniels, M. C. Strain, O. Farkas, D. K. Malick, A. D. Rabuck, K. Raghavachari, J. B. Foresman, J. V. Ortiz, Q. Cui, A. G. Baboul, S. Clifford, J. Cioslowski, B. B. Stefanov, G. Liu, A. Liashenko, P. Piskorz, I. Komaromi, R. L. Martin, D. J. Fox, T. Keith, M. A. Al-Laham, C. Y. Peng, A. Nanayakkara, M. Challacombe, P. M. W. Gill, B. Johnson, W. Chen, M. W. Wong, C. Gonzalez, and J. A. Pople, , *Gaussian 03, Revision C.02 Gaussian, Inc., Wallingford CT, 2004*.
143. Sahu, K.; Mondal, S. K.; Ghosh, S.; Roy, D.; Sen, P.; Bhattacharyya, K., Femtosecond Study of Partially Folded States of Cytochrome C by Solvation Dynamics. *J. Phys. Chem. B* **2005,** *110*, 1056-1062.
144. Sahu, K.; Ghosh, S.; Mondal, S. K.; Ghosh, B. C.; Sen, P.; Roy, D.; Bhattacharyya, K., Ultrafast Fluorescence Resonance Energy Transfer in a Micelle. *J. Chem. Phys.* **2006,** *125*, 044714-8.
145. Jones, G.; Jackson, W. R.; Choi, C. Y.; Bergmark, W. R., Solvent Effects on Emission Yield and Lifetime for Coumarin Laser Dyes. Requirements for a Rotatory Decay Mechanism. *J. Phys. Chem.* **1985,** *89*, 294-300.

146. Tschirschwitz, F.; Nibbering, E. T. J., Femtosecond Pump–Probe and Grating Scattering Study of Condensed-Phase Hydrogen-Bonding Dynamics of Complexes of Coumarin 102. *Chem. Phys. Lett.* **1999,** *312*, 169-177.
147. Liu, Y.-H.; Li, P., Excited-State Hydrogen Bonding Effect on Dynamic Fluorescence of Coumarin 102 Chromophore in Solution: A Time-Resolved Fluorescence and Theoretical Study. *J. Lumin.* **2011,** *131*, 2116-2120.
148. Liptak, M. D.; Gross, K. C.; Seybold, P. G.; Feldgus, S.; Shields, G. C., Absolute Pka Determinations for Substituted Phenols. *J. Am. Chem. Soc.* **2002,** *124*, 6421-6427.
149. Bordwell, F. G.; Cheng, J., Substituent Effects on the Stabilities of Phenoxyl Radicals and the Acidities of Phenoxyl Radical Cations. *J. Am. Chem. Soc.* **1991,** *113*, 1736-1743.
150. Shields, Z. P.; Murray, J. S.; Politzer, P., Directional Tendencies of Halogen and Hydrogen Bonds. *Int. J. Quantum Chem.* **2010,** *110*, 2823-2832.
151. Parker, A. J.; Stewart, J.; Donald, K. J.; Parish, C. A., Halogen Bonding in DNA Base Pairs. *J. Am. Chem. Soc.* **2012,** *134*, 5165-5172.
152. Barman, N.; Singha, D.; Sahu, K., Fluorescence Quenching of Hydrogen-Bonded Coumarin 102-Phenol Complex: Effect of Excited-State Hydrogen Bonding Strength. *J. Phys. Chem. A* **2013,** *117*, 3945-3953.
153. Kumbhakar, M.; Nath, S.; Mukherjee, T.; Pal, H., Effect of Micellar Environment on Marcus Correlation Curves for Photoinduced Bimolecular Electron Transfer Reactions. *J. Chem. Phys.* **2005,** *123*, 034705-11.
154. Ghosh, S.; Sahu, K.; Mondal, S. K.; Sen, P.; Bhattacharyya, K., A Femtosecond Study of Photoinduced Electron Transfer from Dimethylaniline to Coumarin Dyes in a Cetyltrimethylammonium Bromide Micelle. *J. Chem. Phys.* **2006,** *125*, 054509-7.
155. Yeh, J. H.; Shen, T. L.; Nocera, D. G.; Leroi, G. E.; Suzuka, I.; Ozawa, H.; Namuta, Y., Resonance Two-Photon Ionization Spectroscopy of the Aniline Dimer. *J. Phys. Chem.* **1996,** *100*, 4385-4389.
156. Schemmel, D.; Schütz, M., Molecular Aniline Clusters. Ii. The Low-Lying Electronic Excited States. *J. Chem. Phys.* **2010,** *133*, 134307.
157. Schemmel, D.; Schütz, M., Molecular Aniline Clusters. I. The Electronic Ground State. *J. Chem. Phys.* **2010,** *132*, 174303.
158. Kamlet, M. J.; Abboud, J. L. M.; Abraham, M. H.; Taft, R. W., Linear Solvation Energy Relationships. 23. A Comprehensive Collection of the Solvatochromic Parameters, .Pi.*, .Alpha., And .Beta., and Some Methods for Simplifying the Generalized Solvatochromic Equation. *J. Org. Chem.* **1983,** *48*, 2877-2887.
159. Stenutz, R. Kamlet-Taft Solvent Parameters - Home Page of R. Stenutz. http://www.stenutz.eu/chem/solv26.php.
160. Moog, R. S.; Davis, W. W.; Ostrowski, S. G.; Wilson, G. L., Solvent Effects on Electronic Transitions in Several Coumarins. *Chem. Phys. Lett.* **1999,** *299*, 265-271.
161. Molotsky, T.; Huppert, D., Site Specific Solvation Statics and Dynamics of Coumarin Dyes in Hexane–Methanol Mixture. *J. Phys. Chem. A* **2003,** *107*, 2769-2780.
162. Mukherjee, S.; Sahu, K.; Roy, D.; Mondal, S. K.; Bhattacharyya, K., Solvation Dynamics of 4-Aminophthalimide in Dioxane–Water Mixture. *Chem. Phys. Lett.* **2004,** *384*, 128-133.
163. Chakraborty, A.; Seth, D.; Chakrabarty, D.; Hazra, P.; Sarkar, N., Photoinduced Electron Transfer from Dimethyl Aniline to Coumarin Dyes in Reverse Micelles. *Chem. Phys. Lett.* **2005,** *405*, 18-25.
164. Herbich, J.; Kijak, M.; Zielińska, A.; Thummel, R. P.; Waluk, J., Fluorescence Quenching by Pyridine and Derivatives Induced by Intermolecular Hydrogen Bonding to Pyrrole-Containing Heteroaromatics†. *J. Phys. Chem. A* **2002,** *106*, 2158-2163.
165. Martin, M. M.; Ikeda, N.; Okada, T.; Mataga, N., Picosecond Laser Photolysis Studies of Deactivation Processes of Excited Hydrogen-Bonding Complexes. 2. Dibenzocarbazole-Pyridine Systems. *J. Phys. Chem.* **1982,** *86*, 4148-4156.
166. Chowdhury, P. K.; Sugawara, K.; Nakanaga, T.; Takeo, H., Structure of the Aniline–Benzene and Aniline–Cyclohexane Clusters Based on Infrared Depletion Spectroscopy. *Chem. Phys. Lett.* **1998,** *285*, 77-82.

167. Sugawara, K.-i.; Miyawaki, J.; Nakanaga, T.; Takeo, H.; Lembach, G.; Djafari, S.; Barth, H.-D.; Brutschy, B., Infrared Depletion Spectroscopy of the Aniline Dimer. *J. Phys. Chem.* **1996,** *100*, 17145-17147.
168. Spencer, J. N.; Campanella, C. L.; Harris, E. M.; Wolbach, W. S., Solvent Effects on Hydrogen-Bond Formation. *J. Phys. Chem.* **1985,** *89*, 1888-1891.
169. Cook, J. L.; Hunter, C. A.; Low, C. M. R.; Perez-Velasco, A.; Vinter, J. G., Solvent Effects on Hydrogen Bonding. *Angew. Chem. Int. Ed.* **2007,** *46*, 3706-3709.
170. Villa, I.; Sanchez, F.; Lopes, T.; Lopez-Cornejo, P.; Perez-Tejeda, P., Photoinduced Electron-Transfer Reactions: A Study of the Diffusion-Controlled and Activation-Diffusion-Controlled Processes. *J. Phys. Chem. A* **2010,** *114*, 7912-7917.
171. Satpati, A. K.; Kumbhakar, M.; Nath, S.; Pal, H., Roles of Diffusion and Activation Barrier on the Appearance of Marcus Inversion Behavior: A Study of a Photoinduced Electron-Transfer Reaction in Aqueous Triblock Copolymer (P123) Micellar Solutions. *J. Phys. Chem. B* **2007,** *111*, 7550-7560.
172. Song, L.; Dorfman, R. C.; Swallen, S. F.; Fayer, M. D., Influence of Diffusion on Photoinduced Electron Transfer. *J. Phys. Chem.* **1991,** *95*, 3454-3457.
173. Barman, N.; Sahu, K., Anomalous Modulation of Photoinduced Electron Transfer of Coumarin 102 in Aniline-Dimethylaniline Mixture: Dominant Role of Hydrogen Bonding. *Phys. Chem. Chem. Phys.* **2014,** *16*, 27096-27103.
174. Barman, N.; Mondal, K.; Sahu, K., Manuscript Communicated.
175. Barman, N.; Sahu, K., Reduced Fluorescence Quenching of Coumarin 102 at Higher Phenol Mole Fractions in Cyclohexane-Phenol and Anisole-Phenol Solvent Mixtures: Role of Competitive Hydrogen Bonding. *RSC Adv.* **2014,** *4*, 58299-58306.